NTNU

Norwegian University of
Science and Technology

Bottom-Up Modeling of the Nord Pool System Price

Marius Fuglerud
Knut Erik Vedahl

Industrial Economics and Technology Management
Submission date: June 2011
Supervisor: Stein-Erik Fleten, IØT

Norwegian University of Science and Technology
Department of Industrial Economics and Technology Management

Problem description

The objective is to establish a midterm model for the Nord Pool system price. Scenarios for exogenous variables will be created using statistical models. These scenarios will be combined with a mathematical model of the Nordic power system. Resulting price scenarios will yield an indication on the expected future system price, and the uncertainty in future spot prices.

Assignment given: January 17, 2011

Supervisor: Stein-Erik Fleten

Abstract

We develop a bottom-up, midterm model for the Nord Pool system price. Models for consumption, generation and exchange are combined using a market equilibrium approach. Scenarios for the most influential stochastic factors are created using statistical models. Forecasted price scenarios yield an indication on the expected future system price, and the uncertainty in future prices. Compared to stochastic dynamic programming based models, we use an empirical function to approximate the water value. Consequently, our model represents a less computationally intensive method for price forecasting than e.g. the EMPS model.

In addition to providing a picture of the price distribution, the model can be applied to learn about the impact of different variables. In particular, we study the relative influence of the stochastic factors and price risk caused by inflow volatility. The performance of the model is evaluated in numerical examples over a two-year forecast period. Overall, we conclude the model provides realistic forecasts of the system price and its distribution. The performance under normal market conditions may deviate from our results, due to the extraordinary drop in fuel prices caused by the financial crisis.

Preface

This master thesis presents a study within the field of economic modeling in energy markets. It is conducted during the spring of 2011 at the Department of Industrial Economics and Technology Management at Norwegian University of Science and Technology (NTNU), Trondheim.

First, we would like to thank our supervisor, Professor Stein-Erik Fleten, for valuable feedback and guidance. We would also like to thank Ståle Størdal and his colleagues in Eidsiva Energi for sharing their experience and giving advice for the scope of this thesis. Our study is based on large amounts of historical data, and the level of comprehensiveness would not have been possible to achieve without the broad willingness from different organizations to share data with us.

Contents

1. Introduction 1
2. Framework 3
2.1 Stochastic factors 3
2.1.1 HDD and snow reservoirs 4
2.1.2 Reservoir inflow 5
2.1.3 Wind power generation 6
2.1.4 The EEX spot price 6
2.1.5 CO_2 quota prices 8
2.1.6 Fuel prices 9
2.2 Consumption 10
2.2.1 Factors influencing consumption 10
2.2.2 Consumption models 11
2.3 Thermal generation 11
2.3.1 Nuclear power 12
2.3.2 CHP industry 13
2.3.3 CHP district 14
2.3.4 Condensing power 15
2.4 Hydro generation and the marginal water value 16
2.5 Exchange 23
2.6 Load periods 24
2.7 Market equilibrium 25
3. Data 27
3.1 Consumption modeling 27
3.2 Hydrology 29
3.3 Generation modeling 31
3.4 Exchange 34
3.5 Intra-week consumption and prices 37
4. Estimation 38
4.1 Stochastic factors 39
4.1.1 HDD 39

4.1.2 Snow reservoirs 41
4.1.3 Reservoir inflow 42
4.1.4 Wind power generation 44
4.1.5 The EEX spot price 45
4.1.6 Coal, gas and CO_2 prices 48
4.2 Consumption 50
4.2.1 Descriptive statistics 50
4.2.2 Error correction model 51
4.2.3 Dynamic regression model 51
4.3 Thermal generation 53
4.3.1 Nuclear power 53
4.3.2 CHP industry 55
4.3.3 CHP district 56
4.4 Hydro generation and the marginal water value 56
4.5 Exchange 60
4.5.1 The Netherlands, Germany and Poland 60
4.5.2 Russia 61
4.5.3 Estonia 61
4.6 Load periods 62
4.7 Market equilibrium simulations 63
4.8 Case studies 66
4.8.1 Inflow risk 66
4.8.2 The relative influence of the stochastic factors 71
4.8.3 Changes in exchange capacity 72
5. Discussion 74
References 75
Appendix A 82

Appendix B. Source code (zip-file)

1. Introduction

The objective of this thesis is to develop a bottom-up model for the Nord Pool system price. Separate models for consumption, generation and exchange are combined using a market equilibrium approach. Scenarios for the most influential stochastic factors are inputs to the model. The output is a midterm forecast of the price distribution with weekly granularity. In numerical examples, we assess the performance of the model over a period of two years.

Predictions of the future system price distribution are of importance for players in the deregulated Nordic power market. More elaborated models for area prices are also needed, but our model may provide a complementary picture of the price uncertainty in a midterm perspective. The model can improve the decision basis for participants in the power market, such as power producers and energy-intensive industry.

A reasonable price distribution relies on the quality and composition of the underlying models, and our major focus is hence development and combination of these models. Models for each essential variable are established due to their particular characteristics, and interrelations between them are studied.

Bottom-up models for electricity price forecasting are not common in academic literature, but extensively used by the market participants in the Nord Pool area. Most widespread is the EMPS model, which is employed for generation planning and power system analysis in addition to price predictions. The model applies a stochastic dynamic programming (SDP) approach to calculate the marginal water value (SINTEF Energiforskning, 2008). Scenarios for stochastic factors are created directly from historical data: Observed levels for a set of historical years are used to represent potential future realizations (Doorman et al., 2004).

Instead of using historical observations directly as future scenarios, we simulate scenarios from stochastic processes. Consequently, correlation structures between the history and the scenarios are modeled. Inspired by Tipping (2007), we derive an empirical model for the marginal water value, which is a less computationally intensive methodology than the stochastic optimization approach. Tipping demonstrates that an empirical water value function leads to well-performing forecasts of the spot price in New Zealand.

An empirical water value function is also applied in the bottom-up price model of Vehviläinen and Pyykkönen (2005). Vehviläinen and Pyykkönen estimated models for consumption, generation and the marginal water value from historical data for the Nord Pool area. Through a market balance and scenarios for temperature and precipitation, future spot price paths with monthly granularity were created.

Compared to the model developed by Vehviläinen and Pyykkönen, our model is more complex. We introduce additional stochastic factors, model thermal generation as a function of fuel and carbon quota prices, seek to improve the water value equation, include intraweek demand

variations, and model exchange with connected markets. Still, our model represent a more intuitive and less computationally intensive method for system price forecasting than the EMPS model.

A brief overview of the framework is presented in Figure 1. The stochastic factors include heating degree days (HDD), inflow, snow reservoirs, fuel prices, carbon quota prices, the spot price at the German power exchange (EEX), wind power generation and outages of thermal power plants. Electricity generation is modeled for different plant categories: Hydro power, condensing power, industrial CHP (combined heat and power), district CHP and nuclear power in addition to wind power. For the categories which are most flexible with regard to adjustment of the output, generation is assumed to be bid at short run marginal costs. Modeling generation using marginal costs depends on the assumption of an (approximately) efficient power market, which is not obvious due to the large companies dominating the power sector in the Nord Pool area. However, there is no evidence of market power on a system level in the empirical research which Fridolfsson and Tangerås (2009) review. The Nord Pool system price is defined by the intersection of the aggregate supply and demand curves for the entire price area, without taking into account transfer constraints (Nord Pool Spot, 2010). Therefore, internal transmission capacities are not included in our model.

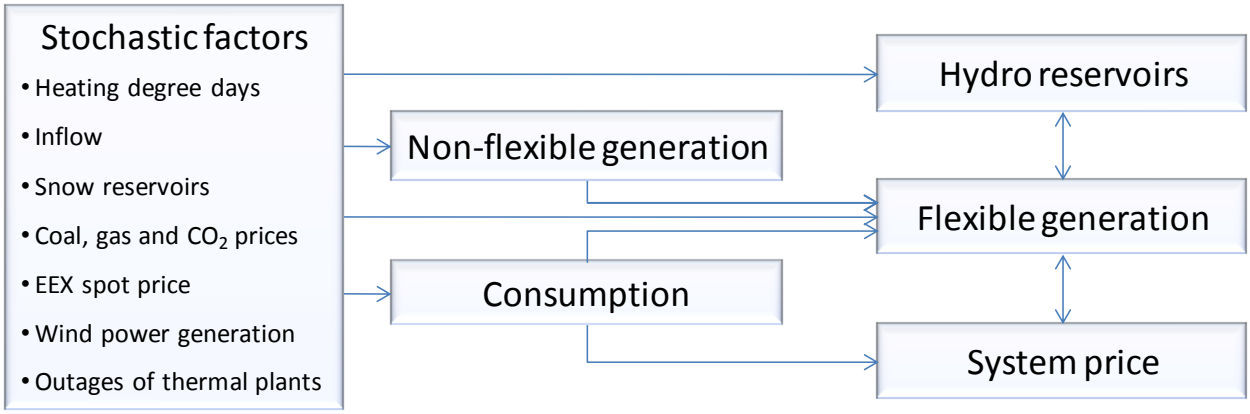

Figure 1. *Overview of the framework*

The next chapter outlines the framework in detail. Chapter 3 provides an overview of the data used to calibrate the models. The estimated models, forecasts and simulations are presented in Chapter 4, while we in Chapter 5 discuss the results and draw conclusions.

2. Framework

A component-wise description of the modeling approach is presented in 2.1-2.6. In Chapter 2.7, we outline how the market equilibrium approach is used to combine the different models. Notations are consecutively introduced. In addition, an overview of the most frequently used notations is given below.

t	Time	R_S	Snow reservoir level
j	Season	$R_{S\%}$	Relative snow reservoir level
Y	Variable to be modeled	I	Reservoir inflow
X	Explanatory variable	MWV	Marginal water value
C	Constant term	NI	Net import
u	Residual term	F	Consumption
		HDD	Heating degree days
		DL	Day length
S_{NP}	Nord Pool system price	RTI	Retail trade index
S_{EEX}	EEX spot price	G_{hydro}	Hydro generation
S_{coal}	Coal spot price	G_{hydroR}	Regulated hydro power generation
S_{gas}	Natural gas spot price	$G_{hydroR\%}$	Relative regulated hydro power generation
S_{CO_2}	CO_2 quota spot price	G_{hydroU}	Unregulated hydro power generation
R_W	Hydro reservoir level	G_{CHPD}	CHP district generation
R_{WCAP}	Hydro reservoir capacity	G_{CHPI}	CHP industry generation
$R_{W\%}$	Relative hydro reservoir level	G_{wind}	Wind power generation

2.1 Stochastic factors

The fundamental quantities influencing the levels of electricity consumption, generation and exchange are modeled as stochastic factors. Temperature affects both consumption and the level of CHP district generation, and is modeled using HDD. Reservoir inflow determines the resources available for hydro power producers, whereas snow reservoirs give indications on future inflow levels. Fuel and carbon quota prices affect the marginal costs which condensing power producers bid to the market. Among the power markets connected to Nord Pool, the largest capacity is shared with the German market. Therefore, the EEX spot price is included as a stochastic factor. The availability of thermal plants varies over time, and we consider how outages can be modeled. Wind power generation is also implemented as a stochastic factor, since the generation level is difficult to predict.

In the following, we describe how the characteristics of each stochastic factor can be modeled. Models for thermal plant outages are deferred to Chapter 2.3.

2.1.1 HDD and snow reservoirs

HDD and snow reservoirs vary in a seasonal pattern throughout the year. The stochastic processes most commonly applied to seasonal time series are deseasonalized ARIMA models, periodic AR (PAR) models and seasonal ARIMA (SARIMA) models (Hipel and McLeod, 1994).

When a deseasonalized ARIMA model is employed, the original time series is deseasonalized by for instance (Hipel and McLeod, 1994):

$$y_{t,j} = \frac{Y_{t,j} - \hat{\mu}_{Y,j}}{\hat{\sigma}_{Y,j}} \tag{1}$$

where Y is the time series to be modeled, y is the deseasonalized series, t is the time period index, j is the season index, $\hat{\mu}_{Y,j}$ is the estimated mean in season j and $\hat{\sigma}_{Y,j}$ is the estimated standard deviation in season j. An ordinary ARIMA model is then fitted to y.

A periodic AR model differs from an ordinary AR model by seasonally dependent coefficients (Hipel and McLeod, 1994):

$$\emptyset_j(B)\nabla^d Y_{t,j} = C + u_t, \qquad u_t \sim N(0, \sigma_u^2) \tag{2}$$

$\emptyset_j(B)$ is an AR polynomial of order p, B is the backshift operator, $\nabla^d = (1-B)^d$ denotes the differencing transformation of degree $d \geq 0$ and C is the intercept. u is the time series of residuals, which should not exhibit autocorrelation. Residuals are also assumed to be normally distributed.

SARIMA models take account of seasonality by seasonal lags. The general, multiplicative form can be written as (Hipel and McLeod, 1994):

$$\emptyset(B^S)\emptyset(B)\nabla_S^D\nabla^d Y_t = C + \theta(B^S)\theta(B)u_t \tag{3}$$

S is the length of one season, i.e. 52 in this case. $\nabla_S^D = (1-B^s)^D$ is the seasonal differencing transformation of degree $D \geq 0$. $\emptyset(B^S)$ is a seasonal AR (SAR) polynomial of order P, $\theta(B)$ is a non-seasonal MA polynomial of order q and $\theta(B^S)$ is a seasonal MA (SMA) polynomial of order Q.

For natural time series as snow reservoirs and HDD, the mean and variance should be (close to) stationary each season. As opposed to SARIMA models, deseasonalized ARIMA and PAR models state explicit that the mean and variance within each season are constant from year to year (Hipel and McLeod, 1994). This is an advantage in favor of deseasonalized ARIMA and PAR models, but leads to a drawback when it comes to calibration. With weekly granularity, the deseasonalized ARIMA model requires estimation of 52 weekly means and standard deviations, while 52 AR models must be estimated when applying the PAR approach. Consequently, a large

number of years of historical data are required to obtain stable parameter estimates[1]. Therefore, we will follow the more parsimonious SARIMA approach in modeling of snow reservoirs and HDD.

To stabilize the seasonally varying mean, the HDD and snow reservoir series will be seasonally differenced ($D = 1$). Seasonally differencing may not completely remove the seasonal pattern, and the remaining seasonality is modeled by SAR and SMA factors. The lag structure *(p, q, P, Q)* will be optimized using an information criterion. However, we restrict $P + Q \leq 1$, as higher orders of seasonal lags have no natural interpretation (Nau, 2010).

2.1.2 Reservoir inflow

The aggregated reservoir inflow stem from snow melting and precipitation, and the inflow is thus negatively correlated with the change in snow reservoirs during the snow melting season. A negative correlation is also present when snow reservoirs increase, as the share of the precipitation which falls as rain decreases when the accumulation of snow reservoirs increases. To incorporate the correlation between inflow and the change in snow reservoirs, we will model reservoir inflow by a dynamic regression model.

A dynamic regression model with one input can be written as (Pankratz, 1991):

$$Y_t = C + v(B)X_t + N_t \tag{4}$$

Y is the output time series, $v(B)$ is a linear transfer function and X is the input time series. In this case, the input series is the change in snow reservoirs. N is the disturbance series, which may be autocorrelated.

After (4) is estimated, the disturbances N are examined for non-stationarity, and the necessary difference operators are added. To get rid of autocorrelation in the disturbances, a SARIMA model (3) will be estimated for N. Substituting the difference operators and the disturbance SARIMA model into (4), the general formulation becomes (Pankratz, 1991):

$$\nabla_S^D \nabla^d Y_t = \nabla_S^D \nabla^d v(B)X_t + \frac{\theta(B^S)\theta(B)}{\emptyset(B^S)\emptyset(B)} u_t \tag{5}$$

The formulation of the transfer function $v(B)$ can be selected by examining the impulse response function. More details on implementation of the methodology are presented along with the estimation results in 4.1.3.

[1] A Fourier transformation approach can solve the overparameterization problem (Hipel and McLeod, 1994), but is not further considered here.

2.1.3 Wind power generation

Wind power generation is simulated using an ARIMA(p,d,q) process. The advantage of an ARIMA model, for instance compared to a Brownian motion, is that the possible autocorrelation in wind speeds from one week to the next will be captured. As the share of wind power in the Nord Pool area is small compared to the other generation categories (Nordel, 2009), we will not develop independent wind power scenarios. Instead, random scenarios will be drawn during the price simulations.

2.1.4 The EEX spot price

Several characteristics of electricity prices have to be considered when developing a model for the EEX spot price (Deng, 2000):

- *Seasonality:* When demand increases, generating units higher on the merit order set the market price. Thus, spot prices increase with demand.
- *Spikes:* Outages of baseload plants or transmission cables force a shift in the supply curve. Depending on the outage size, peak load units with high marginal cost may clear the market in more hours than usually during the week. The same result appears when the demand curve shifts due to a cold/heat wave.
- *Mean Reversion*[2]*:* Sudden changes in the price are often caused by short duration events, like the above mentioned examples. After the event, the price will revert back to the normal level. This level is dependent on marginal costs of generation, and will therefore vary with for instance fuel prices.
- *Jumps:* A sudden price change can also lead to a new long lasting price regime. For instance, prices can jump and remain high in a hydro dominated system if reservoir levels become lower than normal.

The starting point in development of stochastic processes with mean reversion is the arithmetic Ornstein-Uhlenbeck process (Dixit and Pindyck, 1994):

$$dY(t) = \rho\left(\bar{Y} - Y(t)\right)dt + \sigma_{OU}dZ \qquad (6)$$

where ρ (≥ 0) is the speed of mean reversion, $\bar{Y}$ is the long-run equilibrium, σ_{OU} (≥ 0) is the volatility and dZ is the increment to a Wiener process, which creates random moves in the process.

[2] In addition, long-term price dynamics may be explained by mean reversion. With high price levels over time, new suppliers will provide additional generating capacity and push the prices down (and vice versa) (Pilipovic, 1998). As we consider a mid-term horizon, this interpretation is of less importance in our case.

(6) is the limit of the following AR process, which will be used to create scenarios in discrete time (Dixit and Pindyck, 1994):

$$Y_t = Y_{t-1} + \bar{Y}(1 - e^{-\rho}) + (e^{-\rho} - 1)Y_{t-1} + \epsilon_{OU,t}$$
$$\epsilon_{OU,t} \sim N(0, \sigma_\epsilon^2), \ \sigma_\epsilon^2 = \frac{\sigma_{OU}^2}{2\rho}(1 - e^{-2\rho}) \quad (7)$$

The Ornstein-Uhlenbeck process assumes a constant mean reversion speed for all price levels. An alternative is the geometric mean reversion model, where the reversion speed is proportional to Y (Ewald and Yang, 2007):

$$dY(t) = \kappa\big(\theta - Y(t)\big)Y(t)dt + \sigma_{GMR}Y(t)dZ \quad (8)$$

where κ (≥ 0) is the proportional speed of mean reversion, θ is the long-run equilibrium parameter, σ_{GMR} (≥ 0) is the proportional volatility and dZ is the increment to a Wiener process.

In discrete time, (8) can be approximated by a forward Euler discretization (Yang and Yang, 2008):

$$Y_{t+1} = Y_t + (\alpha - \kappa Y_t)Y_t\Delta t + \sigma_{GMR}Y_t\sqrt{\Delta t}\epsilon_{GMR,t+1}$$
$$\epsilon_{GMR,t} \sim N(0,1) \quad (9)$$

where $\alpha = \kappa\theta$ and Δt is the time step. In the following, we assume a time step of one unit.

To model spikes, a jump diffusion component is added to (6) and (8):

$$dY(t) = \rho\big(\bar{Y} - Y(t)\big)dt + \sigma_{OU}dZ + JY(t)d\delta \quad (10)$$
$$dY(t) = \kappa\big(\theta - Y(t)\big)Y(t)dt + \sigma_{GMR}Y(t)dZ + JY(t)d\delta \quad (11)$$

The jump diffusion process is defined according to Cartea and Figueroa (2005), where:

- $d\delta$ is a Poisson process, such that $d\delta = 1$ with probability $\lambda_J dt$ and $d\delta = 0$ with probability (1- $\lambda_J dt$), where λ_J is the spike frequency.
- J is the proportional jump size, which is assumed to be normally distributed: $J \sim N(\mu_J, \sigma_J^2)$.

Since we assume a constant frequency λ_J, spikes will occur with the same likelihood throughout the year. This is a reasonable approximation for supply related events leading to spikes (like plant outages), but a simplification for demand related events. Sudden changes in demand are

more likely to occur in the winter season, and applying a seasonally dependent frequency is thus a possible extension[3].

Discrete time approximations can be written as:

$$Y_t = Y_{t-1} + \bar{Y}(1 - e^{-\rho}) + (e^{-\rho} - 1)Y_{t-1} + \epsilon_{OU,t} + JY_{t-1}\varphi \quad (12)$$

$$Y_{t+1} = Y_t + (\alpha - \kappa Y_t)Y_t + \sigma_{GMR}Y_t\epsilon_{GMR,t+1} + JY_{t-1}\varphi \quad (13)$$

where $\varphi = 1$ with probability λ_J and $\varphi = 0$ with probability $(1 - \lambda_J)$.

Jumps which lead to new permanent price levels can be modeled by for instance regime-switch models (Tipping, 2007). As a simplification, we ignore jumps and model all sudden price changes as spikes.

A simple way to account for seasonality is to subtract the weekly mean of the price history before estimation of parameters (Cartea and Figueroa, 2005). The seasonal behavior of the EEX spot price will be studied in order to evaluate whether deseasonalizing is favorable.

The jump diffusion part and the mean reversion part of (12) and (13) are calibrated separately, by filtration of spikes before estimation. The two models share the same jump diffusion parameters, and model selection is therefore based on comparison of likelihood values for the mean reversion parts. Barz and Johnson (1999) compared arithmetic and geometric mean reversion electricity spot price models with and without jump diffusion in four markets. The models with jump diffusion performed consistently better than those without, while the geometric mean reversion jump diffusion model resulted in higher likelihood values than the arithmetic model in 75% of the cases[4].

2.1.5 CO_2 quota prices

Daskalakis et al. (2009) evaluate different processes for CO_2 spot prices in European markets, including geometric Brownian motion and various mean reverting processes with and without jump diffusion. They found the prices have a non-mean reverting structure with jumps, and conclude the price process is best approximated by a geometric Brownian motion (GBM) augmented by jumps. An ordinary geometric Brownian motion was found to perform better than other processes without jumps.

The empirical study by Daskalakis et al. was based on price data during EU's first emission trading scheme (2005-2007), and their conclusions may not necessarily be applicable to succeeding trading schemes. As our base case, we assume the price process follows an ordinary geometric Brownian motion. The status of the European quota market will be assessed in

[3] We do not apply seasonally dependent spike frequencies due to the limited number of observations available for calibration (the EEX market opened in 2000). With a limited number of spikes, robust estimation of spike parameters is difficult.

[4] The models were fitted to hourly, not weekly, price data over periods of two months.

Chapter 3.3, to evaluate whether inclusion of jump diffusion is a necessary extension. The geometric Brownian motion process is written as (Vose, 2008):

$$dY(t) = \mu_{GBM} Y(t)dt + \sigma_{GBM} Y(t)dZ \quad (14)$$

where μ_{GBM} is the drift rate, σ_{GBM} is the volatility and dZ is the increment to a Wiener process.

A discrete-time approximation of (14) is developed by applying Itô's lemma with $F(Y) = ln(Y)$ and integrating from t to $t + \Delta t$ (Vose, 2008):

$$Y_{t+\Delta t} = Y_t \, e^{(\mu_{GBM} - 0.5\,\sigma_{GBM}^2)\Delta t + \sigma_{GBM}\sqrt{\Delta t}\,Z} = Y_t \, e^{r_{\Delta t}} \quad (15)$$

$$r_{\Delta t} \sim N\big((\mu_{GBM} - 0.5\sigma_{GBM}^2)\Delta t, \sigma_{GBM}^2 \Delta t\big)$$

The log return over period Δt, $r_{\Delta t} = ln(Y_{t+\Delta t}) - ln(Y_t)$, is normally distributed with parameters $(\mu_{GBM} - 0.5\sigma_{GBM}^2)\Delta t$ and $\sigma_{GBM}^2 \Delta t$. Hence, the mean and variance of historical log returns can be used to calibrate the GBM process parameters. A time step of Δt = 1 will be applied in the simulations.

The CO_2 price model may be improved by taking fuel prices into consideration. Prices of CO_2 emission allowances are indirectly linked to fuel prices, as allowance demand increases with fuel combustion levels. Hence, inclusion of fuel prices as an explanatory variable is a reasonable extension, see e.g. Mansanet Bataller et al. (2007).

2.1.6 Fuel prices

Pindyck (2001) discusses the dynamics of commodity prices in competitive markets. Prices of oil, natural gas and many other commodities exhibit high volatility, which vary over time. Short run price movements are caused by shifts in demand and supply in the cash and storage markets. In the long run, spot prices are likely to revert to long-run marginal costs. Consequently, fuel prices may be modeled as mean revering processes.

Geman (2007) conducted empirical research on oil and natural gas prices from 1994 to 2004. Time series are tested for unit root, in order to determine whether the prices are mean reverting or follow a random walk. There is evidence of a mean reversion pattern in natural gas prices until 1999, which changes into a random walk as from 2000. Also, crude oil prices have followed a random walk since 2000. As there is mixed results, we will determine whether to apply a mean reverting process (6) or a geometric Brownian motion (14) based on characteristics of collected fuel prices.

2.2 Consumption

2.2.1 Factors influencing consumption

Electricity consumption in the Nordics is affected by a variety of variables. In the EMPS model, consumption is separated into two categories: Price elastic and firm consumption. Price elastic consumption typically includes power intensive industry and dual-fuel boilers, whereas the remaining consumption is categorized as firm (Doorman, 2009). Price elastic consumption is separated into groups, where the plants within a group are assumed to switch off consumption at a certain threshold level. Firm consumption may also be modeled as price dependent, as is done by Johnsen and Willumsen (2010). In their model for firm consumption in Norway, they also apply HDD, day length, wind speed, price of alternative fuels, economic activity level and holiday dummies as explanatory variables. The intuition of including these variables can be summarized as follows:

- *HDD:* Electricity consumption in the Nordics is closely tied to the temperature, since electricity is one of the most important heating sources. The concept of HDD provides an intuitive link between temperature and heating demand, by assuming the heating demand starts at a certain temperature, the critical temperature. The HDD for a given period is here defined as the number of degrees the average temperature of the period is below the critical temperature, in line with Murray and Ringwood (1994).
- *Day length:* The demand for lightning increases when the day length decreases.
- *Wind speed:* An increase in the average wind speed reduces the effective temperature, and thus the heating demand should increase.
- *Electricity price:* The electricity demand should decrease when the price increases.
- *Price of alternative fuels:* If the price of substitutes to electricity increases, the electricity consumption should increase.
- *Economic activity level indicator:* If the aggregated level of consumer spending increases, it is reasonable that also electricity consumption increases.
- *Holiday dummies:* Electricity consumption may be reduced in holidays, when factories are temporarily shut down and office buildings closed.

By including the electricity price as a factor influencing firm consumption, the firm consumption cannot be simulated independently from the price model. The price elasticity of firm consumption has historically been low in both the long and short term[5] (Doorman, 2009). To limit the calculation time required for the market equilibrium simulations, we therefore exclude the electricity price as an explanatory variable.

To establish a realistic model for price elastic consumption, the threshold levels must be derived from the operating margins of each plant group. The operating margins depend on output prices,

[5] However, the price elasticity has been slightly growing in the recent years due to the increased coupling between consumer and spot prices (Doorman, 2009).

and prices of outputs from power intensive industry in the Nordics (aluminum, pulp and paper etc.) must be introduced as additional stochastic factors. In order to keep the number of stochastic factors at a reasonable level, we will not model price elastic consumption explicitly. Instead, all consumption will be modeled as firm consumption.

2.2.2 Consumption models

We will compare two classes of models, both frequently applied to model electricity consumption: Error correction models and dynamic regression models, the latter introduced in 2.1.2.

Error correction model

The general error correction model with one explanatory variable can be written as (Brooks, 2008):

$$\Delta Y_t = \beta_{EC1}\Delta X_t + \beta_{EC2}(Y_{t-1} - \gamma X_{t-1}) + u_t \quad (16)$$

where γ is the cointegrating coefficient and β_{EC1} and β_{EC2} are parameters to be estimated.

The model can be extended with more explanatory variables; in our case all variables listed in 2.2.1 will be applied. (16) assumes Y is integrated of order one and that Y and X are cointegrated, hence the linear combination $Y_t - \gamma X_t$ must be stationary. The model states that Y changes from $t-1$ to t due to changes in X, but also due to eventual disequilibrium from the long-term relationship $Y_{t-1} - \gamma X_{t-1}$ (Brooks, 2008). Johnsen and Willumsen (2010) used an error correction model in their work. Albeit good fit with historical data (R^2 = *89%*), the model had two weaknesses:

- Residuals were autocorrelated.
- The consumption data used in the model was found to be stationary, hence an error correction model should not be the appropriate choice.

Dynamic regression model

To model consumption, the dynamic regression model (4) is generalized to take more than one input. Given the characteristics of electricity consumption, it is reasonable that the consumption immediately responds to changes in the explanatory variables. Therefore, we will not include any lags of the inputs in the transfer function.

2.3 Thermal generation

Nuclear power, industrial CHP, district CHP and condensing power are the different types of thermal generation in the Nord Pool area. CHP and nuclear generation are characterized by high capacity utilization. Condensing generation has higher flexibility, and the generation level is to a larger extent dependent on the spot price (Doorman, 2009). In the following, the characteristics of each technology are used to establish models for the generation level.

2.3.1 Nuclear power

When operating at the installed capacity, nuclear power is the thermal generation technology with lowest operating costs. Weight and von Hirschhausen (2008) estimated the average operating cost of nuclear units in Germany to be 9 EUR/MWh in 2006, where fuel costs accounted for 3 EUR/MWh. Those figures can be compared with an average marginal cost of coal generation at about 33 EUR/MWh for the same year. The time required to adjust the output level and start/stop costs are higher for nuclear than for other thermal technologies. For nuclear units in the Nordics, startup times range from 10 to 36 hours, dependent on the generator size (Nord Pool Spot, 2011a). Combining these aspects, the optimal generation plan for a nuclear unit is simply to run at the maximum level all the time (Patterson, 1983).

Planned and forced outages make the realized generation to deviate from the maximum level. Planned outages are caused by maintenance needs, and are typically allocated to periods when the electricity price is low (Gerger, 2011). Forced outages occur randomly as a consequence of technical failures (Doorman, 2009). An outage of a nuclear unit will force a shift of generation to units with higher marginal costs. The nuclear generation capacity in the Nordics consists of 14 reactors (at 5 plants) with an average capacity of 840 MW. Thus, a single outage may have impact on the system price.

Vehviläinen and Pyykkönen forecast nuclear generation by the historical mean for each week. In the EMPS model, deterministic maintenance periods can be specified for each plant. Forced outages are represented by the expected incremental cost method: The outage possibility for a plant or plant group is modeled by an increased expected marginal cost for units higher on the merit order (SINTEF Energiforskning, n. d.). While Vehviläinen and Pyykkönen take account of the expected failure rate only, the impact of a wider range of outages can be modeled when the expected incremental cost method is applied. However, certain aspects of the stochastic behavior of plant outages are not captured by the expected incremental cost method, including the correlation in outages from week to week and the distribution of outage sizes[6]. To incorporate such aspects of nuclear plant outages, we will model stochastic processes for forced outages. While improving the accuracy of the model, a stochastic modeling approach will also increase the computation time required in the price simulations.

A model for forced plant outages has three components: A process for the time to the next failure, a process for the repair time and a distribution of outage sizes. To reduce the complexity of the model, we introduce some assumptions. The time to failure for the different reactors is assumed to be independent, so that failure arrival processes can be estimated independently for each reactor. Alternatively, a single process covering all plants could be calibrated. By using

[6] The expected incremental cost method implements the different outage possibilities by introducing more steps on the merit order. To limit computation time, the availability of a single unit is either 0% or 100% of the capacity (SINTEF Energiforskning, n. d.). Empirical data shows that outage sizes are continuously distributed (Nord Pool Spot, 2011a).

individual failure arrival processes, the variation in failure frequencies caused by differences in for instance age and maintenance policies are covered. When a given reactor has an outage (less than the reactor capacity), we assume additional outages of that reactor do not occur until the reactor is repaired. The size of the outage is assumed to be constant. In reality, available capacity will gradually increase at the end of the outage, due to the long startup times. Furthermore, the repair time is assumed to have the same distribution for all reactors. For planned outages lasting longer than expected, the additional time is considered as a forced outage.

Two widely used distributions in reliability modeling are the exponential distribution and the Weibull distribution, given by the density functions (17) and (18). The exponential distribution models the time between events in a Poisson process, where the key property is a constant expected event frequency λ_E. Thus, the expected time to the next event from now is independent of when the previous event occurred. The Weibull distribution is a generalization of the exponential distribution, where the event rate may increase or decrease with time. A shape parameter k_W less than one indicates that the event rate decreases with time. (Ross, 2007)

$$f_E(Y;\lambda_E) = \begin{matrix} \lambda_E e^{-\lambda_E Y} & Y \geq 0 \\ 0 & Y < 0 \end{matrix} \tag{17}$$

$$f_W(Y;\lambda_W,k_W) = \begin{matrix} \frac{k_W}{\lambda_W}\left(\frac{Y}{\lambda_W}\right)^{k_W-1} e^{-(Y/\lambda_W)^{k_W}} & Y \geq 0 \\ 0 & Y < 0 \end{matrix} \tag{18}$$

Anderson and Davison (2005) argue that the exponential process is sufficient to describe the time to failure of a power plant. On the other hand, repair times are undoubtedly nonexponential, and a Weibull process is more appropriate. Following their approach, we model the individual failure processes by the exponential distribution, while repair times are assumed Weibull distributed. Nuclear outage sizes are continuously distributed with the reactor capacity as the upper limit, but a bulk of the failures cause the reactor to shut down entirely (Nord Pool Spot, 2011a). Fitting a distribution for outage sizes would therefore be difficult, and we will instead use bootstrapping of historical outage sizes for each plant.

A deterministic model for planned outages makes sense, since they generally occur at the same time each year. Therefore, we will model nuclear generation as the sum of:

- the historical weekly mean corrected for forced outages, and
- the process for forced outages.

2.3.2 CHP industry

At an industrial CHP plant, heat from the combined heat and power generation is utilized as process steam at a connected mill (Nordel, 2009). Industrial CHP is mostly used in relation to pulp mills in the Nord Pool area (Nord Pool Spot, 2011b). Electricity is only a byproduct of the

mills[7], and the generation level is typically directly coupled to the production of the mill's core product. Adjusting the production level to the electricity price is generally not profitable, and the electricity generation is therefore almost constant over time. (Lyngfelt, 2011)

Due to the relative constant generation level, generation in week t is forecasted as the historical average for that week:

$$G_{CHPI,t} = \bar{G}_{CHPI,t} \tag{19}$$

By using the historical average, the forecast takes account of temporary shutdowns during holidays and the average rate of forced outages. As the generation capacity at a typical industrial CHP plant is considerably lower than the capacity of an average nuclear plant (Nord Pool Spot, 2011b), an outage of an industrial CHP plant will have less impact on the system price. Consequently, we will not implement a stochastic process for outage risk of industrial CHP.

2.3.3 CHP district

The level of CHP district generation varies with the temperature, as CHP district plants have an obligation to serve a local heat demand (Manczyk and Leach, 2002; Rolfsman, 2004). Like industrial CHP plants, the electricity generation is directly tied to the level of heat production. For suppliers with ability to cover the heat demand by heating plants in addition to CHP district plants, electricity will be generated at least as long as the short-run marginal cost of electricity generation is covered by the spot price[8] (Pedersen, 2011):

$$SRMC_{CHPDel,t} = SRMC_{CHPDtot,t} - MI_{CHPDheat,t} \leq S_{NP,t} \tag{20}$$

where $SRMC_{CHPDel}$ is the short run marginal cost of electricity generation, $SRMC_{CHPDtot}$ is the total short run marginal cost of the plant and $MI_{CHPDheat}$ is the marginal income from heat generation.

Low electricity prices and excess capacity at heating plants, with corresponding switching from CHP district plants, are not likely in periods of low temperatures. Thus, it makes sense to model CHP district generation as a function of temperature only. Vehviläinen and Pyykkönen (2005) propose the following model:

$$G_{CHPD,t} = \beta_{CHPD1} + \beta_{CHPD2}[(T_t - T_{min})^+ - (T_t - T_{max})^+] \tag{21}$$

The generation is constant (β_{CHPD1}) for temperatures above T_{max}, a linear function of temperature in the interval $[T_{max}, T_{min}]$, and continues at the maximum generation capacity for

[7] In fact, several mills with CHP production in the Nord Pool area are net consumers of electricity (Lyngfelt, 2011).

[8] With costless instantaneous switching between the CHP plant and the heating plant, switching to the heating plant should take place when the spot prices decrease to the short run marginal cost of electricity generation. Else, the spot price threshold will be lower.

temperatures lower than T_{min}. The constants β_{CHPD1} and β_{CHPD2} are estimated from historical data.

We apply HDD instead of temperature, and the generation is assumed to be constant when the temperature exceeds the critical temperature. Thus, the model transforms to:

$$G_{CHPD,t} = \beta_{CHPD1} + \beta_{CHPD2}\left[HDD_t - \left(HDD_t - HDD_{max,t}\right)^+\right] \quad (22)$$

Without including the maximum generation capacity, the model simplifies to a linear equation:

$$G_{CHPD,t} = \beta_{CHPD1} + \beta_{CHPD2} HDD_t \quad (23)$$

Whether the generation level is best modeled by (22) or (23) will be determined in 4.3.3.

2.3.4 Condensing power

Condensing plants are more flexible than CHP plants, as condensing plants are used for electricity generation only. Therefore, condensing plants are assumed to bid generation at their short run marginal costs. Vehviläinen and Pyykkönen (2005) approximate the ask price curve by a linear function of the generation level. The merit order is in reality not linear, and ask prices vary over time with fuel costs. To develop a more realistic model for condensing generation, we follow the EMPS approach, where the marginal cost function is modeled for different plant groups (Doorman, 2009). We separate condensing generation into five groups according to fuel type and plant characteristics: Coal extraction plants[9], coal condensing plants, gas extraction plants, combined cycle gas turbines and peak load units.

For coal fueled units, different efficiencies will be applied for each country, as the age of the plant portfolio varies across the borders (Thema Consulting Group, 2011). In reality, the peak load category consists of both gas turbines and oil condensing plants. To avoid introducing the oil price as an additional stochastic factor, all peak load units are assumed to be gas turbines. Similar to the CHP models, a stochastic process for capacity unavailability is not modeled. Instead, capacities are adjusted by an average plant availability factor based on historical data. Assuming a constant aggregated availability is reasonable given the number of condensing generation units, although the expected incremental cost method may be a more accurate alternative.

The short run marginal cost $SRMC_{CONDu,t}$ of a condensing unit u in period t is calculated as the sum of fuel costs, variable operation costs and costs of emissions (Weigt and von Hirschhausen, 2008). As a simplification, start-up and shutdown costs are neglected[10]. Fuel costs are found by dividing the fuel price ($S_{fuel,t}$) by the net plant efficiency η_{CONDu}. Costs of emissions are the

[9] An extraction plant is a condensing plant with some extraction of steam from the turbine (Pierre, 2002).

[10] Unit commitment of condensing plants is not modeled, hence start-up and shutdown costs cannot be included.

product of the CO_2 quota price ($S_{CO2,t}$) and the CO_2 content in fuel ($m_{CO2,u}$) divided by the plant efficiency. Adding variable operation costs ($C_{CONDvar,u}$), the short run marginal cost is given by:

$$SRMC_{CONDu,t} = \frac{1}{\eta_{CONDu}} S_{fuel,t} + C_{CONDvar,u} + \frac{m_{CO2,u}}{\eta_{CONDu}} S_{CO2,t} \quad (24)$$

Empirical evidence shows that costs for staying idle and capital costs are included in the bids of peak load units (Schemde, 2011). This practice contradicts with the perfect competition theory of ask price equal to short run marginal cost. In modeling of marginal costs, this aspect will be incorporated by increasing the variable operation costs of peak load units.

2.4 Hydro generation and the marginal water value

Hydro power producers continuously face the problem of maximization of the value of their reservoirs. If an amount of water is released now, the value is given by the spot price. However, the value may be higher if the water is stored until prices are higher and the availability of water more constrained. The expected marginal water value[11] is the expected opportunity cost of producing a marginal unit today instead of storing that water to a later period (Tipping, 2007; Wangensteen, 2007). Neglecting other variable costs, the marginal cost and consequently the asking price to a hydro producer equals the water value of the reservoirs to that producer.

Hydro producers typically use stochastic dynamic programming to estimate the water value of their reservoirs. As mentioned, the EMPS model is an example of a widely used implementation of the SDP approach. The strength of SDP is the ability to model intertemporal consequences of the decision of release versus storage (Doorman, 2009). We will use a less computationally intensive approach, and instead establish an empirical approximation of the aggregated water value curve in the Nord Pool area. In the following, we describe the factors influencing the water value and how they can be included in an empirical model.

Hydro and snow reservoirs

Tipping (2007) points out that the median historic storage trajectory of a hydro reservoir is a reasonable approximation of the optimal reservoir management strategy. The optimal strategy is to keep the water value constant over time, as long as this is possible given reservoir constraints: If the marginal hydro unit has a higher expected value in the next period than in the present, it is optimal to allocate that unit to the next period. Water will then be a more constrained resource in the present period and less scarce in the next, and the difference in water values between the two periods will be smoothed out. Combining these aspects, the water value can be approximated as constant along the median trajectory.

Due to the stochastic nature of e.g. inflow and demand, it is not possible to keep the reservoir equal to the median trajectory in every period. If the reservoir level in a given week is lower than

[11] *Expected marginal water value* is from now denoted *water value.*

the historic median for that week, there is an increased risk of running out of water in the next weeks. The value of storing water will therefore increase. On the other hand, if the reservoir level is higher than the median, the risk for future spills will increase; hence the water value will decrease. Water values calculated by SDP based reservoir management models (Figure 2) illustrate this relationship: The water value increases exponentially when the reservoir level decreases, and decreases exponentially when the reservoir level is increasing (Tipping 2007, Batstone 2003).

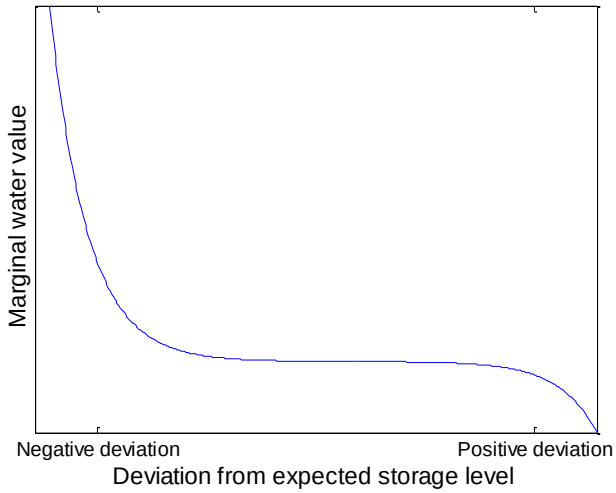

Figure 2. *Conceptual illustration of the relationship between the water value and the hydro storage level, from Batstone (2003)*

The impact of a deviation from the median trajectory is seasonally dependent. If the reservoir level in the winter season is lower than the average, this should increase the water value more than the same deviation in the summer season. In the winter, inflow is low and demand is high. Thus, the risk of running out of water is much higher than in the summer, when the inflow is high relative to the demand. This intuitive relationship is confirmed by an empirical study by Johnsen (2001).

With background in the above aspects and empirical evidence from the market in New Zealand, Tipping (2007) proposes the following function to approximate the water value:

$$MWV_t = \beta_{NZ1,j} + \beta_{NZ2,j} e^{\beta_{NZ3,j}(\beta_{NZ4,j}+0.01RSL_{t-1})^{\beta_{NZ5,j}}} \quad (25)$$

RSL_t is the relative storage level in period t, which is defined by Tipping as the difference between the actual storage level and the 45-day moving average of the tenth percentile trajectory. $\beta_{NZ1,j}$, $\beta_{NZ2,j}$, $\beta_{NZ3,j}$ (≤ 0), $\beta_{NZ4,j}$ and $\beta_{NZ5,j}$ are constants to be estimated for each season j.

In the Nord Pool area, snow reservoirs in the mountains account for a high degree of the total hydro storage. The relationship between snow reservoirs and the water value depends on season and generation flexibility. In the winter season (i.e. the snow accumulation period), snow

reservoir levels provide an indication on the inflow levels during the next hydrological cycle[12]. For hydro producers with ability to store water from a hydrological cycle to the next, a decrease in the relative snow reservoir level leads to an increase in the water value, as the expected scarcity of water in the next cycle increases. Producers with less reservoir capacity will not have the flexibility to allocate water between hydrological cycles, and remaining water at the end of each cycle has no value. Thus, the snow reservoir level will not influence their water values during the winter. In the summer season (i.e. the snow melting period), snow reservoir levels provide information about the scarcity of water in the current hydrological cycle, and snow reservoir levels will also affect the water values to these producers with less flexibility (Johnsen, 2011).

A water value approximation suggested by Vehviläinen and Pyykkönen (2005) include the impact of snow reservoirs, although the inclusion of snow reservoirs through the linear factor $R_{TOT,t} - C_{TOT,t}$ lacks a clear motivation:

$$MWV_t = \beta_{WVslope}\left(R_{TOT,t} - C_{TOT,t}\right)\left(1 + e^{-\beta_{ResPenalty}\left(R_{W\%,t} - \beta_{ResMin\%}\right)}\right) + \beta_{WVLevel} \qquad (26)$$

where

- $R_{TOT,t}$ is the total (snow and hydro) reservoir in period *t*.
- $C_{TOT,t}$ is the historical average total reservoir in period *t*.
- $R_{W\%,t}$ is the filling degree of the hydro reservoir in period *t*, calculated as $R_{W,t}/R_{WCAP}$.
- $\beta_{WVslope}, \beta_{ResPenalty}, \beta_{ResMin\%}$ and $\beta_{WVLevel}$ are constants to be estimated.

(26) states that the water value is proportional to the deviation from the historical average total reservoir, but increases exponentially if the hydro reservoir decreases to an estimated limit, $\beta_{ResMin\%}$. Thus, the water value is assumed to depend on the deviation from a constant storage level and not the relative storage level. We will follow the reasoning of Tipping and instead model the water value as a function of the relative storage level.

Generation level and plant characteristics

Figure 3 illustrates the conceptual relationship between generation level and water value, according to ECON (2004) and Sandsmark and Tennbakk (2010). The curve may be representative for both the supply curve to an individual producer and the merit order of all hydro plants in the market.

[12] In this thesis, the hydrological cycle is defined as the yearly period which commences when snow melting in the mountains starts.

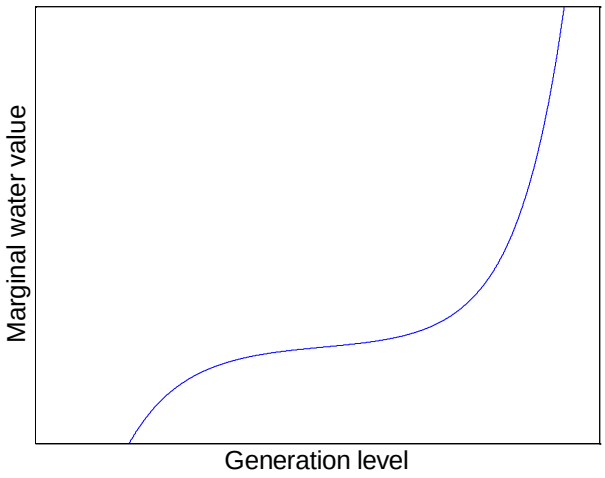

Figure 3. *Conceptual illustration of the relationship between the water value and hydro generation level, from Sandsmark and Tennbakk (2010)*

First, we discuss the shape in context of a single plant. If inflow and reservoir level are high, some generation may be supplied at a price close to zero due to the spillage risk. When the generation level increases, the marginal hydro unit not released in the present period may with an increasing probability be stored and produced in a later period, instead of spilled. Higher generation level today means less water available for future generation, and the opportunity cost of producing the marginal unit today will increase.

Considering the aggregated supply curve, the shape of the curve can also be used to explain differences between producers. As an example, consider a market consisting of the five hydro producers A, B, C, D and E. A is a run-of-the-river plant without storage capacity, and has to produce all inflow immediately. Thus, the water value for plant A is zero. B and C have identical relative storage levels today, but B has higher storage capacity than C. B is able to store the marginal unit of water longer than C, hence B can wait longer for higher prices. Consequently, the water value for B is higher than for C. D has the same relative storage level and storage capacity as B, but a bigger turbine capacity. D has better ability than B to produce in the hours with highest prices, which results in a higher water value than B. E is identical to plant B, except a lower present relative storage level and consequently a higher water value.

In this thesis, estimation of the aggregated supply curve[13] is of interest. The simplest approach is to aggregate hydro reservoirs and turbine capacities for all plants in the market into one equivalent plant, thus assuming all producers share the same water value. As the above discussion illustrates, the result will be an exaggeration of the flexibility of generation. Modeling the water value curve as a function of the total hydro generation level is a crude way to take account of plant specific capacities and reservoir levels. Given the scope of this thesis, increasing the accuracy by modeling individual plants or plant groups is not considered feasible.

[13] The aggregated supply curve (or merit order) of all hydro plants in the market is in this thesis also denoted *market water value curve*, or simply *water value curve*.

Vehviläinen and Pyykkönen model generation with water value of zero and close to zero through a division between regulated and unregulated generation[14]. Unregulated generation is equal to unregulated inflow, which is assumed to be of the form:

$$I_{U\%,t} = \beta_{U\%1} + e^{\beta_{U\%2}(1-R_{W\%,t})} \quad (27)$$

$$G_{hydroU,t} = I_{U\%,t} I_t \quad (28)$$

$I_{U\%,t}$ denotes unregulated inflow as percentage of total inflow, whereas $\beta_{U\%1}$ and $\beta_{U\%2}$ are constants to be estimated.

A constant share of the inflow, $\beta_{U\%1}$, pass through run-of-river hydro plants without storage capacity. Of the (1-$\beta_{U\%1}$)% of the inflow which arrives to plants with storage capacity, $e^{\beta_{U\%2}(1-R_{W\%,t})}$% are sent directly through the turbines in order to avoid future spillage.

We will use Vehviläinen and Pyykkönen's approach to model unregulated generation. Therefore, the water value of regulated generation will be modeled as a function of regulated generation and not the total generation level.

Expected future inflow and spot prices

The expected value of storing water to later periods depends on the expected distribution of future inflow levels and spot prices (Tipping, 2007). As pointed out, snow reservoir levels yields information about expected inflow during the snow melting season. Precipitation levels are more difficult to forecast. Most players in the Nord Pool area use raw data from the European Centre for Medium-Range Weather Forecasts (ECMWF) in their inflow models, which provide 10-day-ahead forecasts (ECMWF, 2009). We will therefore assume producers have access to accurate forecasts of the inflow level for the next week, such that the expected inflow is (approximately) equal to the realization. By modeling the water value as a function of the hydro and snow reservoirs in the end of the week rather than the observed levels at the start of the week, the influence of inflow expectations are included[15].

Futures prices reflect expectations regarding future spot prices. When modeling the water value for an individual plant, the time to maturity for the chosen futures contract should be tied to the producer's ability to store water (Sandsmark and Tennbakk, 2010). Thus, it is difficult to choose the relevant time to maturity when we model the water value curve for the whole market. Futures prices are therefore not included in our water value model.

[14] The terms *regulated* and *unregulated* will in this thesis be used to characterize hydro generation, not to describe the market structure.

[15] The weekly generation level is implicitly known from the end-of-week hydro reservoir level. Thus, it makes no sense to model the water value to an individual producer as a function of both the generation level and the end-of-week reservoir level. However, the approach to model water value as a function of generation level explained above will still be used to describe differences in water values between producers.

Marginal costs of thermal generation

Marginal costs of technologies competing with hydro power influence the water value, since a decrease in hydropower generation have to be compensated by an increase in output from other technologies[16]. A change in output of hydropower is assumed to mainly affect the generation level of coal plants, as coal generation typically is the technology closest to hydropower on the merit order (ECON, 2004).

The water value equation

Combining the above discussed aspects, we propose the following empirical approximation of the water value curve:

$$MWV_t = \left(\beta_{MWV1,j} + \beta_{MWV2,j} SRMC_{coal,t}\right)\left(1 + e^{-\beta_{MWV3,j}\left(R_{W\%,t} - C_{W\%,t}\right)}\right) \left(1 + e^{-\beta_{MWV4,j}\left(R_{S\%,t} - C_{S\%,t}\right)}\right) e^{\beta_{MWV5,j} G_{hydroR\%,t}} \quad (29)$$

where

- $R_{W\%,t} - C_{W\%,t}$ is the relative storage level of the hydro reservoirs in the end of week t. $C_{W\%,t}$ may either be the mean reservoir level, the median, the tenth percentile or a moving average of one of these; the representation will be selected based upon fit with historical data.
- $R_{S\%,t} - C_{S\%,t}$ is the relative storage level of the snow reservoirs in the end of week t.
- $G_{hydroR\%,t}$ is the level of regulated hydro power production in week t relative to the installed turbine capacity. For a particular value of $G_{hydroR\%,t}$, the equation should return the water value to the marginal hydro unit producing.
- $\beta_{MWV1,j} \ldots \beta_{MWV5,j}$ are parameters to be estimated.
- $j \in \{1,2\}$ is the season index. Season 1 is the snow melting period (summer season), characterized by high inflow and increasing hydro reservoirs. Season 2 is the snow accumulation period (winter season), when inflow is low relative to demand and the hydro reservoirs are declining.

Seasonality is partly accounted for by the factor approximating plant characteristics, since the regulated generation level is highest in the winter season. Seasonally dependent parameters are included in order to test whether further seasonal adjustment is needed. The decrease in water value for high relative storage levels and low generation levels is not modeled in (29), but accounted for through the division of unregulated and regulated inflow.

[16] Since the price elasticity of consumption is assumed to be zero.

Statistical benchmark: Artificial neural network

Despite (29) is formulated according to fundamental considerations, selection of the exact functional form is based on judgment only. To get an idea of how well the formulation performs, we compare (29) with a statistical model using the same input variables. Due to the nonlinear relationship between the water value and the explanatory variables, an artificial neural network will be used as benchmark.

An artificial neural network consists of neurons organized in parallel layers: An input layer, one or more hidden layers and an output layer. As illustrated in Figure 4, each neuron in the hidden and output layers takes a set of inputs (including a constant bias), forms a weighted sum and transforms the sum through a transfer function. The use of nonlinear transfer functions makes the network able to map the nonlinear relationship between the water value and the input variables. The appropriate mapping is found by training the network. During training, the input weights for each neuron are adjusted using a backpropagation algorithm. The final weights depend on the initial weights assigned to the inputs. (Bishop, 1995; Hassoun, 1995)

As (29) contains no lags of the water value or the inputs, we will use a feedforward network without input delays. Only one hidden layer will be applied. More hidden layers increase the amount of data needed to calibrate the network, and studies using neural networks to model electricity prices have found that one hidden layer is appropriate (see e.g. Catalão et al. (2007) and Pao (2007)). To find a well-performing network, several networks with different combinations of initial input weights and number of hidden neurons must be tested.

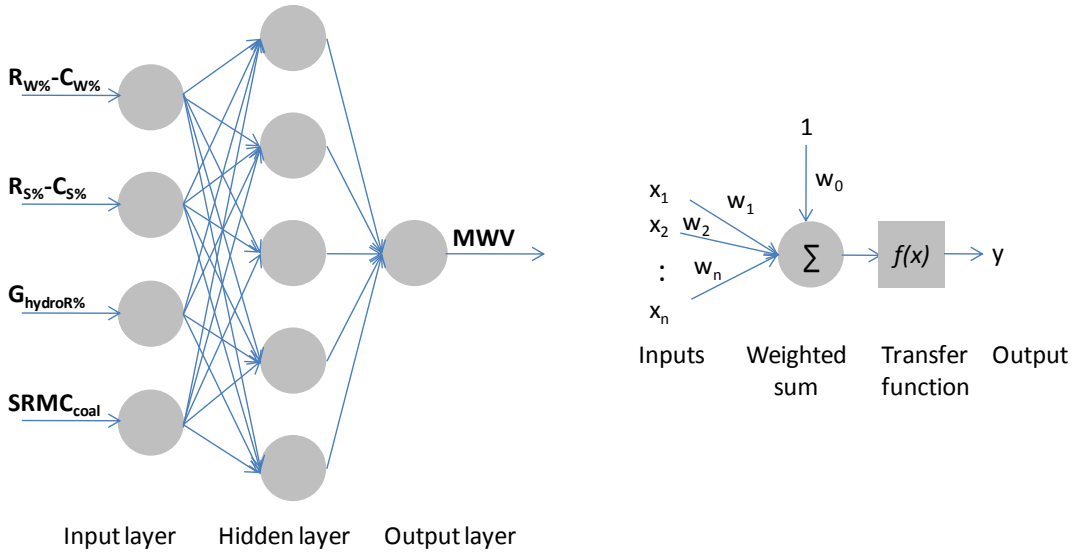

Figure 4. *Artificial neural network structure*

Reservoir balance

To keep track of the hydro reservoir, the following reservoir balance is used:

$$R_{W,t} = R_{W,t-1} + I_t - G_{hydroR,t} - G_{hydroU,t} - Spill_t, \qquad R_{W,t} \leq R_{WCAP} \tag{30}$$

The change in reservoir level from period $t-1$ to period t is calculated as inflow less hydro generation (regulated and unregulated) and spills in the period. Spills arise when reservoirs are full or when hydro producers release water without producing in order to prevent full reservoirs.

2.5 Exchange

The Nord Pool system price is influenced by electricity exchange with the Netherlands, Germany, Poland, Estonia and Russia. In this section, we consider possible approaches to model exchange. Characteristics of the price in the markets connected to Nord Pool, presented in 3.4, will later be used to select suitable exchange models for each market.

Electricity exchange between two markets is influenced by the price difference and restricted by transmission capacities. As an illustration, consider two connected markets M_1 and M_2 during a short time period when the prices are constant in both markets. A domestic market equilibrium with higher price in M_1 (S_{M1}) than in M_2 (S_{M2}) will lead to exchange from M_2 to M_1. Parts of the demand in M_1 are then covered by M_2, and the need for domestic supply in M_1 is reduced. Hence, the demand curve shifts to the left on the merit order in M_1, whereas it shifts to the right in M_2. This implies lower price in M_1 and higher price in M_2, compared to a situation without exchange. The exchange volume is either the volume which equalizes the prices or equal to the transmission capacity (Wangensteen, 2007).

In case of S_{M1} constantly higher or lower than S_{M2}, the exchange will be equal to the available capacity in every period. Historic exchange volumes, reflecting the average available capacity, can then be used to forecast future exchange.

With S_{M1} and S_{M2} in the same range, the domestic market equilibrium and the shift in demand curves caused by exchange must be computed for each period. As spot prices are cleared with hourly steps, the period length should ideally be one hour. To reduce computing time, we will aggregate hours in the week for which prices are approximately equal. The selection of these periods is elaborated in Chapter 2.6. When using this approach, we assume that exchange between Nord Pool and the connected market influence the price in Nord Pool only. Exchange can then be modeled without considering the merit order of the connected market. Due to the size of the continental markets connected to Nord Pool, this approximation is reasonable.

Compared to the above multi-period approach, a more straightforward way to estimate weekly exchange levels is to specify a simple linear model:

$$NI_t = K_{cap,t}\left[\beta_{NI1} + \beta_{NI2}\left(S_{NP,t} - S_{F,t}\right)\right], \qquad NI_{min} \leq NI_t \leq NI_{max} \tag{31}$$

Net import[17] to Nord Pool is thus modeled as a function of the difference between the weekly averages of the Nord Pool system price and the foreign price (S_F). K_{cap} incorporates changes in installed capacity, while NI_{min} and NI_{max} restrict the feasible range. The equation is calibrated using historical exchange volumes. While simple, this single-period approach is likely to have significant drawbacks: With high price variations during the week, the difference in average prices may have limited ability to explain exchange volumes. In both the multi-period and single-period approach, we neglect the impact of transmission fees on exchange volumes.

To forecast available exchange capacity, a stochastic process for cable outages similar to the nuclear outage model would be the most accurate approach. To keep the number of stochastic factors at a computationally acceptable level, available capacity will instead be forecasted by the historical average availability of cables in operation at the end of the estimation period.

As several of the markets connected to Nord Pool are highly interconnected, aggregation of markets by using a common reference price can reduce the complexity of the exchange model without significant loss of accuracy.

2.6 Load periods

The intraweek variation in consumption makes different generation units to be marginal, and hence the price to vary in a similar pattern. Consequently, the merit order should be evaluated for different subperiods of the week. In the EMPS model, weekly consumption estimates are typically divided into four to eight load periods using relative factors (Doorman, 2009; Matilainen et al., 2009). In addition to consumption, we apply this approach to capture the intraweek variation in the EEX price. The intraweek EEX estimates will then be used to forecast exchange when using the multi-period approach. For computationally simplicity, the same subperiods will be applied to consumption and the EEX price.

We will select load periods such that the historical average consumption and EEX profiles can be replicated in an acceptable way. The relative factors for each period are then calculated as the levels which minimize the squared deviation between the factor and historical values. Restrictions are applied to ensure consistency with the aggregated weekly forecasts.

For consumption, minimization of the squared deviation yields:

$$min \sum_{k \in K} \sum_{j \in W} \sum_{i \in H} \left(f_{ijk} - \hat{f}_k\right)^2 \tag{32}$$

K is the set of all subperiods within the week, W is the set of the historical weeks used in calibration of the relative factors and H is the set of all hours in the week. The relative consumption f_{ijk} is the actual consumption in hour i, week j and period k divided by the average

[17] Total import less total export.

consumption in week j. $\hat{f}_k$ is the estimator for the relative consumption in period k. The sum of consumption estimates in all subperiods during the week must equal the total weekly (forecasted) consumption, which is equivalent to:

$$\sum_{k \in K} \hat{f}_k M_k = M \tag{33}$$

M is the number of hours per week, while M_k is the length of period k. The Lagrange formulation of (32) - (33) and the corresponding optimality conditions are attached in Appendix A.1.

The similar procedure applied to the EEX price gives the following optimization problem:

$$min \sum_{k \in K} \sum_{j \in W} \sum_{i \in H} \left(s_{EEX,ijk} - \hat{s}_{EEX,k}\right)^2 \tag{34}$$

$$\sum_{k \in K} \hat{s}_{EEX,k} M_k = M \tag{35}$$

The relative EEX price $s_{EEX,ijk}$ is defined as the actual price in hour i, week j and period k divided by the average price in week j. $\hat{s}_{EEX,k}$ is the estimator for the relative price in period k. The constraint (35) ensures that the weighted average of intraweek prices equals the forecasted weekly average price.

2.7 Market equilibrium

When simulating the system price, the models for generation, consumption and exchange are combined to find the market equilibrium. The generation levels of nuclear, CHP industry, CHP district, unregulated hydro and wind power are assumed to be independent of the price, as previously described. Together with exchange with markets characterized by prices constantly above or below the Nord Pool price, these technologies are stacked to the left of the merit order. The marginal water value curve is then combined with condensing generation to form an aggregated supply curve of the price dependent technologies.

A preliminary price is found by calculation of the intersection with the consumption curve. This market equilibrium is adjusted to account for exchange with markets whose prices are in the same range as the Nord Pool price, such as the German market. As explained in 2.5, the exchange forces a shift of the demand curve. In the particular example illustrated by Figure 5, the foreign price (the EEX price) is higher than the preliminary Nord Pool price, and the demand curve is shifted to the right. As equalization of prices is impossible given the exchange capacity, the exchange volume becomes equal to the capacity.

If demand exceeds the maximum level of supply, load shedding occurs. The value of lost load will not be modeled, but is instead set to 1000 EUR/MWh, well above the marginal costs for hydro and condensing power.

The above procedure is repeated for each subperiod of the week, during all weeks, for all price scenarios. As the water value curve is assumed to depend on the end-of-week hydro reservoir, all intraweek equilibriums are solved simultaneously. The weekly system price is calculated as the weighted average of the intraweek prices.

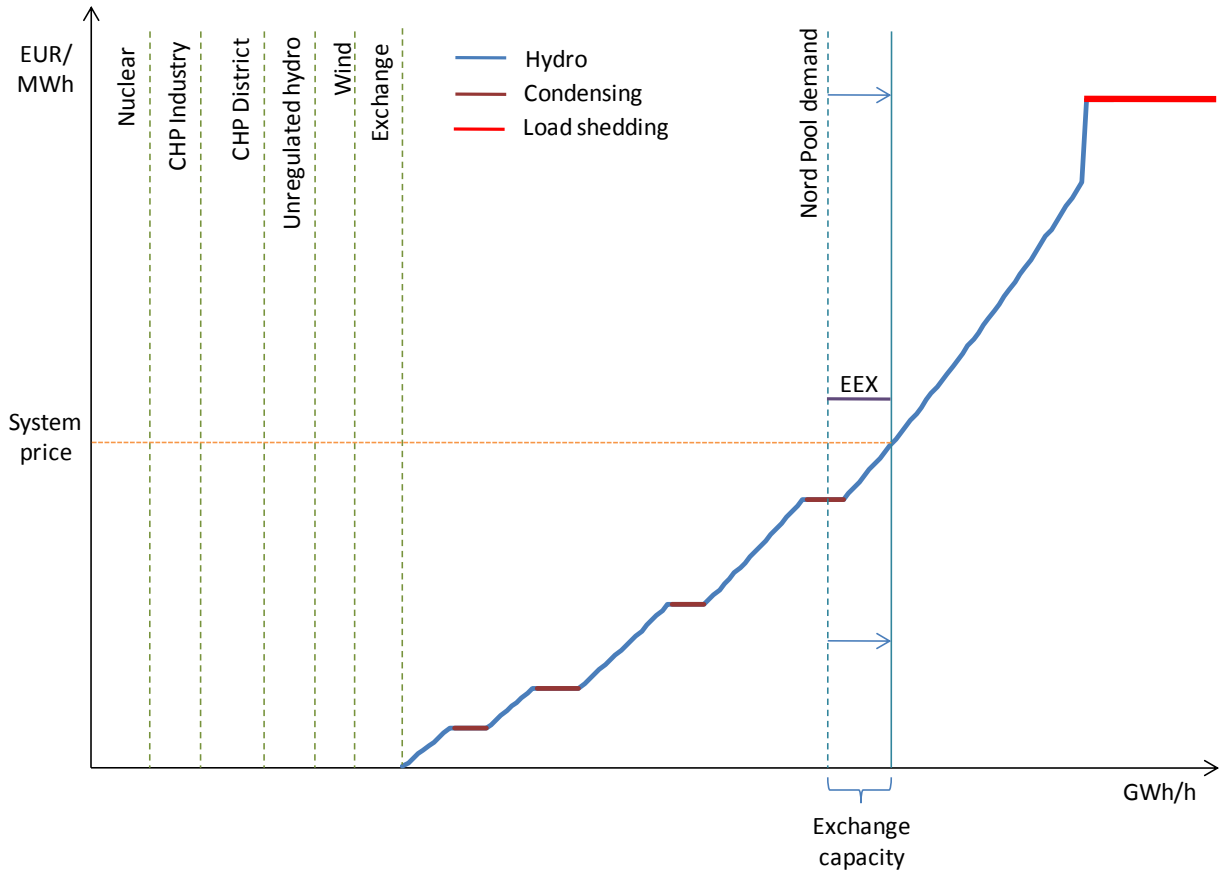

Figure 5. *Conceptual merit order example*

3. Data

Data are collected from Denmark, Finland, Norway and Sweden, and then aggregated to representative levels for the whole Nord Pool area. Time series are converted to weekly basis and divided into an estimation period and a forecast period. In order to enable out-of-sample forecasts for two years, the forecast period commences week 27, 2008.

3.1 Consumption modeling

Information on time series which may be applied in consumption modeling is summarized in Table 1, including period, granularity and source.

Table 1. *Consumption data*

Description	Period	Granularity	Source
Consumption	2000-2010	Hourly	Nord Pool Spot
Temperature, Norway	1993-2010	Daily	Norwegian Meteorological Institute
Temperature, Finland	1993-2010	Daily	Finnish Climate Centre
Temperature, Sweden	1993-2010	Daily	Swedish Meteorological and Hydrological Intitute (SMHI)
Temperature, Denmark	1993-2010	Daily	SMHI
Day length	-	Daily	Norwegian Water Resources and Energy Directorate (NVE)
Heating oil prices	2000-2010	Monthly	Statistics Norway
Retail trade index, Norway	2000-2010	Monthly	Statistics Norway
Retail trade index, Sweden	2000-2010	Monthly	Statistics Sweden
Retail trade index, Finland	2000-2010	Monthly	Statistics Finland
Retail trade index, Denmark	2000-2010	Monthly	Statistics Denmark

Daily mean temperatures over 17 years are collected for locations which are assumed to be representative for the respective countries. The most populated locations are chosen, since the temperatures are to be applied in consumption modeling. Coast climate are characteristically for all these sites, which may be disadvantageous due to more varying inland temperatures.

The temperature in Stockholm is collected from Sweden, whereas the temperature in Harmaja, near Helsinki, is used for Finland. In lack of available Danish data, the temperature in Malmö is assumed to reflect the temperature in Copenhagen. For Norway, temperatures in Oslo, Bergen, Værnes and Tromsø are weighted according to population in the region in which they are located.

Since HDD is applied instead of temperature, modeled consumption will only be affected by temperatures below the critical temperature. The critical temperature is selected as 16 degrees Celsius, consistent with Johnsen and Willumsen (2010). Daily HDD values for each country are summed up to weekly figures and the four series are weighted according to consumption in the respective countries. This leads to weekly accumulated weighted HDD, illustrated in Figure 6.

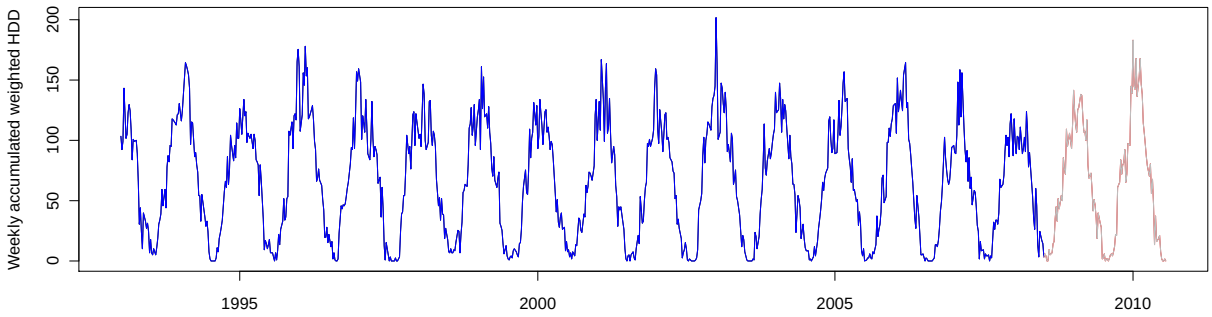

Figure 6. *HDD time series*

Data for day length (time from sunrise to sunset) is collected for each day of the year. Retail trade indexes are weighted due to consumption in each country, and a 12 month moving average will be used as an indicator of the trend in consumer expenditures. Heating oil can act as a substitute for electricity, and the development in heating oil prices is illustrated in Figure 7. The rapid growth in the end of the estimation period complicates modeling of the further progression. Representative wind speed data for the whole area is hard to obtain, and will not be implemented in the model.

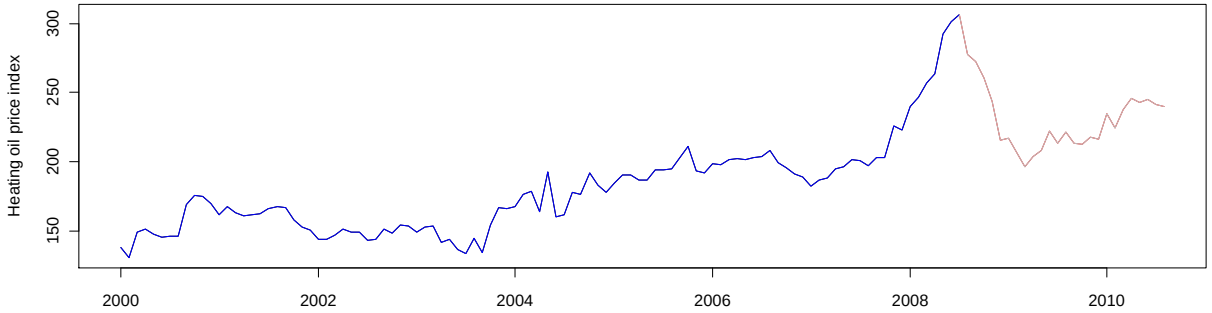

Figure 7. *Heating oil price index time series*

A consumption model based on an appropriate selection of these data will be compared with the real consumption series in Figure 8. Consumption and HDD have similar seasonality, suggesting that HDD is the most important explanatory variable. Consumption figures include TSO consumption, i.e. system losses.

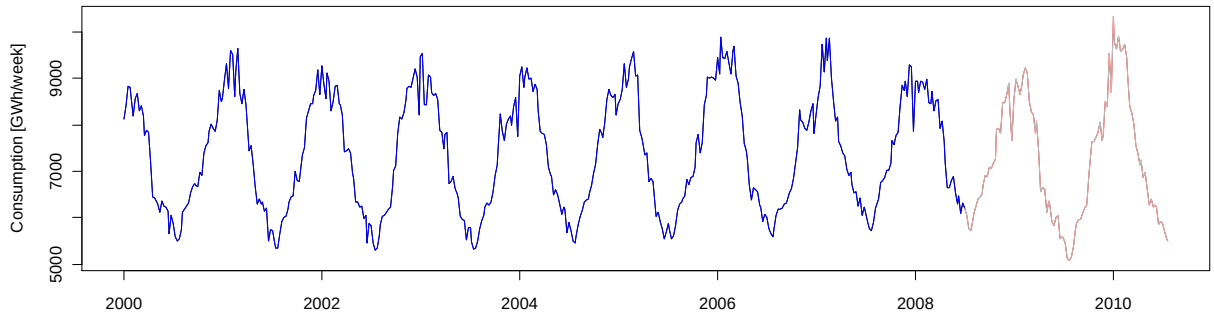

Figure 8. *Consumption time series*

3.2 Hydrology

A brief summary of collected hydrological data (inflow, snow reservoirs and hydro reservoirs) is presented in Table 2.

Table 2. *Hydrological data*

Description	Period	Granularity	Source
Inflow	1995-2010	Weekly	Nord Pool Spot
Snow reservoirs, Norway	1993-2010	Daily	NVE
Median culmination, Norway	1971-2000	-	NVE
Median culmination, Sweden	1981-2005	-	SMHI
Hydro reservoirs, Norway	1993-2010	Weekly	NVE
Hydro reservoirs, Sweden	1993-2010	Weekly	Svensk Energi
Hydro reservoirs, Finland	1993-2010	Weekly	Finnish Environment inst.

Total weekly inflow to the hydro reservoirs in Norway, Sweden and Finland is plotted in Figure 9. Due to snow melting, inflow levels are highest from April and throughout the spring and summer. The inflow may still be high in the autumn, depending on precipitation levels. From the end of November, precipitation falls mainly as snow in the mountain areas and inflow levels remain low until snow melting starts.

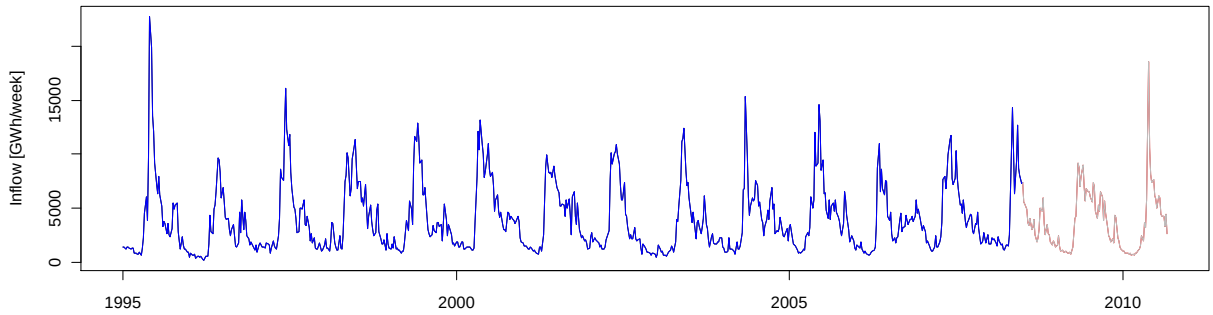

Figure 9. *Inflow time series*

Figure 10 illustrates historical energy content of the Norwegian snow reservoirs which drain to hydro reservoirs. End-of-week energy content is graphed as a percentage of median culmination. The median culmination is the maximum value of the annual profile of median snow reservoirs, based on data from 1971 to 2000. Snow reservoirs are generally overestimated throughout the year, and NVE therefore set the energy content to zero each autumn to avoid escalating levels in the data (Holmquist, 2010). For that reason, a rapid decrease in reported reservoir levels appears at this time some years. In order to convert the energy content into TWh, the values are multiplied by the median culmination. The median culmination in Norway is no easy factor to decide due to lack of measurements, and consequently a major source of error. It is probably between 40 and 70 TWh (Holmquist, 2010), and 60 TWh will be applied in our model, similar to Johnsen and Willumsen (2010).

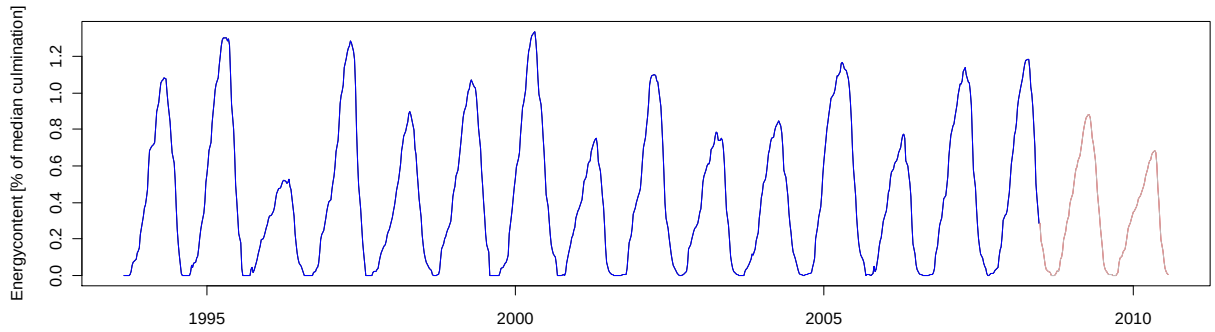

Figure 10. *Snow reservoir time series*

Calculations by SMHI indicate a median culmination of approximately 24 TWh in Sweden (Johansson, 2010). Historical time series for the energy content of snow reservoirs in Sweden was not available, and the Norwegian time series is thus assumed to be representative for Sweden. There is also lack of time series for snow reservoirs in Finland. Due to different topography and lower levels of hydropower generation, neglecting the Finnish snow reservoirs should not be a significant source of error. Hence, the total snow reservoir is calculated by multiplying the relative energy content of Norwegian reservoirs by 84 TWh.

The end-of-week aggregated hydro reservoir level for the three hydropower nations is presented in Figure 11. Logically, the seasonality is opposite to that of the snow reservoirs. Data for hydro spillage and the division between regulated and unregulated inflow are not found.

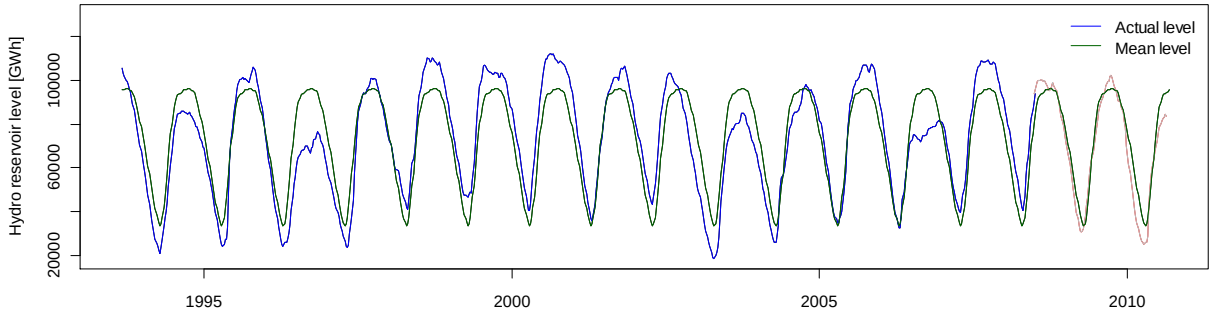

Figure 11. *Historical hydro reservoir levels*

3.3 Generation modeling

Historical fuel prices and generation levels as well as plant characteristics will be applied in generation modeling. Table 3 gives an overview of the collected data.

Table 3. *Generation data*

Description	Period	Granularity	Source
Electricity generation per technology, Finland	2000-2010	Weekly	Finnish Energy Industry
Electricity generation per technology, Sweden	2000-2010	Weekly	Svensk Energi
Electricity generation per technology, Denmark	2000-2010	Hourly	Energinet.dk
Electricity generation, Norway	2000-2010	Weekly	Nord Pool Spot
Nuclear outages	2000-2010	-	Nord Pool Spot UMM Service
Generation at the Barsebäck plant	2000-2005	Weekly	Vattenfall
Coal spot prices	2000-2010	Weekly	McCloskey
Gas spot prices	2000-2010	Daily	Reuter Ecowin, Nord Pool Gas
CO_2 futures prices	2005-2010	Daily	NASDAQ OMX Commodities Europe
Capacities, efficiencies, operating costs and emissions for condensing plant categories	-	-	Thema Consulting Group, SKM Market Predictor

Historical electricity generation from the different technologies is illustrated in Figure 12. Hydro, CHP district and nuclear generation vary in a seasonal pattern, peaking during the winter. Condensing generation is less seasonally dependent, CHP industry generation is almost constant, whereas wind generation is random.

Norwegian generation is dominated by hydro power, with a share of 98.6% in 2008 (Nordel, 2009). As an approximation, the entire Norwegian generation is assumed to stem from this category. Time series for hydro, nuclear, condensing, CHP district, CHP industry and wind generation are collected for Sweden and Finland. Generation data from Denmark is separated into central generation, decentral generation and wind generation (Energinet.dk, 2010). According to Rasch (2010), decentral generation mainly stems from municipal CHP units. Danish CHP industry generation is small, there is no nuclear power and hydro power is negligible (Nordel, 2009). Therefore, condensing generation is set equal to the central generation.

The nuclear generation curve has an uneven shape because of plant outages. Information concerning frequency, size and duration of forced outages are collected from Nord Pool Spot's Urgent Market Message (UMM) archive. Only outages lasting at least one day are considered. Additionally, separate generation data from the Barsebäck nuclear plant is gathered. Barsebäck closed in 2005, and the historical mean generation level applied in our model is adjusted for the capacity reduction associated with this shutdown.

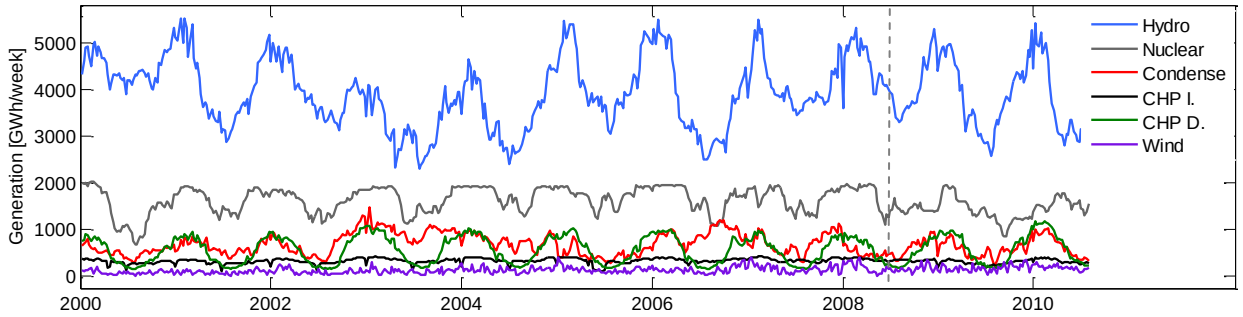

Figure 12. *Generation per technology*

Coal, gas and CO_2 quota prices are required in modeling of marginal costs for condensing units. Time series for steam coal prices in USD/ton delivered CIF (including cost, insurance and freight) within the ARA (Antwerpen/Rotterdam/Amsterdam) zone are collected[18]. Differences in freight rates to the ARA zone compared to plants in the Nord Pool area will be neglected. Natural gas prices on the EEX market are used throughout the estimation period, whereas prices on the Nord Pool Gas exchange are considered past mid 2009, when the liquidity in this new market had improved. Figure 13 shows a rapid growth in the fuel prices prior to the end of the estimation period, complicating modeling of the further price path.

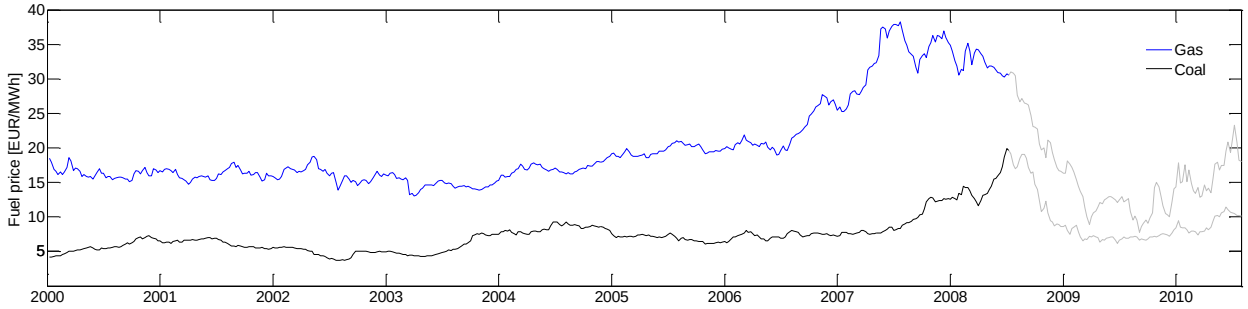

Figure 13. *Fuel price time series*

EUA (European Union Allowance) futures prices for CO_2 emissions in EUR/ton are illustrated in Figure 14. In particular, the curve corresponds to current futures prices at NASDAQ OMX Commodities whose time to expiry is shortest, as from the European CO_2 market was established. There is an increasing trend in the price until April 2006, when it suddenly drops by more than 50 percent in three days due to news regarding lower than expected CO_2 emissions. Some nations had reported too high emissions in order to receive large quotas, which led to oversupply (Bjerke, 2006; Daskalakis et al., 2009). The price declines further due to the low scarcity of quotas, until the second phase of the European Union Emission Trading Scheme (ETS 2) commenced in 2008. The jump diffusion behavior pointed out by Daskalakis et al. (2009) is to a high extent tied to the price drop in April 2006. Neglecting the possibility for such events, approximating the price process as an ordinary Geometric Brownian Motion seems reasonable.

[18] In order to convert the prices to EUR/MWh, they are divided by the corresponding USD/EUR exchange rate and a heating value of 7 MWh/ton, suggested by Nyland (2011).

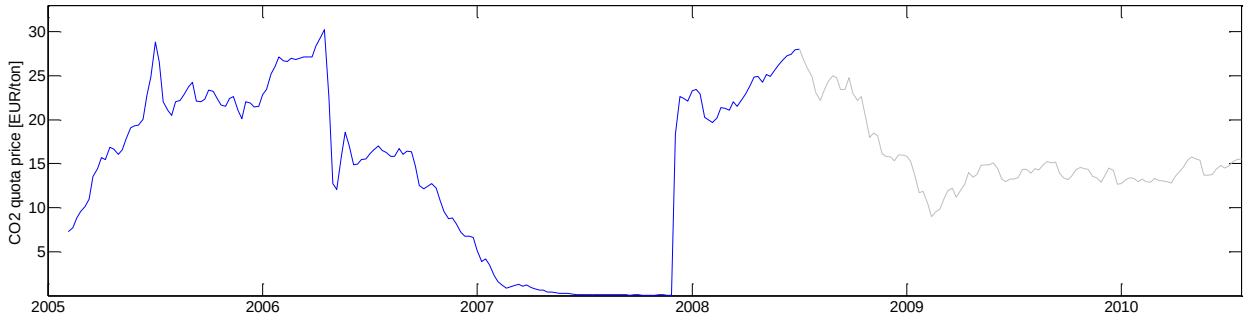

Figure 14. *CO_2 futures prices*

Figure 15 gives an overview of generation capacities for each condensing plant category. Efficiencies, operational costs and CO_2 emissions are specified for these categories, based upon estimates by Thema Consulting Group (2011) and SKM Market Predictor (2011). Aggregated plant data are associated with uncertainty, and the chosen estimates are not necessary identical to those used in other power market models. Variable operational costs are approximated to 3 EUR/MWh, except for peak load units (gas turbines) where costs of 25 EUR/MWh also reflects capital costs and costs associated with staying idle. A carbon content of 0.34 ton per MWh input is used for coal, whereas the corresponding value is 0.20 for gas. The efficiency is assumed to be 54% for CCGT power plants, 39% for gas extraction plants and 35 % for peak load units. Coal condensing plants in Denmark are assumed to have an efficiency of 43%, somewhat higher than for Finish plants at 41%. Efficiencies of coal extraction plants are 42% and 40% in Denmark and Finland respectively. In particular, these figures represent average total plant-efficiencies at maximum output.

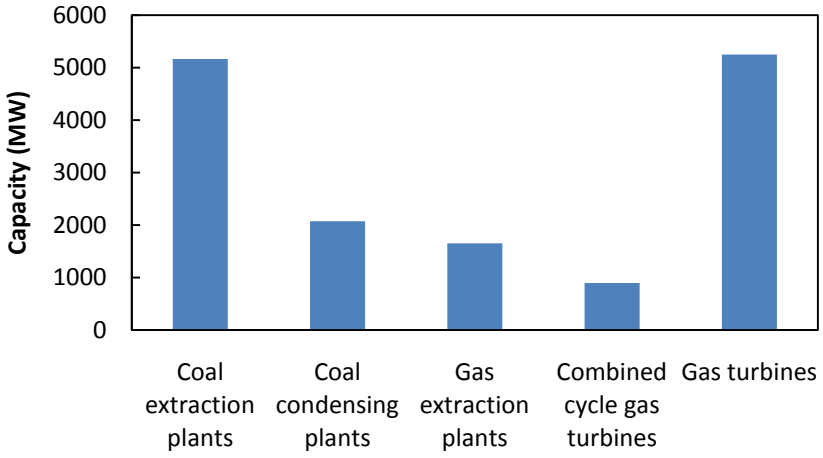

Figure 15. *Condensing generation capacities (Thema Consulting Group, 2011)*

As no aggregate availability statistics for condensing plants in the Nordics are found, the average energy availability for fossil fueled units in Germany from 2000 to 2007 of 86.2% is applied to the model (VGB, 2010).

3.4 Exchange

Historical exchange data, transmission capacities and spot prices are collected (Table 4). Figure 16 displays net electricity import from each country connected to Nord Pool. Electricity spot prices in Nord Pool, Germany[19] and Poland[20] are plotted in Figure 17. Another view of the German price is presented in Figure 18, which shows the annual EEX price variation during the estimation period.

Table 4. *Exchange and price data*

Description	Period	Granularity	Source
Exchange with connected markets	2000-2010	Weekly	Nord Pool Spot
Transmission capacities	2000-2008	-	Nord Pool Spot, Nordel, Energinet.dk
Nord Pool system price	2000-2010	Hourly	Nord Pool Spot
EEX spot price	2000-2010	Hourly	EEX
POLPX (IRDN) spot price	2000-2010	Weekly	Polish Power Exchange

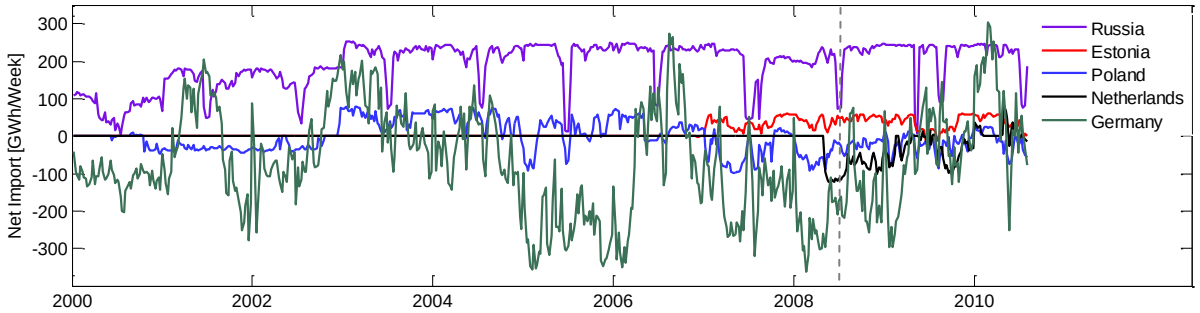

Figure 16. *Net import time series*

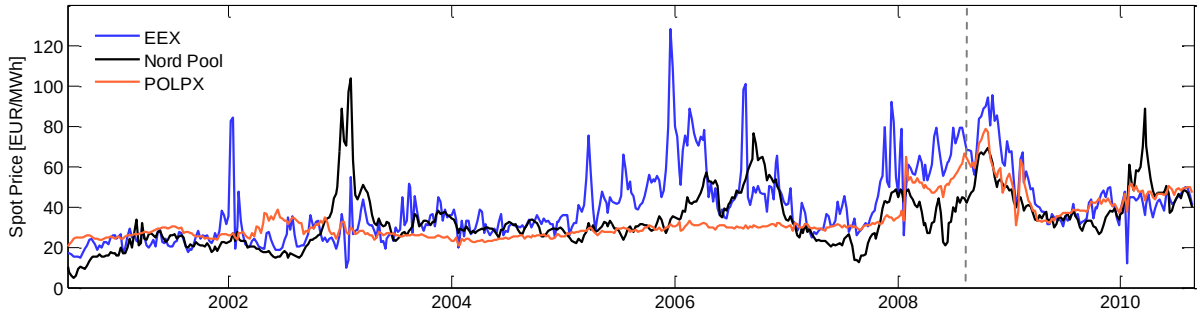

Figure 17. *Nord Pool, EEX and POLPX spot price time series*

[19] The Phelix price at the European Energy Exchange (EEX), here referred to as the EEX price.
[20] The IRDN index at the Polish Power Exchange (POLPX), here referred to as the POLPX price.

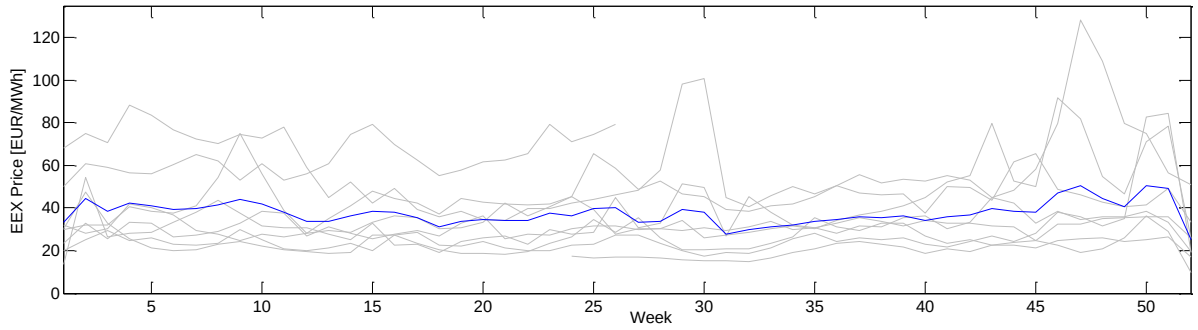

Figure 18. *Annual EEX price paths*

Germany

As evident from Figure 17, the EEX price has a higher mean and is more volatile than the Nord Pool price. The average price is highest during the winter season (Figure 18), a seasonality which seems to be more tied to increased frequency of spikes than higher base prices. Also apparent is the fast mean reversion after price jumps, indicating that spikes are more relevant to model than regime-switching jumps.

Exchange volumes presented in Figure 16 are consistent with the price behavior: The exchange varies to a large extent, although the volumes are positive in direction of Germany over time. Large transmission capacity enables the high exchange volumes: Onshore interconnections, the Kontek cable and the Baltic cable have a total capacity of 2100 MW to Nord Pool and 2650 MW from Nord Pool. However, the effective capacity of the Baltic cable is reduced because of limitations in the German network (Nordel, 2009).

The Netherlands

The NorNed cable has been in operation between Norway and the Netherlands since May 2008, with a capacity of 700 MW (NordREG, 2008). The Dutch spot price (APX spot) exhibits a strong degree of correlation with the EEX price (Morsy et al., 2008), and consistently net exchange volumes are variable over time (Figure 16). Given this strong correlation and the modest capacity, it is reasonable to use the EEX price as reference in modeling of exchange with the Netherlands.

Poland

The POLPX price remained relatively stable during most of the estimation period, but the volatility and the correlation with the EEX price increased considerably in the end. The correlation was 71% from 2007 to the end of the estimation period, compared to 34% from 2000 to 2007. Nord Pool is connected to Poland via a 600 MW submarine cable, the SwePol link, which entered operation in June 2000 (NordREG, 2008). Introducing the Polish spot price as a separate stochastic factor may not be beneficial due to the size of the interconnection and the increased correlation with EEX.

Russia

Finland is connected to Russia by a total capacity of 1400 MW (NordREG, 2008). Due to technical restrictions, import to Finland is possible only (ENTSO-E, 2010). Exchange is possible in both directions between Norway and Russia, but the capacity is limited to 50 MW. There is an electricity surplus in northwestern Russia, and generation is dominated by low-cost nuclear power. The prices are consequently lower than in the Nordics, typically around 20 EUR/MWh (Eliassen, 2011). For that reason, import levels are close to the maximum capacity throughout the year, except for maintenance periods typically taking place in the summer. Due to the low Russian electricity prices, forecasting exchange by historical volumes is appropriate.

Estonia[21]

A 350 MW interconnection (Estlink) links Finland to Estonia (NordREG, 2008). The import from Estonia is stable during the winter, but tends to be more variable in the summer. Due to a power surplus (EIA, 2011), electricity prices in Estonia are among the lowest in Europe. For instance, industrial power prices were the third lowest among the EU member states in 2006 (European Commission, 2007). Given spot prices below those in Nord Pool, historical exchange volumes can be used to predict future exchange.

Available capacities

When using the multi-period approach, historical average available capacity of connections in operation at the end of the estimation period will be applied to restrict exchange volumes. Average available capacities between Nord Pool and the Netherlands, Germany and Poland are compared to installed capacities in Table 5, whereas the time series of available capacity is illustrated in Figure 19. The variability for some of the connections indicates that using average available capacities is a rather crude method to restrict exchange volumes.

Table 5. *Transmission capacities for connections between Nord Pool and the Netherlands, Germany and Poland, January 2007 – June 2008.*

	Installed capacity (MW)		**Average available capacity (MW)**	
	To Nord Pool	From Nord Pool	To Nord Pool	From Nord Pool
SwePol Link[22]	600	600	98	468
Baltic cable	600	600	509	392
Denmark West - Germany	950	1500	920	1316
NorNed cable	700	700	668	668
Kontek cable	550	550	441	435
Total	3400	3950	2636	3280

[21] Note that the Estonian power market is moving in direction of deregulation, and Estonia was included in the Nord Pool Spot area in April 2010 (Nord Pool Spot, 2011c).

[22] The available capacity of the SwePol link has been reduced because of grid constraints in Poland and Sweden (Andruszkiewicz, 2010).

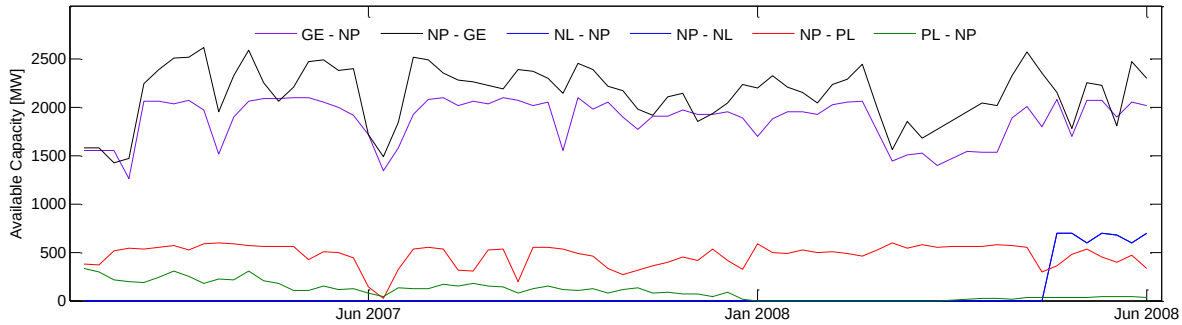

Figure 19. *Transmission capacities between Nord Pool and the Netherlands, Germany and Poland*

3.5 Intra-week consumption and prices

The shapes of historical weekly load profiles are illustrated in Figure 20. Consumption follows approximately the same pattern all weekdays, whereas weekend levels are somewhat lower. The average profile of the Nord Pool system price is plotted together with the load profiles, both scaled by the weekly average level. The average price and consumption profiles are highly correlated; indicating that consumption is the main driver behind intraweek price differences.

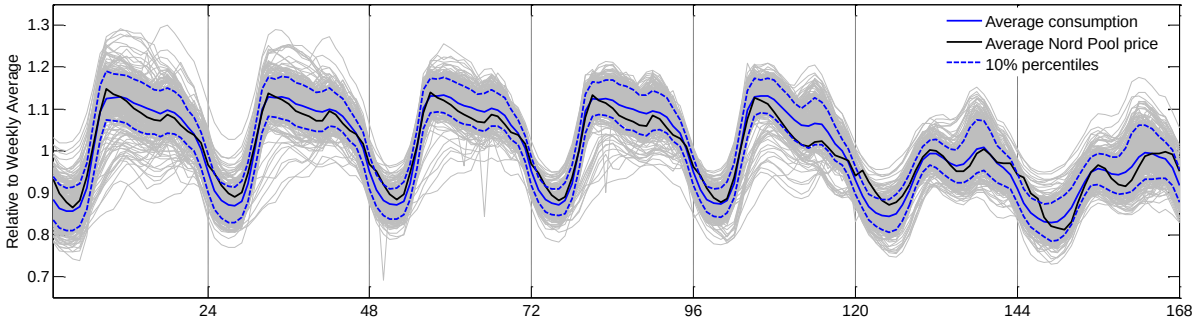

Figure 20. *Historical intraweek load profiles*

Figure 21 displays the variation in the EEX price within the week. Compared to Nord Pool, the peak price (and consequently peak consumption) appears later in the day. The higher variation in the average EEX profile is tied to the use of hydro reservoirs to smooth out price differences in the Nord Pool area.

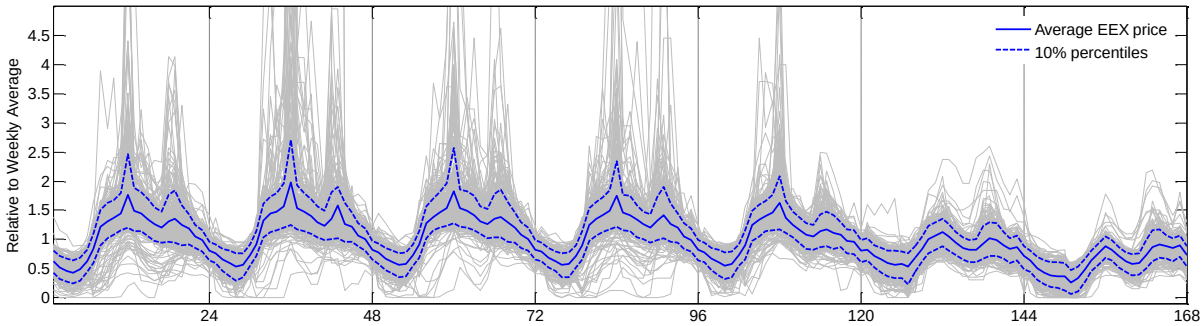

Figure 21. *Historical intraweek EEX price paths*

4. Estimation

Each part of the framework described in Chapter 2 is modeled by either a statistical equation, a fundamental equation or as an integral part of the price simulations (Table 6). For the statistical and fundamental equations, statistical software are applied to find optimal coefficient estimates. Time series models are calibrated in R, whereas other estimations are performed in EViews. MATLAB is used for simulations of stochastic factors and calculation of the market equilibrium, including determination of system price, hydro generation, condensing generation, hydro reservoirs and exchange. Source code is attached in Appendix B.

***Table 6**. Overview of the modeling approach*

Model	**Modeling approach**		
	Statistical equation	Fundamental equation	Within simulation model
Stochastic factors	X		
Consumption	X		
CHP industry generation		X	
CHP district generation		X	
Condensing generation			X
Hydro power generation			X
Water value		X	
Exchange		X	X

As the total number of simulations grows exponentially with the number of scenarios for each stochastic factor, the number of scenarios for each factor is kept relatively low (Table 7). In total, 22 500 scenarios for the system price are simulated. The computation time is approximately 1.5 seconds for each market equilibrium scenario path (108 weeks), using a PC with a CPU of 3.33 GHz and a RAM of 3.8 GB.

***Table 7**. Number of scenarios for each stochastic factor*

Stochastic factor	**Number of scenarios**
Inflow[23]	5
Snow reservoirs	5
HDD	5
EEX price	5
Nuclear generation	5
Wind power generation	-
Coal price	4
Natural gas price	3
CO_2 quota price	3

[23] Each inflow scenario corresponds to a snow reservoir scenario.

The statistical models are evaluated based on tests for stationarity, parameter stability, residual autocorrelation and residual distribution. For the simple fundamental equations, it is likely that not all relevant explanatory variables are included. Thus, residuals will typically exhibit autocorrelation. The parameter estimates are still unbiased when residuals are autocorrelated, but standard error estimates are generally not correct (Brooks, 2008). Therefore, t-ratios cannot be used to assess parameter significance. The practical consequences of this are limited; since the fundamental models are selected according to an underlying theory, all included parameters should be significant.

4.1 Stochastic factors

4.1.1 HDD

As outlined in 2.1.1, a SARIMA(p,d,q)(P,D,Q)$_S$ model with $D = 1$, $S = 52$ and $P + Q \leq 1$ is selected in order to capture the seasonality in the HDD time series. Models are estimated for all possible combinations of AR and MA lags, up to an upper limit of 9 lags, using maximum likelihood estimation. In case of autocorrelated residuals, the estimated model is rejected. From the remaining models, the one with lowest value of Akaike's information criterion is selected. The script for implementation of this procedure in R is attached in Appendix B.

The Ljung-Box test is applied to detect autocorrelation in the residuals. The null hypothesis of no autocorrelation until lag n is rejected if the p-value is less than 10%. The parameter n is set to 5% of the length of the series, as the test starts to deteriorate when number of lags exceeds this level (Burns, 2002).

Stationarity of the seasonally differenced HDD series is tested with the Augmented Dickey-Fuller test. Schwarz' information criterion is used to choose the lag length. As the test yields a p-value less than 1%, the null hypothesis of non-stationarity is rejected. We therefore start to consider models without non-seasonal differencing.

Without non-seasonal differencing, none of the evaluated models pass the Ljung-Box test. Following the suggestion of Brooks (2008), non-seasonal differencing ($d = 1$) is applied to remove autocorrelation. As deseasonalized HDD is stationary and follows a mean-reverting process, adding non-seasonal differencing may lead to overdifferencing. Overdifferencing is typically characterized by a first lag autocorrelation of -0.5 or less (Nau, 2010). For the differenced HDD series, the first lag autocorrelation is well within this limit (-0.32), and we assume overdifferencing is avoided.

A model with 6 AR-terms, 6 MA-terms and an SMA-term is selected. Due to the SMA term, the model can be interpreted as a seasonal exponential weighted moving average (EWMA) model. The weights applied to observations in previous seasons decline exponentially, and are given

by $\theta_s^{k-1}(1+\theta_s)$ where k is the number of seasons back in time (Pankratz, 1991). Since the SMA coefficient equals -1, all past seasons are given equal weight in the forecast. Table 8 summarizes the coefficient estimates.

Table 8. *Coefficients in the HDD model*

AR1	AR2	AR3	AR4	AR5	AR6	
0.5203	-0.0634	-0.299	-0.0866	0.6954	-0.1545	
MA1	**MA2**	**MA3**	**MA4**	**MA5**	**MA6**	**SMA**
-1.0863	0.1355	0.3178	-0.0362	-0.9782	0.6473	-1

Characteristics of the residuals are presented in Appendix A.2, including sample autocorrelation function (SACF) plot, normal quantile plot and Ljung-Box p-values for different number of lags. The Ljung-Box test indicates no autocorrelation in the residuals for the selected lag length and significance level. A Shapiro-Wilk normality test yields a p-value near zero, and the null hypothesis of normally distributed residuals is clearly rejected. This conclusion is supported by the density plot (Figure 22), which reveals that the residual distribution has excess kurtosis and fat tails. Normally distributed residuals are not critical for obtaining good parameter estimates (Hipel et al., 1977), but standard error estimates assume normally distributed residuals (Brooks, 2008). Hence t-ratios cannot be used to assess the significance of the parameters. All coefficients are therefore assumed significant and included the model.

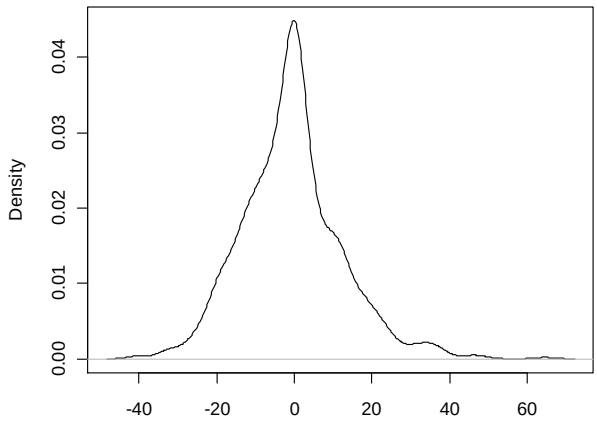

Figure 22. *Density of HDD residuals*

A CUSUM test is performed to check the stability of the model parameters. The CUSUM chart (Figure A.10) indicates that the parameters of the HDD model are stable. See Appendix A.3 for further details.

The residual distribution will be used in simulation of HDD scenarios. Since the residuals are non-normally distributed, we use historical residuals to bootstrap an empirical distribution. For any distribution, percentiles are uniformly distributed (McDonald, 2006). Bootstrapping is therefore performed by drawing the residual corresponding to a given percentile generated from an $U(0,1)$-distribution. Instead of using a pseudorandom number generator to simulate the

uniform distribution, we apply a Sobol sequence. A Sobol sequence is a low-discrepancy sequence of quasi-random numbers more evenly distributed than a similar series of pseudo-random numbers (Glasserman, 2004). Due to the higher uniformity, a Sobol sequence is better suited to represent the $U(0,1)$-distribution than pseudo-random numbers. The consequence is HDD scenarios converging more rapidly to the theoretical forecast, which is critical due to the low number of scenarios applied.

The high number of historical observations indicates that the bootstrapping procedure will perform well. Alternatively, a theoretical distribution could have been fitted to the residuals or a Box-Cox transformation could have been applied to the HDD series in search for normally distributed residuals (Hipel et al., 1977).

Figure 23 illustrates how realized HDD evolves compared to five simulated scenarios and the forecasted level. The forecast tracks the realized HDD well, except in the cold winter of 2010. In this period, the actual level was higher than all scenarios. The mean of the simulations are close to the forecasted level, indicating that a sufficient number of scenarios are simulated.

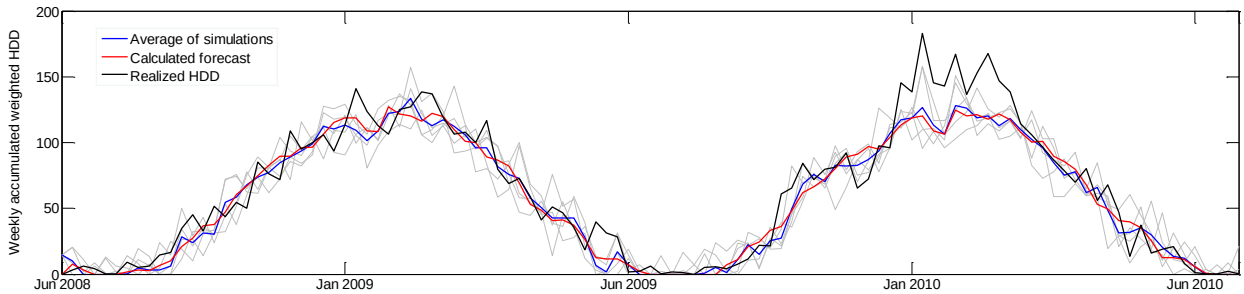

Figure 23. *HDD forecast and scenarios*

4.1.2 Snow reservoirs

SARIMA models for snow reservoirs are estimated according to the procedure presented in 4.1.1. Since the median culmination is uncertain (as pointed out in 3.2), we choose to model the relative energy content ($R_{S\%}$) instead of the absolute reservoir level. The ADF test for the seasonally differenced data yields a p-value less than 1%, which confirms stationarity. Estimation of models without non-seasonal differencing leads to alternatives which pass the Ljung-Box test. However, we do not find any model whose parameters are proven to be stable, even not when increasing the lag length limit. A SARIMA$(9,0,9)(0,1,1)_{52}$ model is chosen, as it has the lowest AIC value and the most promising CUSUM chart among the alternatives.

The CUSUM chart (Appendix A.3) yields indications of instability, but we cannot conclude that the parameters are unstable at a 1% significance level. Natural time series are generally stable over time, and applying a longer historical series for calibration may result in stable parameter estimates. Given the high variation in snow reservoirs from year to year, stability problems are not unexpected when a limited number of years are available for calibration.

Coefficient estimates for the selected model are presented in Table 9. The residual characteristics (Appendix A.2) show that the residuals are non-normally distributed, while it is clear that the model pass the Ljung-Box test for the given specifications.

Table 9. *Coefficients in the snow reservoir model*

AR1	AR2	AR3	AR4	AR5	AR6	AR7	AR8	AR9	
0.0849	-0.1794	0.2637	0.3953	0.5084	0.3840	-0.0210	0.2229	-0.7998	
MA1	**MA2**	**MA3**	**MA4**	**MA5**	**MA6**	**MA7**	**MA8**	**MA9**	**SMA**
1.2570	1.5101	1.3323	0.8607	0.1588	-0.4179	-0.6482	-0.9584	-0.2494	-0.9263

Historical snow reservoirs (Figure 10) are near continually increasing in the snow accumulation period and continually decreasing in the snow melting period, a behavior not captured by SARIMA models. To explicitly model this behavior, scenarios could instead be drawn from historical snow reservoir paths. By using historical paths instead of a time series model, the correlation between the end of the estimation period and the forecast period will not be modeled. Therefore, we do not reject the SARIMA approach, but restrict the scenario generation process to only accept scenarios which are in accordance with the historical behavior.

Five scenarios are simulated using the procedure presented in 4.1.1. Figure 24 illustrates realized, forecasted and simulated levels. The forecast fit reasonable well for the 2008-2009 season, while the low snow reservoirs in the next season cause the forecast to fail.

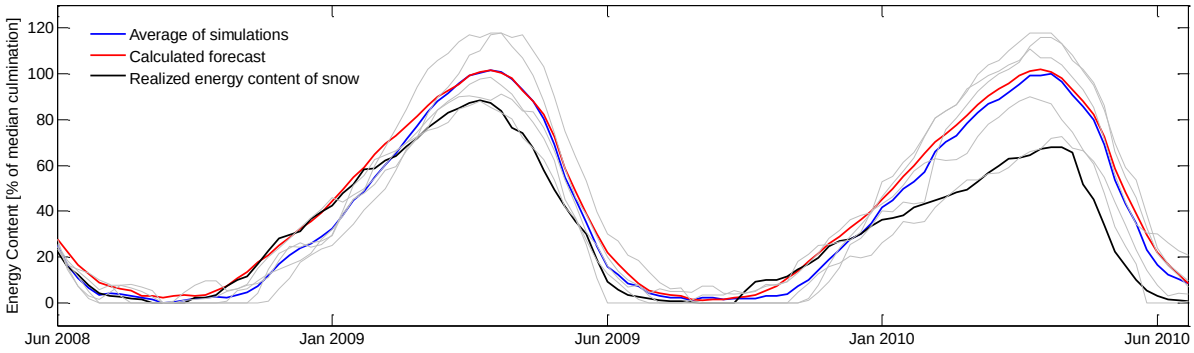

Figure 24. *Snow reservoir forecast and scenarios*

4.1.3 Reservoir inflow

The correlation between inflow and the change in snow reservoirs is -79% in the estimation period[24], confirming that inclusion of snow reservoirs is advantageous in inflow modeling. Snow reservoir changes in week t and $t-1$ are significant in explaining inflow in week t, as evident from the impulse response function (Appendix A.4). As a slight simplification, we will model inflow as a function of the change in the week t snow reservoir only (i.e., $v(B) = \beta_{S\%}$).

[24] The coefficient is in the same range in the snow melting season and the snow accumulation season. Thus, we do not apply seasonally dependent coefficients in the inflow model.

First, a regression similar to (4) is estimated by ordinary least squares:

$$I_t = C + \beta_{S\%}\,\Delta R_{S\%,t} + N_t \tag{36}$$

The seasonal lags of the residual autocorrelation function decay slowly, thus seasonally differencing of (36) is necessary. The new regression is:

$$\nabla_{52}\, I_t = \beta_{S\%}\,\nabla_{52}\,\Delta R_{S\%,t} + N'_t,\;\; N'_t = \nabla_{52} N_t \tag{37}$$

The ADF test applied to N'_t yields a p-value close to zero, and non-seasonal differencing is not applied. A SARIMA model with 5 AR-terms, 7 MA-terms and an SMA-term is selected for N'_t according to the AIC criterion. Hence, the final model is:

$$\nabla_{52} I_t = \beta_{S\%}\,\nabla_{52}\Delta R_{S\%,t} + \frac{(1-\theta_1 B^1 - \cdots - \theta_8 B^7)(1-\theta_{52} B^{52})}{1-\emptyset_1 B^1 - \cdots - \emptyset_6 B^5} u_t \tag{38}$$

Residual characteristics (Appendix A.2) reveal that the residuals u are non-normally distributed. The plot of Ljung-Box p-values implies the model satisfies the requirements related to residual autocorrelation. Table 10 summarizes the coefficient estimates, which stability is confirmed by the CUSUM chart (Appendix A.3).

Table 10. *Coefficients in the inflow model*

AR1	AR2	AR3	AR4	AR5		$\beta_{S\%}$	
-0.4125	-0.0620	-0.1276	0.2660	0.8544		-6922	
MA1	**MA2**	**MA3**	**MA4**	**MA5**	**MA6**	**MA7**	**SMA**
1.1251	0.6131	0.4190	0.0124	-0.9113	-0.5434	-0.1297	-0.8319

We simulate five inflow scenarios, each corresponding to a snow reservoir scenario. The scenarios are simulated using bootstrapping of residuals and a Sobol sequence. Except for a period of extremely high inflow in the spring of 2010, the forecast is in the same range as the realization. The inflow forecast is calculated using forecasted snow reservoir levels as input.

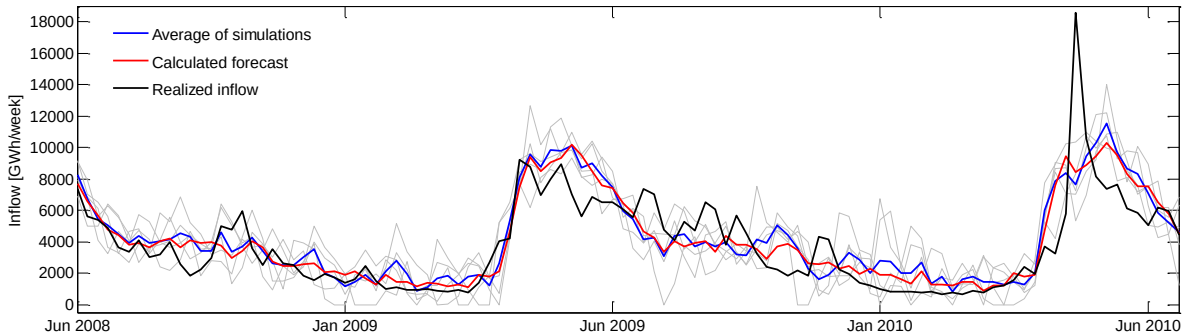

Figure 25. *Inflow forecast and scenarios*

A disadvantage by not applying a Box-Cox transformation to the inflow series is evident from the scenarios in Figure 25: The variance in simulated inflow during the summer is higher than what seems realistic from historical data (Figure 9). As implied by the historical series, the variance in inflow increases with the magnitude. The appropriate Box-Cox transformation may stabilize the variance of the series to be modeled, and also result in a residual distribution closer to the normal distribution (Hipel and McLeod, 1994). In this case, a logarithmic transformation is reasonable due to the rise in variance with the inflow level. However, we choose to not use Box-Cox transformations. The physical relationship between inflow and the change in snow reservoirs is linear, and a transformation will thus reduce the explanatory power of the dependent variable. Pianosi and Raso (2008) discuss this shortcoming of the transformation approach in more detail, and shows that values of the input variable exceeding the maximum value used in calibration can lead to significant overestimation of the inflow[25].

Modeling the variance structure of inflow is discussed in Chaper 4.8.1, where the impact of inflow on price variations is considered in detail.

4.1.4 Wind power generation

The ARIMA(p,d,q) process for wind power generation is estimated using maximum likelihood. Models are compared for different numbers of AR and MA lags. From models without autocorrelation in the residuals, the alternative with lowest AIC is chosen.

Due to convergence problems, the logarithm of wind generation is modeled instead of absolute levels. The ADF test of the transformed series yields a p-value of 59%, and non-seasonal differencing is applied. A model with 5 AR-terms, 7 MA terms and a constant term is selected. The constant term implies an increasing trend in wind generation, reflecting the growth in installed capacity.

Table 11. *Coefficients in the wind power generation model*

AR1	**AR2**	**AR3**	**AR4**	**AR5**		**Constant**
-0.2796	0.2150	-0.5375	0.0226	0.7752		0.0016
MA1	**MA2**	**MA3**	**MA4**	**MA5**	**MA6**	**MA7**
-0.3477	-0.5824	0.6080	-0.3118	-0.9671	0.5070	0.0941

The residual characteristics (Appendix A.2) show non-normally distributed residuals, characterized by excess kurtosis and skewness. Results from Ljung-Box tests demonstrate that requirements concerning residual autocorrelation are satisfied.

[25] Pianosi and Raso (2008) forecast inflow with precipitation as the dependent variable, and use a deseasonalized ARMAX model instead of a SARIMA based dynamic regression model. The results are yet transferable to our case. Due to the shortcomings of the ARMAX method, they propose a nonlinear model which includes the dependent variable as a linear term. With a rather complicated calibration method required, we consider this approach to be outside the scope of our study.

Figure 26 displays some example scenarios along with the realized generation. Both simulated and actual generation levels oscillate randomly.

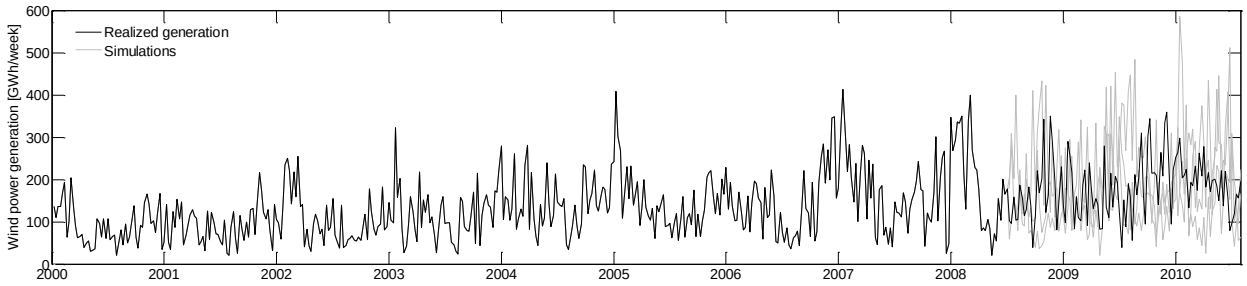

***Figure 26**. Simulations of wind power generation*

4.1.5 The EEX spot price

EEX spot prices are modeled by the mean reverting jump diffusion models proposed in 2.1.4. The common jump diffusion part is estimated before calibrating the different mean reversion parts. For numerical convenience, we choose to model the logarithm of the price.

Spikes are removed from the series of historical logarithmic returns by implementation of a recursive filtration algorithm. Returns located outside a selected quantile level of the normal distribution fitted to the return series are removed. This process is repeated iteratively with remaining returns until no new spikes are identified (Clewlow and Strickland, 2000). Following Cartea and Figueroa (2005), the quantile level is defined such that returns with absolute values higher than three times the standard deviation are filtered. Properties of the identified spikes are summarized in Table 12. Prices are not deseasonalized, as the slightly higher prices in the winter season seemed to be a result of increased spike frequency, not higher base prices.

***Table 12**. Spike properties*

Property	**Value**
Frequency, λ_J	0.05263
Mean, μ_J	0[26]
Standard deviation, σ_J	0.7650

Since the mean reversion process is a log-normal diffusion process (Guimarães Dias, 2008), returns should be normally distributed. The Shapiro-Wilk test demonstrates lack of normality for unfiltered returns. Removal of fat tails through filtration makes the normality assumption more realistic, albeit the null hypothesis still is accepted at the 1% level only. Normality is accepted at

[26] Robust estimation of the mean is difficult to obtain (Clewlow and Strickland, 2000), and consequently we define the mean to be zero. The data yielded a slightly negative mean of -0.0166.

the 5% level for spikes. Thus, assuming normally distributed jump sizes is reasonable. See Appendix A.5 for details.

To estimate the discretization of the Ornstein-Uhlenbeck process (7), the following regression is specified:

$$\xi_{EEX,t} - \xi_{EEX,t-1} = a_{OU} + b_{OU}\,\xi_{EEX,t-1} + \epsilon_{OU,t} \tag{39}$$

where $\xi_{EEX} = ln\,(S_{EEX})$.

The parameters are calculated according to Dixit and Pindyck (1994):

$$\hat{\xi}_{EEX} = -\frac{\hat{a}_{OU}}{\hat{b}_{OU}} \tag{40}$$

$$\hat{\rho} = -\,ln\,(1 + \hat{b}_{OU}) \tag{41}$$

$$\hat{\sigma}_{OU} = \hat{\sigma}_{\epsilon}\sqrt{\frac{2\,ln(1+\hat{b}_{OU})}{\left(1+\hat{b}_{OU}\right)^2 - 1}} \tag{42}$$

Parameter values turn out to be $\hat{\xi}_{EEX}$ = 3.437, $\hat{\rho}$ = 0.08292 and $\hat{\sigma}_{OU}$ = 0.1478. Figure 27 presents 30 simulated price paths from the combined Ornstein-Uhlenbeck jump diffusion model. The simulated mean is reasonable close to the actual level, except for week 52 in 2009 and during the autumn of 2008. Notably, the realized price path experiences a lower spike frequency in the forecast period than in the estimation period.

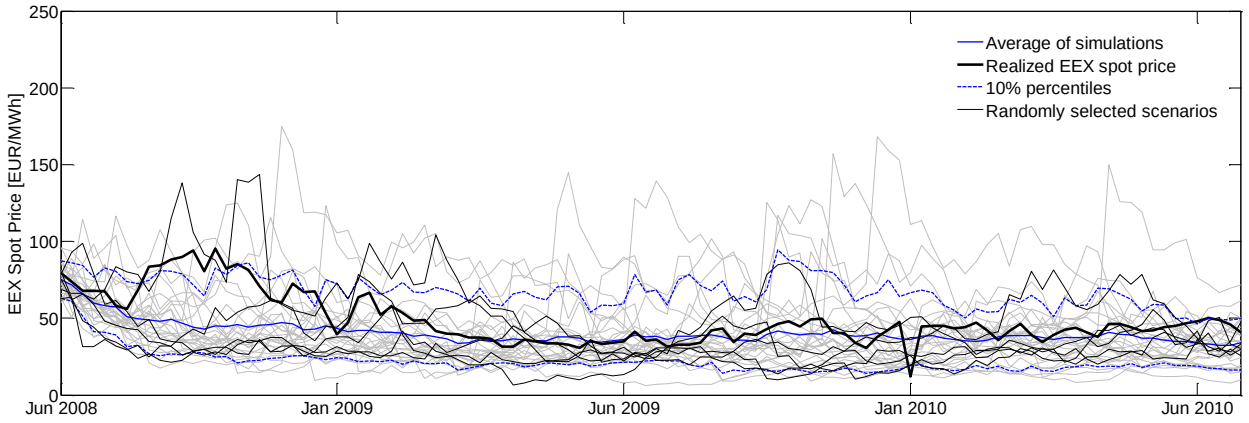

Figure 27. *EEX scenarios created from the Ornstein-Uhlenbeck jump diffusion model*

The regression approach (39) for calibration of the Ornstein-Uhlenbeck model provides the maximum likelihood parameter estimates (Brigo et al., 2009). The likelihood function for the Ornstein-Uhlenbeck model is (based on Franco, 2003):

$$f(\boldsymbol{Y}|Y_0, \bar{Y}, \rho, \sigma_{OU}, \Delta t) = (2\pi)^{-\frac{1}{2}}\left(\frac{\sigma_{OU}^2}{2\rho}(1-e^{-2\rho\Delta t})\right)^{-\frac{1}{2}n} exp\left(-\frac{\rho}{\sigma_{OU}^2}\sum_{i=1}^{n}\frac{\left(Y_i-\bar{Y}-(Y_{i-1}-\bar{Y})e^{-\rho\Delta t}\right)^2}{1-e^{-2\rho\Delta t}}\right) \quad (43)$$

Given the parameter estimates, the log-likelihood value is 574.15[27], which will be compared to the log-likelihood of the geometric mean reversion model.

For the discretization of the geometric mean reversion model, Yang and Yang (2008) derive the following likelihood function of the parameters:

$$f(\boldsymbol{Y}|Y_0, \alpha, \kappa, \sigma_{GMR}, \Delta t) = \frac{1}{\left(\sqrt{2\pi\Delta t}\sigma_{GMR}\right)^n \prod_{i=0}^{n-1} Y_i} exp\left(-\frac{\Delta t}{2\sigma_{GMR}^2}\sum_{i=0}^{n-1}\left(\frac{Y_{i+1}-Y_i}{Y_i}-\alpha+\kappa Y_i\right)^2\right) \quad (44)$$

where $\boldsymbol{Y} = (Y_1, Y_2, \dots, Y_t, \dots, Y_n)$ is the vector of historical prices (except the start price Y_0)[28].

In Appendix A.6, we derive the maximum likelihood parameter estimates from (44). For the proportional mean reversion speed κ, we obtain:

$$\hat{\kappa} = \frac{\sum_{i=0}^{n-1}(Y_{i+1}-Y_i) - \frac{1}{n}\left(\sum_{i=0}^{n-1} Y_i\right)\left(\sum_{i=0}^{n-1}\frac{Y_{i+1}-Y_i}{Y_i}\right)}{\frac{1}{n}\left(\sum_{i=0}^{n-1} Y_i\right)^2 - \sum_{i=0}^{n-1} Y_i^2} \quad (45)$$

Given the estimate of κ, $\hat{\alpha}$ and $\hat{\sigma}_{GMR}^2$ are calculated as:

$$\hat{\alpha} = \frac{1}{n}\sum_{i=0}^{n-1}\frac{Y_{i+1}-Y_i}{Y_i} + \frac{\hat{\kappa}}{n}\sum_{i=0}^{n-1} Y_i \quad (46)$$

$$\hat{\sigma}_{GMR}^2 = \frac{\Delta t}{n}\sum_{i=0}^{n-1}\left(\frac{Y_{i+1}-Y_i}{Y_i}-\hat{\alpha}+\hat{\kappa}Y_i\right)^2 \quad (47)$$

Numerical values are $\hat{\kappa}$ = 0.02384, $\hat{\alpha}$ = 0.08643 and $\hat{\sigma}_{GMR}$ = 0.04038. Figure 28 displays the simulated price paths. As expected, spikes simulated by the geometric-mean reversion model revert faster than those simulated by the Ornstein-Uhlenbeck model.

[27] Note that a positive likelihood value is possible for a continuous distribution.

[28] The vector $\boldsymbol{Y}$ is not static due to spike filtration. Consider a spike at $t = k$. The term $\frac{Y_{k+1}-Y_k}{Y_k}$ is included in (44) to capture mean reversion after the spike, while the relative spike return $\frac{Y_k-Y_{k-1}}{Y_{k-1}}$ is not included.

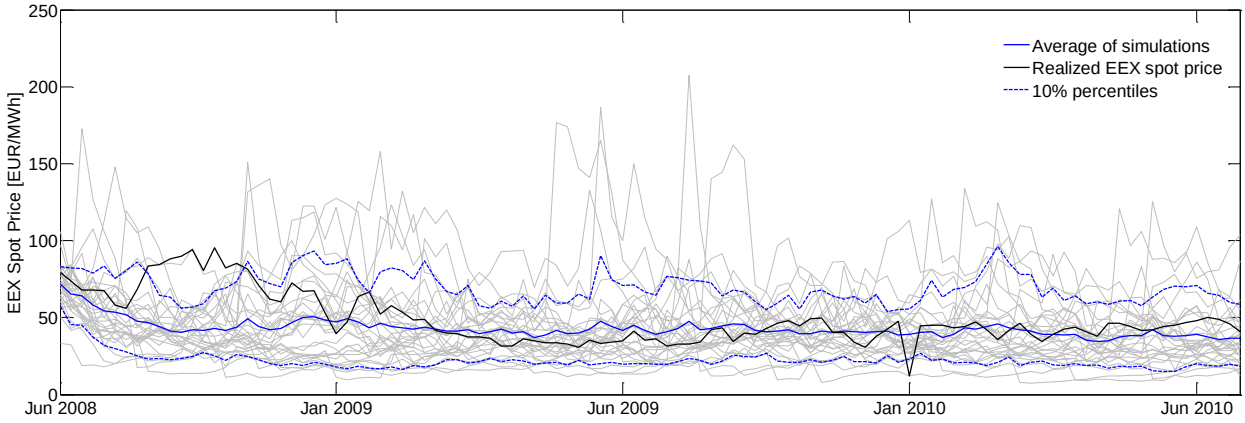

Figure 28. *EEX scenarios created from the geometric mean reversion jump diffusion model*

The log-likelihood value for the geometric mean reversion model (44) is 213.07. Since the Ornstein-Uhlenbeck jump diffusion model yields the highest log-likelihood value, it is selected to simulate the EEX spot price. Five randomly selected scenarios, displayed in Figure 27, will be applied in the market equilibrium simulations.

After the peak period in 2008, the realized price reverts to a level near the historical mean. Consequently, the forecasts of both mean-reverting models fit the realized price well. As pointed out in 2.1.4, the equilibrium price level is dependent on e.g. fuel prices. Thus, the performance obtained by the mean-revering models may not be representative for other periods. Extending the model by adding fuel prices as explanatory variables is therefore a possible extension.

4.1.6 Coal, gas and CO_2 prices

Gas and coal prices (Figure 13) as well as CO_2 prices (Figure 14) started to fall rapidly in the beginning of the forecast period, caused by the financial crisis. No econometric model is able to predict the price fall related to this crisis, and forecasts will diverge tremendously from actual prices. Based on historical data, prices are expected to increase or fluctuate around the current level. In order to provide a realistic picture of the influence of coal, gas and CO_2 prices on the electricity price, the processes for these prices are calibrated using realized data from the forecast period. The intention is to show how the electricity price distribution model works, not to create a valid forecast. If the latter is the objective, fuel prices must of course be modeled using historical prices.

CO_2 prices

CO_2 prices are simulated according to (15), where the mean and variance of the log returns are estimated using data from the forecast period. Figure 29 shows three scenarios for the CO_2 price.

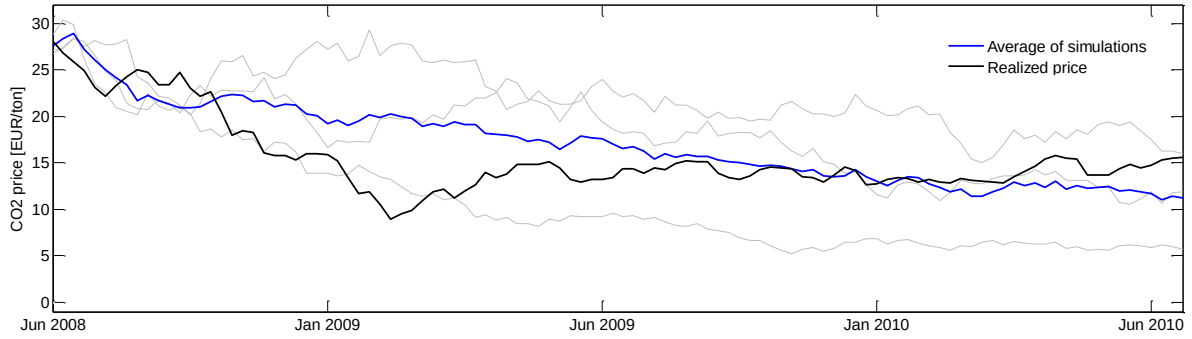

Figure 29. *Scenarios for the CO_2 price*

Coal and natural gas prices

In order to capture the steep decrease in fuel prices in the forecast period, mean reverting scenarios are simulated around the actual prices. Figure 30 and 31 illustrate four scenarios for the coal price and three for the natural gas price, respectively.

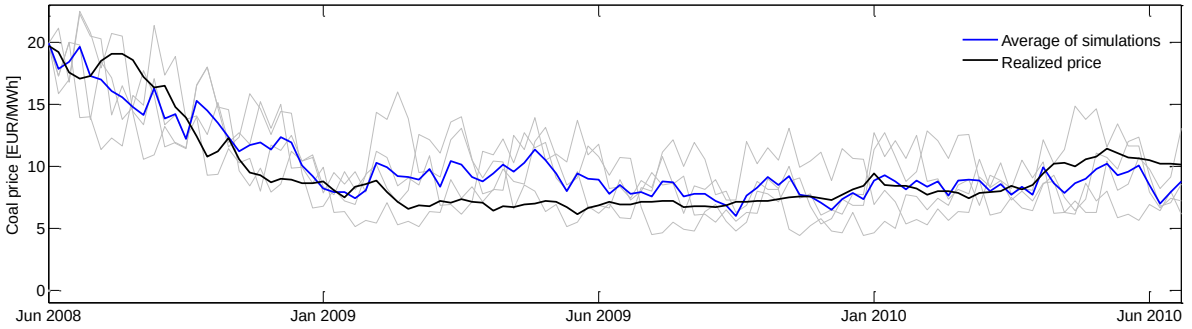

Figure 30. *Scenarios for the coal price*

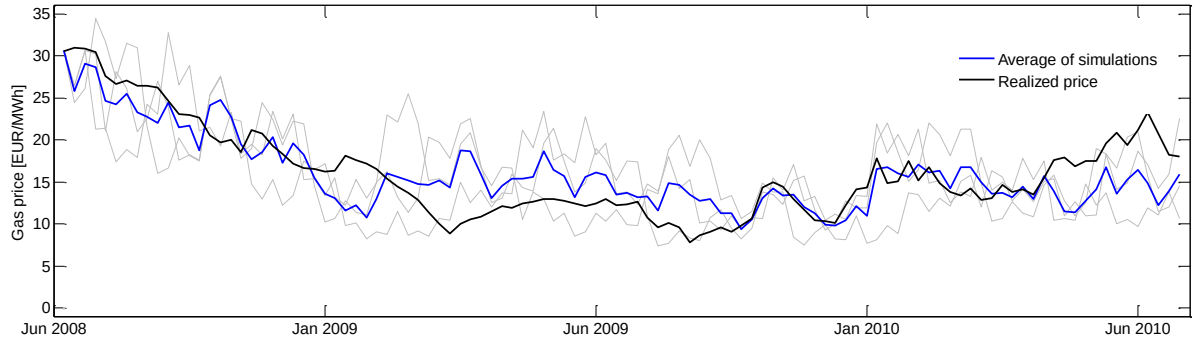

Figure 31. *Scenarios for the natural gas price*

4.2 Consumption

4.2.1 Descriptive statistics

Table 13 presents the correlations between consumption and relevant explanatory variables introduced in 2.2.1.

Table 13. *Correlations between consumption and explanatory variables*

Dependent variable	Correlation
HDD	95.6 %
Day length	-83.0%
RTI	70.7 %
Heating oil price	9.6%

As apparent, consumption is closely tied to the HDD. The correlation with day length is also high. However, HDD and day length are correlated by a coefficient of -74%, which can cause collinearity problems in the estimations. The retail trade index (RTI) is compared with a 52-week moving average of consumption. The correlation of 71% demonstrates that the index is well suited to explain the growth pattern in consumption over time. Deseasonalized consumption values are used to assess the impact of heating oil prices. As the correlation is low and the rapid growth in the end of the estimation period makes forecasting of heating oil prices difficult, we exclude heating oil prices from the model.

The scatter plot in Figure 32 adds further insight to the relation between consumption and HDD. The electricity consumption in the Nord Pool area seems to be around 6000 GWh per week when no heating is required, and increases thereafter linearly with the HDD.

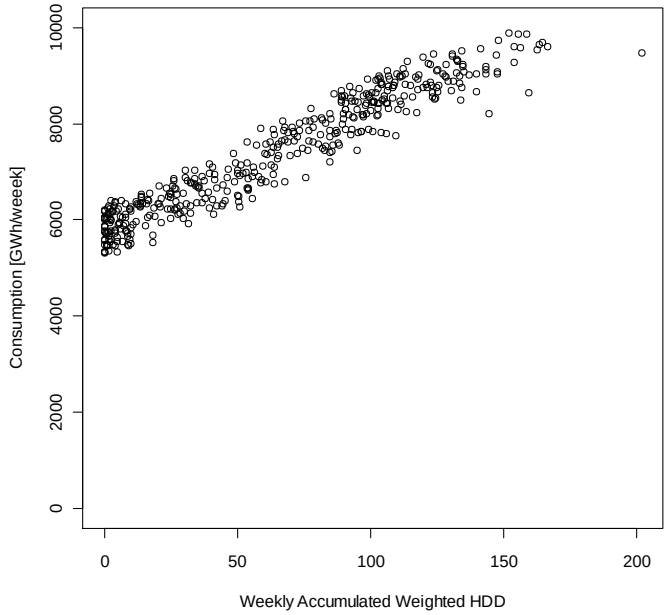

Figure 32. *Correlation between consumption and HDD*

4.2.2 Error correction model

The Augmented Dickey-Fuller test applied to the historical consumption series yields a p-value of 31%, hence the null hypothesis of a unit root cannot be rejected. While Johnsen and Willumsen (2010) found that the Norwegian consumption series in their study was stationary, we conclude that the Nordic consumption series is non-stationary. Consequently, an error correction model should be appropriate. The following cointegration relationship is modeled:

$$F_t = \beta_{EC1} + \beta_{EC2} HDD_t + \beta_{EC3} DL_t + \beta_{EC4} ln(RTI_t) + \beta_{EC5} D_{1,t} + \beta_{EC6} D_{2,t} + u_t \qquad (48)$$

where

- RTI_t is the 12-month moving average retail trade index in week t.
- DL_t is the average day length in week t.
- $D_{i,t}$, $i \in \{1, 2\}$ are holiday dummies for the summer holiday (3 weeks) and the Christmas holiday, respectively.
- β_{EC1} ... β_{EC6} are constants to be estimated.

After estimating (48), the Engle-Granger test is applied to confirm that the estimated equation is cointegrated, i.e. that the residual series is stationary. Using a lag length of 31 based on the AIC criterion, the Engle-Granger test gives a p-value of 48%. Therefore, the null hypothesis of no cointegration cannot be rejected. If instead the SBIC criterion is used to select the lag length, a length of 3 is suggested, yielding an Engle-Granger p-value close to zero. This ambiguous result continues when applying the ln-transformation to consumption and day length.

Assuming that the variables are cointegrated, we estimate the whole error correction model (16). The residuals show clear signs of autocorrelation, even when multiple lags of the difference terms in (16) are applied. As a consequence of the autocorrelation problems and doubt whether the variables are cointegrated, we conclude that a dynamic regression model may be a better choice for our data.

4.2.3 Dynamic regression model

First, a regression similar to the cointegration expression in (48) is estimated by OLS:

$$F_t = \beta_{DR1} + \beta_{DR2} HDD_t + \beta_{DR3} DL_t + \beta_{DR4} ln(RTI_t) + \beta_{DR5} D_{1,t} + \beta_{DR6} D_{2,t} + N_t \qquad (49)$$

An R^2 value of 97.3% indicates a good fit. A model with only HDD as input yields a fit of 92.1 %, illustrating that HDD is the by far most influential variable.

Seasonally differencing is applied, as the seasonal lags of the sample autocorrelation function for the residuals from (49) decay slowly. The residual series is stationary according to the ADF test (which yields a p-value close to zero), but non-seasonal differencing ($d = 1$) is applied to remove autocorrelation. The first lag autocorrelation of the differenced consumption series

($\nabla_{52}\nabla F_t$) is less than 0.5 (-0.26), and consequently there are no indications of overdifferencing. The new regression is:

$$\begin{aligned}\nabla_{52}\nabla F_t = {} & \beta_{DR2}\nabla_{52}\nabla HDD_t + \beta_{DR3}\nabla_{52}\nabla DL_t + \beta_{DR4}\nabla_{52}\nabla ln(RTI_t) \\ & + \beta_{DR5}\nabla_{52}\nabla D_{1,t} + \beta_{DR6}\nabla_{52}\nabla D_{2,t} + N_t' \\ & N_t' = \nabla_{52}\nabla N_t\end{aligned} \tag{50}$$

Not unexpected, the differenced day length and HDD series turn out to be collinear, and day length is excluded as an input to the model. Furthermore, the retail trade index and both holiday dummies are not significant in the new model. Therefore, the model has boiled down to a single-input model with HDD as the only explanatory variable (51). With R^2 at 75 % for the differenced model, the fit is still good[29].

$$\nabla_{52}\nabla F_t = \beta_{DR}\nabla_{52}\nabla HDD_t + N_t' \tag{51}$$

Evaluation of SARIMA models for N_t' leads to a $(6,1,8)(0,1,1)_{52}$ model, and the final consumption model is thus:

$$\nabla_{52}\nabla F_t = \beta_{DR}\nabla_{52}\nabla HDD_t + \frac{(1-\theta_1 B^1 - \cdots - \theta_8 B^8)(1-\theta_{52}B^{52})}{1-\emptyset_1 B^1 - \cdots - \emptyset_6 B^6}u_t \tag{52}$$

Estimation results are summarized in Table 14, whereas Appendix A.2 contains the residual characteristics.

Table 14. *Coefficients in the consumption model*

AR1	AR2	AR3	AR4	AR5	AR6	β_{DR}		
-1.7676	-1.3180	0.0099	1.1595	1.1227	0.2294	15.5028		
MA1	**MA2**	**MA3**	**MA4**	**MA5**	**MA6**	**MA7**	**MA8**	**SMA1**
1.3333	0.2569	-1.0487	-1.4544	-0.6339	0.4766	0.2330	-0.0335	-0.9963

Figure 33 compares forecasted consumption and realized levels. Note that forecasted, not actual, HDD is used as input. The forecast fits the realized consumption well, but the consumption is generally somewhat overestimated. The overestimation can be explained by the economic downturn following the financial crisis. Due to reductions in operating margins, power intensive industry reduced the consumption levels by permanent and temporary shutdowns (Hydro, 2010; Vattenfall, 2011). On the other hand, consumption is underestimated in the period from December 2009 to February 2010. This is due to the high HDD in this period, which is not captured by the HDD forecast.

[29] Remark that R^2 for a differenced and an undifferenced model are not comparable.

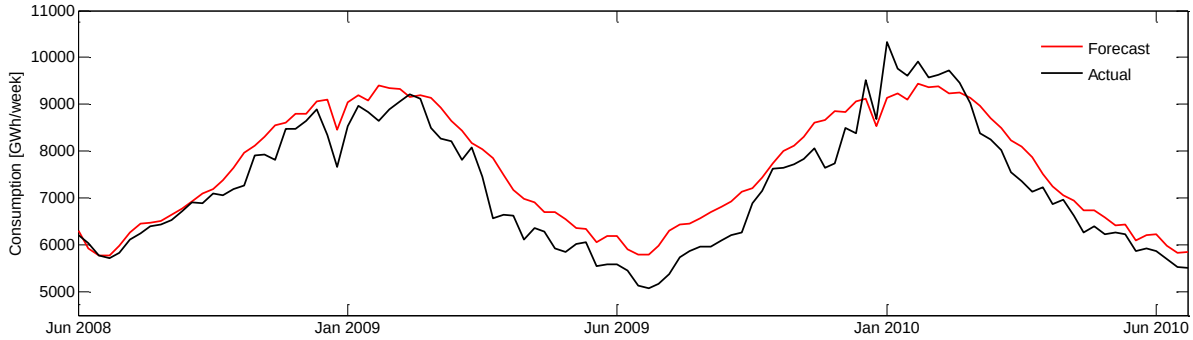

Figure 33. *Consumption forecast*

4.3 Thermal generation

4.3.1 Nuclear power

As explained in 2.3.1, the model for nuclear power generation consists of a deterministic part and a process for forced outages. The historical mean generation level throughout the year, adjusted for forced outages and the Barsebäck shutdown, is presented in Figure 34. As expected, generation levels are high and stable during the winter. The highest amount of planned outages occurs around week 23, when the inflow level from snow melting peaks, and in week 31-34 (holiday period), when the consumption is low.

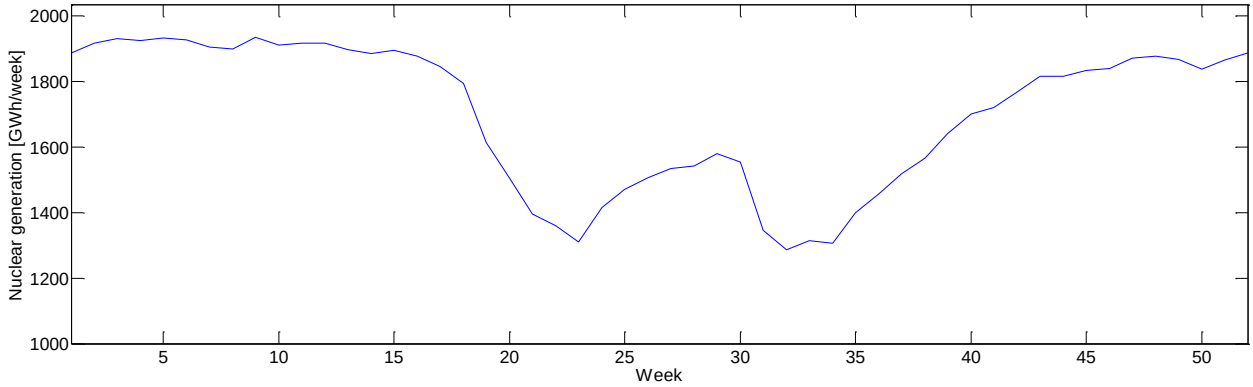

Figure 34. *Historical outage-adjusted mean nuclear generation level*

Table 15 displays historical failure rates[30]. The variation among the different reactors is quite high.

[30] Defined as the number of failures in the estimation period divided by the total time the reactor operated without failures.

Table 15. *Estimated failure rates at nuclear reactors*

Reactor	Failure rate (λ_E)
Loviisa[31]	0.001993
Okiluoto[31]	0.003587
Oscarshamn 1	0.007017
Oscarshamn 2	0.002287
Oscarshamn 3	0.002927
Forsmark 1	0.003368
Forsmark 2	0.005864
Forsmark 3	0.001294
Ringhals 1	0.006361
Ringhals 2	0.004747
Ringhals 3	0.006164
Ringhals 4	0.003606

Since only outages lasting at least one day are covered, the Weibull distribution is fitted to historical repair times subtracted one day. The resulting distribution is characterized by a scale parameter λ_W = 4.326 and a shape parameter k_W = 0.572. As k_W < 1, the expected remaining time to repair increases with the time the outage has lasted. In Figure 35, the fitted distribution is compared to the distribution of historical repair times.

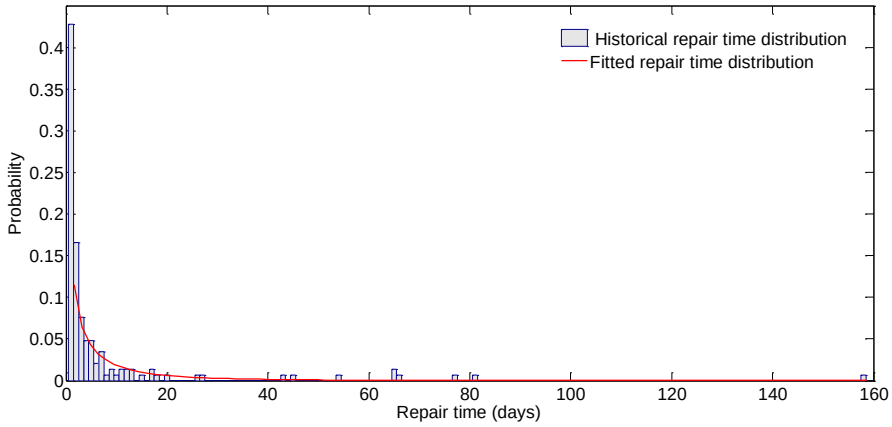

Figure 35. *Weibull distribution fitted to repair times*

When simulating generation paths for the forecast period, failure and repair processes are discretized to daily resolution. Figure 36 illustrates the simulation results. The average of the simulated paths deviates from the historical mean at the start of the forecast period, due to an ongoing outage at Forsmark 2. After some weeks, the expected generation level converges to the historical mean. However, the fit between scenarios and realized generation is low. Throughout most of the forecast period, Swedish nuclear generation experienced serious operational

[31] Due to the low failure frequency at Loviisa and Okiluoto, the failures at the individual reactors at each plant are aggregated.

problems (NVE, 2010a; NVE, 2010d). Frequent outages and delayed restarts after maintenance resulted in realized generation lower than the historical minimum for long periods. Those events were impossible to foresee in advance, and our scenarios reflect the outage risk that seemed realistic at the end of the estimation period. In the market equilibrium simulations, five randomly drawn scenarios will be employed.

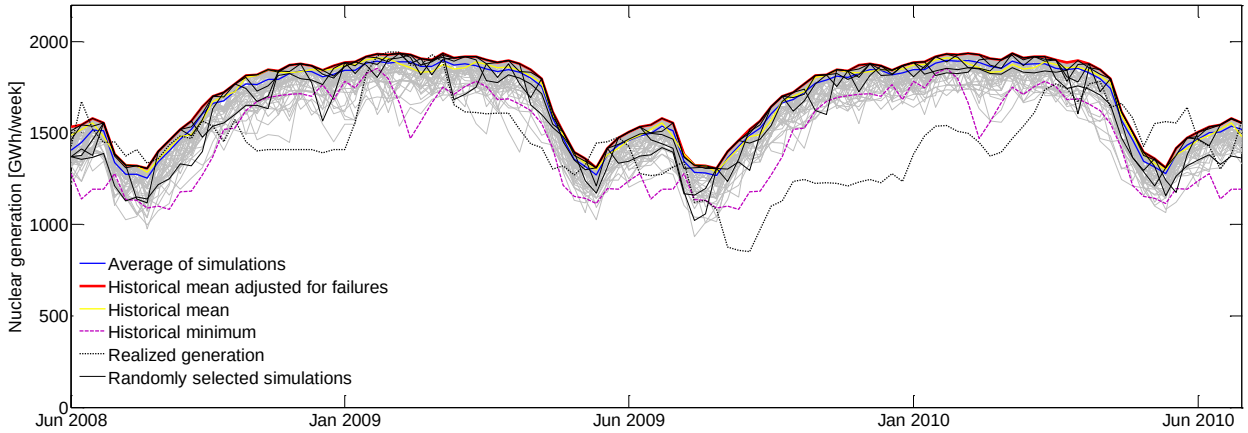

Figure 36. *Simulated nuclear generation in the forecast period (converted to weekly granularity)*

4.3.2 CHP industry

CHP industry generation forecasted by the historical average is compared with actual generation in Figure 37. As evident, the historical mean provides a good prediction of future generation.

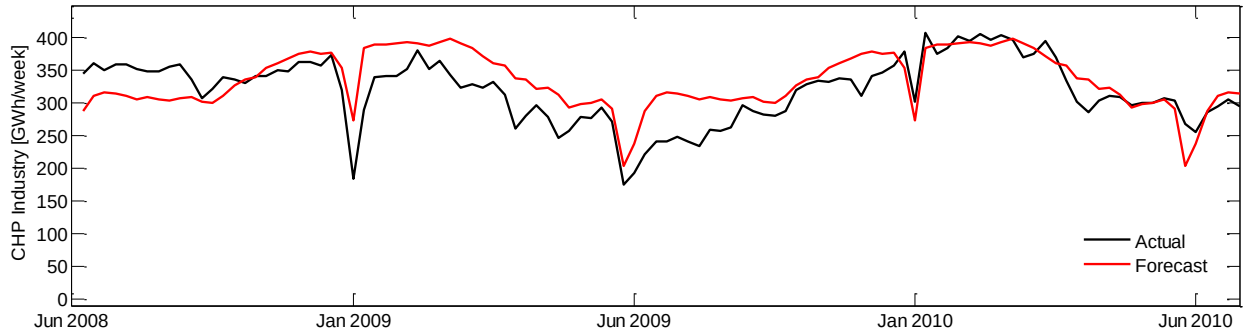

Figure 37. *Actual and forecasted CHP industry generation*

4.3.3 CHP district

Figure 38 illustrates the strong correlation between weekly CHP district generation and weekly HDD, and thus backs up the functional form of the models proposed in 2.3.3. The models (22) and (23) are estimated by ordinary least squares. Limiting the maximum generation does not improve the goodness of fit. Model (23) is therefore preferred, with a fit of 96%:

$$G_{CHPD,t} = 189.3 + 5.84HDD_t \left[\frac{GWh}{week}\right] \quad (53)$$

CHP district generation is forecasted by inserting the HDD forecast into the above model. Figure 39 illustrates the forecasted generation compared to the actual. In the first year, the forecast fits the realized values well. The generation is underestimated during most of the second year, as result of a HDD forecast below the actual levels.

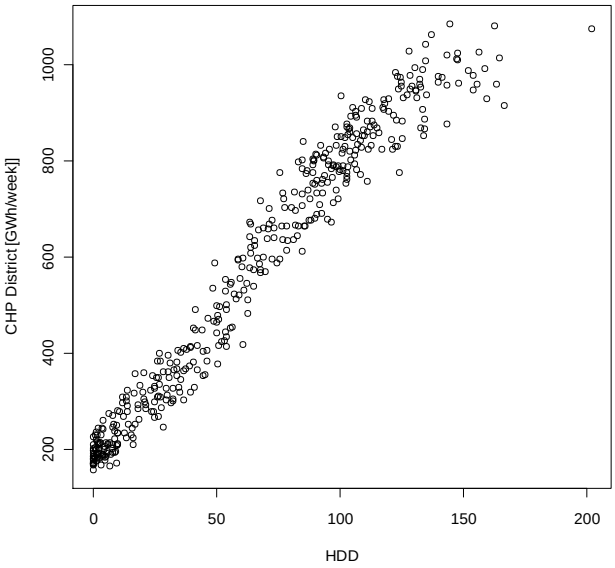

Figure 38. *CHP district generation versus HDD*

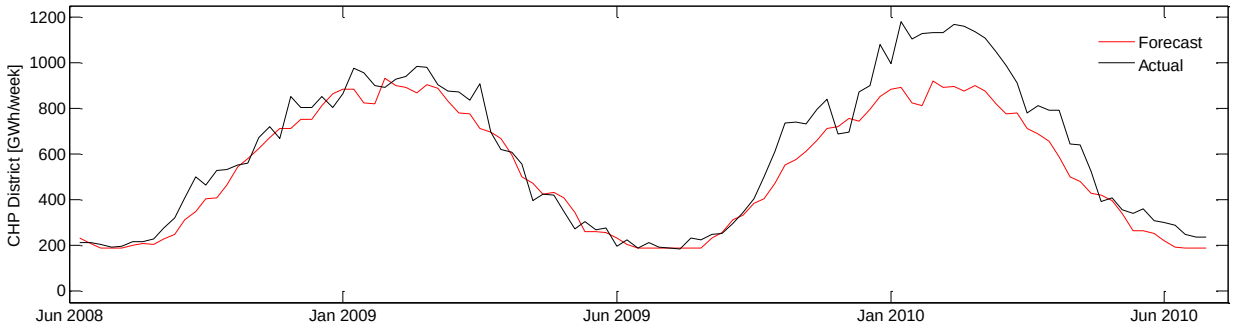

Figure 39. *CHP district generation forecast*

In the market equilibrium simulations, the maximum allowable generation level will be specified as equal to the capacity.

4.4 Hydro generation and the marginal water value

Equation (29) is a model for the market water value curve. Given a particular level of regulated hydro generation as input, the equation should return the water value to the marginal hydro producer. As water values are not public available information, several assumptions must be introduced when calibrating the equation.

First, we assume a hydro plant is the marginal unit which bid is accepted. In reality, also condensing plants or import from EEX may clear the market. To increase the likelihood of the assumption being valid, we will approximate water values using prices from the NO1 price area, where the share of hydro power is high.

The short run marginal cost of condensing plants is assumed constant during a week. Since the water value curve is modeled as a function of the end-of-week hydro and snow reservoirs, the only explanatory variable changing during the week is the level of regulated hydro generation. A reasonable approach would therefore be to calibrate the equation using generation levels and area prices for each hour of the week.

However, data on hydro generation was found with weekly granularity only. Thus, the area prices used in calibration should reflect the water value to the marginal hydro producer during the week. Consistent with the assumption of hydro being the marginal technology, the maximum weekly area price can be used for calibration.

A drawback by using the maximum weekly price is sensitivity to special circumstances, such as short-duration outages of plants or transmission lines. Such events can increase the maximum weekly price without affecting the total weekly level of regulated hydro generation to a high extent, and thus deteriorate the relationship between generation level and water value which we try to capture in the water value equation.

To avoid such problems, we will use the median of the daily NO1 peak prices as our water value proxy. Choosing the median is founded on the approximation of constant daily profiles for regulated hydro generation within a particular week, except for the hours in which extraordinary events lead to deviations.

As explained above, the shape of the modeled water value curve is constant during the week. A relatively constant water value curve over a week may also be a reasonable approximation in reality: Although water values vary continuously as new information arrives, producers will use their flexibility trying to follow the optimal constant water value policy.

A constant daily profile of regulated hydro generation in combination with a constant water value curve yields the same water value for the marginal unit each weekday. To remove the effects of events as e.g. outages, the median of the daily peak prices during the week is used to approximate the water value to the marginal hydro unit.

Table 16 displays the historical correlations between the water value approximation and the dependent variables. The signs of all correlation factors are consistent with the theory outlined in 2.4.

Table 16. *Correlations between the water value and explanatory variables*

Dependent variable	Correlation
$SRMC_{coal}$	40.0%
$R_{W\%} - R_{WMEAN\%}$	-63.8%
$R_{S\%} - R_{SPERC\%}$	-40.8%
$G_{hydroR\%}$	15.8%

Calibration of (29) by nonlinear least squares estimation gives the coefficient estimates in Table 17. The seasonal differences in the parameter estimates turns out to be small; hence, we apply the same parameter values for both seasons. Using the mean hydro filling degree ($R_{WMEAN\%}$) as $C_{W\%,t}$ and the lower tenth percentile of the snow reservoir ($R_{SPERC\%}$) as $C_{S\%,t}$ yielded the best fit. In particular, the fit of the chosen equation is 74% in the estimation period.

Table 17. *Coefficient estimates*

Coefficient	Value
β_{MWV1}	3.178
β_{MWV2}	0.111
β_{MWV3}	6.003
β_{MWV4}	2.128
β_{MWV5}	0.675

Figure 40 shows the realized water value approximation along with fitted values in the estimation period and out-of-sample calculated water values in the forecast period. The estimated series tracks the realized water value approximation in an overall convincing way, although the fit is low during some periods with price jumps. Considering the forecast period (Figure 41), sizing of peaks is still the main weakness of the model[32].

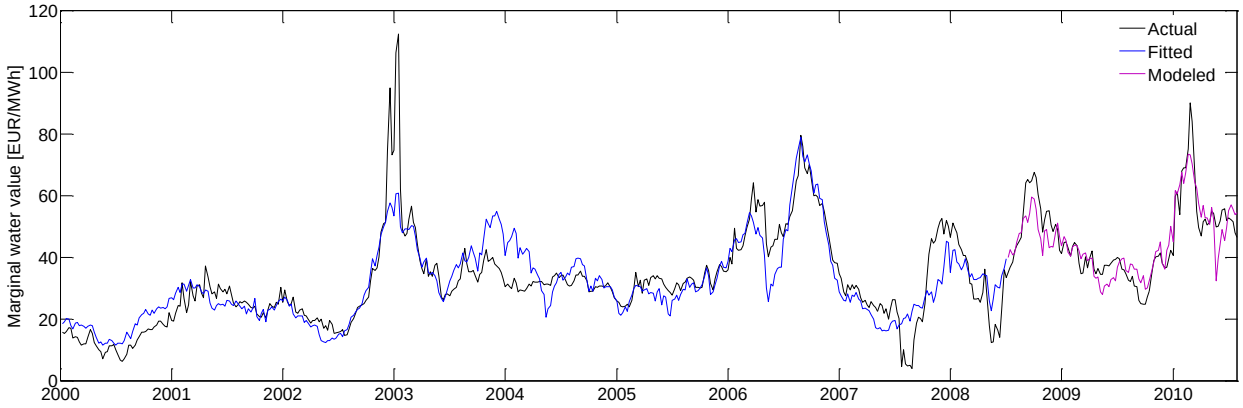

Figure 40. *Fitted and modeled values of the water value approximation*

[32] In addition, a downward jump is modeled for week 20, 2010. This week was characterized by a steep increase in inflow levels (NVE, 2010a). The resulting increase in unregulated hydro generation resulted in a downward jump in low-load prices, but the peak prices used in calibration of the water value curve was only minorly affected.

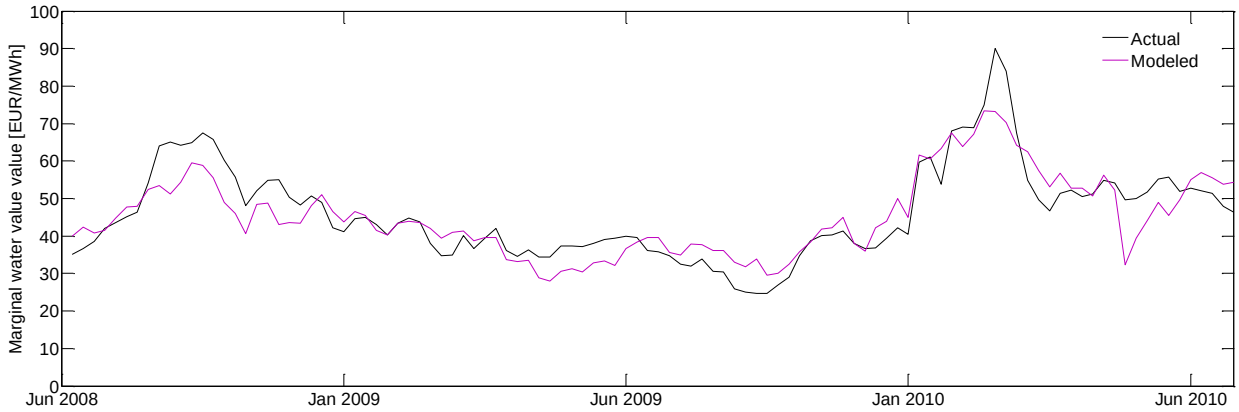

Figure 41. *Modeled and realized values of the water value approximation in the forecast period*

The feedforward neural network for the water value is estimated using MATLAB's Neural Network Toolbox. Networks with up to 20 hidden neurons are trained several times with randomly chosen initial weights. A network with 10 hidden neurons resulted in the highest fit with realized values in an independent test sample[33]. Figure 42 shows the simulated water value path from this network, using realized values of the input variables. Modeled water values are in the same range and seem to vary similar to the realized water value approximation. However, the magnitude of the peak in early 2010 is underestimated. As the hydro reservoir level was critical at this time, the gap between modeled and realized values indicates that the impact of the relative storage level is not properly captured by the network. Due to the trial and error approach applied in network selection, networks with improved fit may be possible to obtain.

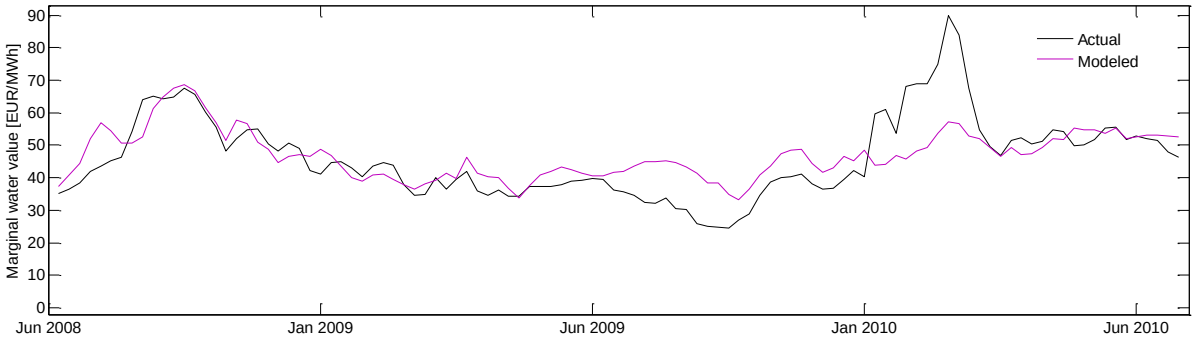

Figure 42. *Comparison of water values modeled with neural network and realized values*

The water value equation has a fit of 77% in the forecast period, while the neural network has a fit of 55%. Thus, we have not found any better input-output mapping than the water value equation, and we conclude that the equation is a reasonable approximation of the dynamics influencing the water value. Of course, the equation can be subject for improvements, especially regarding the sizing of peaks.

[33] The test sample contains 20% of the observations in the estimation period, and is selected randomly.

Due to lack of data for the division between regulated and unregulated hydro generation, we apply the coefficient estimates found by Vehviläinen and Pyykkönen in (27):

$$I_{U\%,t} = 0.2 + e^{-13.3(1-R_{W\%,t})} \quad (54)$$

An empirical spillage function could have been fitted to implied spill levels from historical reservoir balances. However, this approach is not appropriate as the aggregated reservoir and inflow data are too inaccurate. Consequently, hydro spillage is neglected.

4.5 Exchange

4.5.1 The Netherlands, Germany and Poland

Due to high correlation between the APX price and EEX, increased correlation between the POLPX price and EEX, and modest capacities of the connections with the Netherlands and Poland, exchange with the Netherlands, Poland and Germany is modeled together. The EEX price is thus applied as a common reference price for those markets.

With the single-period approach, (31) is calibrated with NI_{min} equal to historical minimum net import (-481 GWh/week) and NI_{max} equal to historical maximum net import (291 GWh/week). As no capacity extensions were known at the end of the estimation period, K_{cap} is held constant during the forecast period. The forecast turns out to be:

$$NI_{GE-NL-PL,t} = -19.0 + 11.7\left(S_{NP,t} - S_{EEX,t}\right), \; NI_{GE-NL-PL,t} \in [-481, 291] \; (GWh/week) \quad (55)$$

The fit in the estimation period is 57%. Figure 43 illustrates the out-of-sample performance, where the actual net import is compared to net import calculated using the realized price difference.

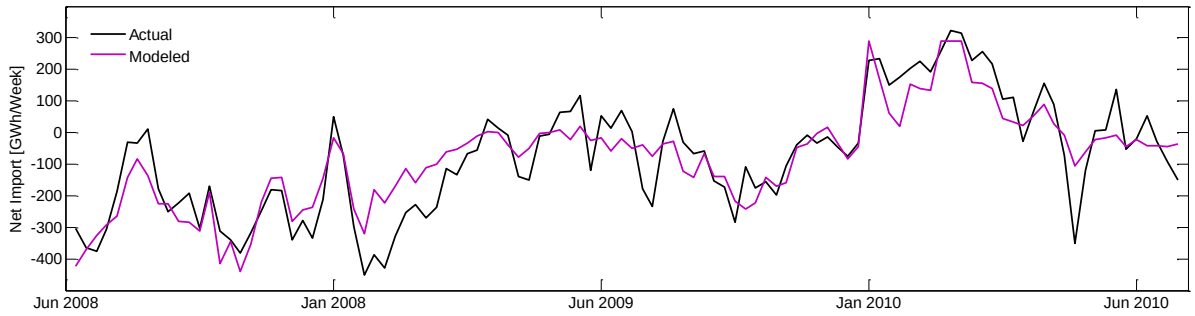

Figure 43. *Actual and modeled net import from the Netherlands, Germany and Poland*

In the multi-period approach, exchange levels are computed simultaneously with the system price during the simulations. The unsatisfactory fit of (55) throughout the estimation period indicates that the more computationally intensive multi-period approach is necessary. Results for this methodology are discussed in Chapter 4.7, along with other simulation results.

4.5.2 Russia

Import from Russia is represented by a constant value, as the levels stay near the maximum capacity for most of the estimation period and the maintenance periods are hard to predict. The import is assumed to be equal to the maximum of the historical weekly average:

$$NI_{RU,t} = 238\ (GWh/week) \tag{56}$$

The value is obtained using data from 2003 and onwards, when the last of the three lines between Russia and Finland was put in operation (RAO, 2002). Realized import is compared with the forecast in Figure 44.

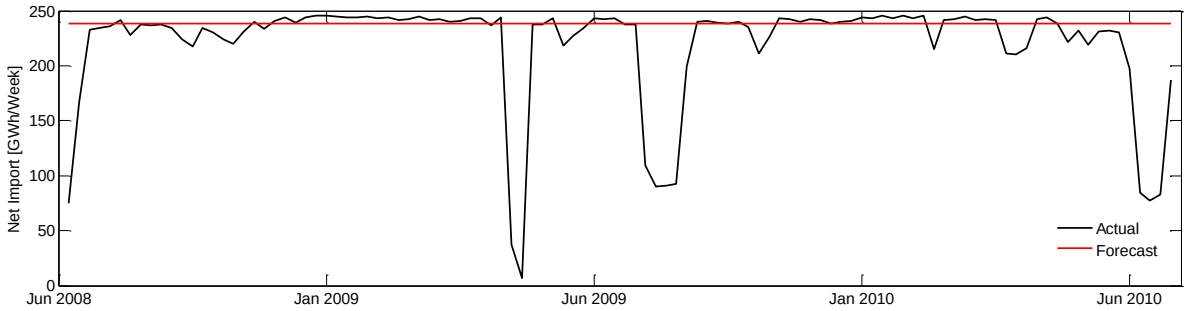

Figure 44. *Actual and forecasted import from Russia*

4.5.3 Estonia

As the import from Estonia varies with the season, it is forecasted by different constants for summer and winter. Weekly import during the summer (week 17-35) is set equal to the historical average for the summer season, and vice versa for the winter.

$$NI_{ES,t} = \begin{cases} 27, summer\ season \\ 42, winter\ season \end{cases} \quad (GWh/week) \tag{57}$$

Figure 45 shows realized and predicted import levels.

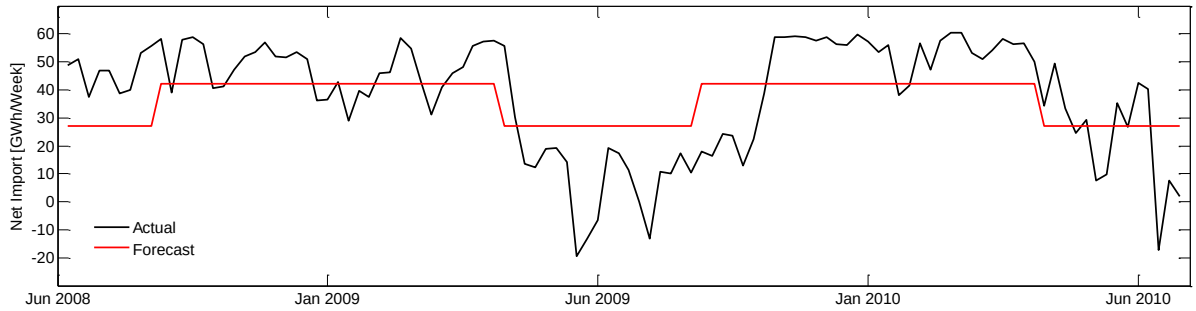

Figure 45. *Actual and forecasted net import from Estonia*

4.6 Load periods

The week is divided into five load periods: Peak, day, morning and evening, night and weekend day. The duration of these load periods and the corresponding relative factors, calculated according to (32) - (35), is presented in Table 18.

Table 18. *Load periods and relative factors*

Period	Duration	Relative factors	
		Consumption	EEX
Morning and evening	6 - 8 and 20 - 24	1.0217	1.0296
Day	8 -10 and 15 - 20	1.0973	1.3058
Peak	10 - 15	1.1127	1.5036
Night	24 - 6	0.8758	0.6025
Weekend day	6 - 24	0.9540	0.7920

The fitted consumption profile is compared to the historical average in Figure 46. Similarly, the fitted EEX price profile is displayed in Figure 47. As the consumption and EEX profiles have somewhat different shapes, the selection of load periods is a tradeoff between the fit with the two profiles. More subperiods would have improved the fit, but likewise increased the calculation time required for the market equilibrium simulations.

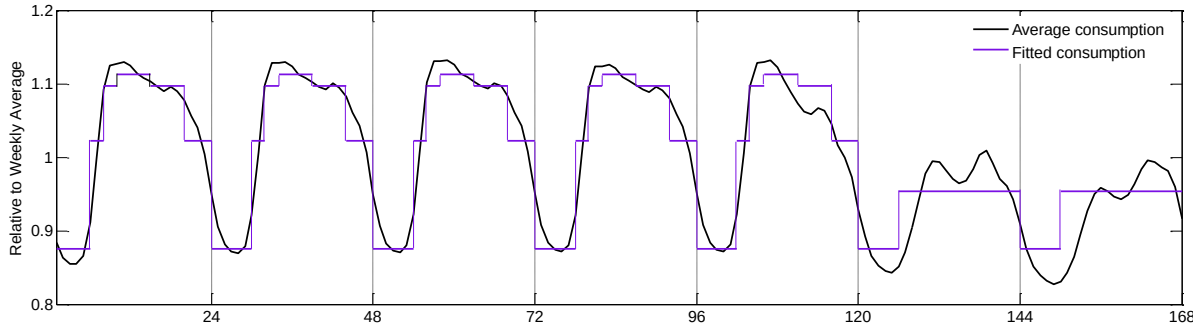

Figure 46. *Approximated variation in consumption within the week*

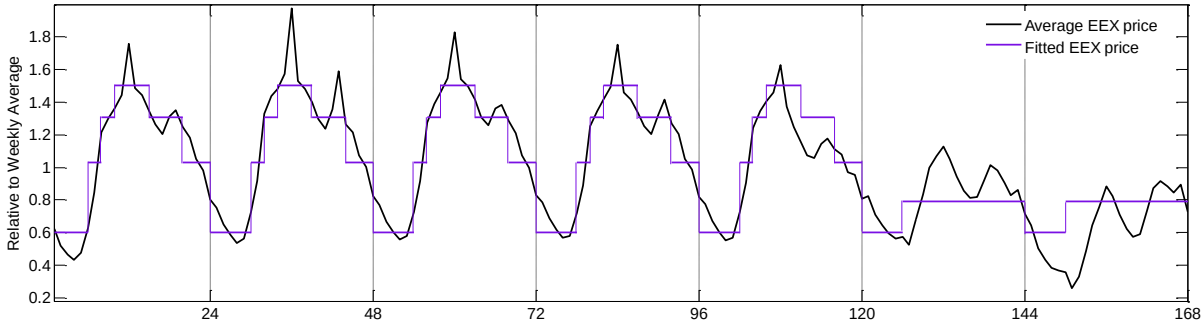

Figure 47. *Approximated EEX price variation within the week*

4.7 Market equilibrium simulations

Models for generation, consumption and exchange are combined as explained in 2.7, to find the supply-demand equilibrium. Condensing generation, regulated hydro generation, hydro reservoir levels, exchange and the system price are determined implicit from the merit order. In this section, simulated scenarios for these variables will be presented and discussed.

Calculated scenario paths for the aggregated hydro reservoir are shown in Figure 48, along with the realized reservoir series, the historical mean and the upper and lower 10% percentiles of the simulations. The expected reservoir series (the average of the scenarios) is close to the realized series the first weeks, and approaches subsequently the historical average. This behavior is as expected: Most stochastic factors are mean-reverting, thus the expected hydro reservoir conditioned on information from week 26 in 2008 and backwards converges to the unconditional expectation with time. A complementary interpretation can be raised from the idea behind the water value equation (Chapter 4.4): Since the optimal reservoir management policy is approximated to be the strategy which keeps the hydro reservoir at the long-term mean, the price formation should drive the reservoir level towards the mean.

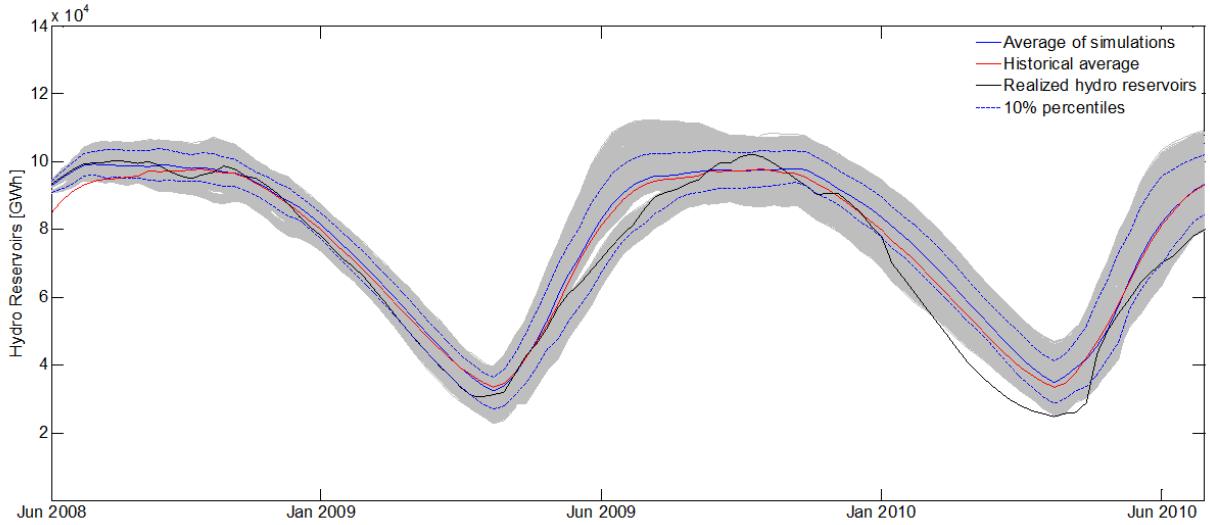

Figure 48. *Hydro reservoir scenarios*

A slight deviation from the mean trajectory is present in the 2009-10 winter season. The deviation is likely to be a result of several factors, including neglected spills, inaccurate input data and a slight overestimation of the expected inflow compared to the historical average in some periods.

Until January 2010, the realized reservoir series stays within the 10% percentiles. The rapidly decrease in the reservoir in the 2009-10 winter season has two main reasons: High levels of hydro generation due to massive nuclear outages in Sweden the fourth quarter of 2009 (4.3.1), and lower than normal inflow throughout the whole period (NVE, 2010b; NVE, 2010c). High temperatures in the spring of 2010 resulted in early snow melting, and consequently the realized

hydro reservoir turns back within the 10% percentiles. However, the total snow reservoir was lower than normal (NVE, 2010d), which again led to a deviation from the expected range at the end of the forecast period.

Simulation results for regulated hydro generation are displayed in Figure 49. A high reservoir level resulted in a water value lower than average in the start of the forecast period. As fuel prices were still high, the marginal cost of condensing generation was higher than normal. Consequently, hydro was more competitive than average compared to condensing power, and the simulated and realized levels of regulated hydro generation exceed the historical average. The level of regulated hydro generation converges towards the historical mean with time, although the fit is somewhat varying.

The largest deviations between realized and forecasted generation levels occur in the 2009-10 winter season. As mentioned, nuclear outages resulted in high levels of hydro generation in the fourth quarter of 2009. The combination of low hydro reservoirs, low inflow expectations due to dry weather and small amounts of snow in the mountains (NVE, 2010c) increased the opportunity cost of hydro power production in the second half of the winter. As a result, the generation level fell below the lower tenth percentile of the simulations.

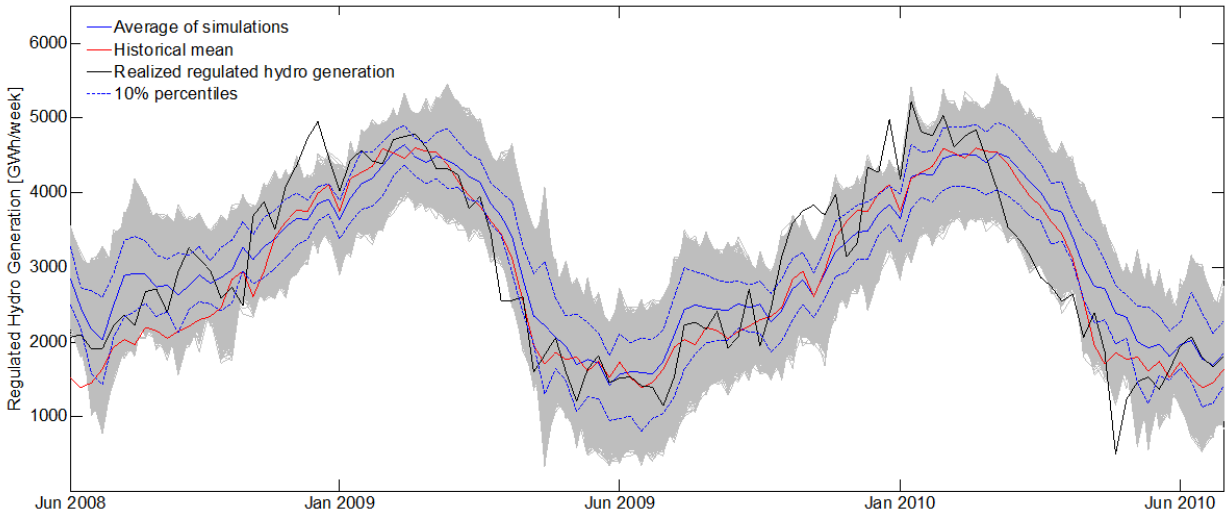

Figure 49. *Scenarios for regulated hydro generation*

Figure 50 shows simulated condensing generation compared to realized levels. Realized generation stays within the 10% percentiles most of the period, but are higher than all simulated values the first weeks. In these weeks, marginal costs of condensing units were high because of the high fuel prices, whereas hydro power was attractive due to the reservoir filling. Given the low consumption in the summer, no condensing generation was implicated from the merit order.

However, there was some condensing generation in reality, due to internal bottlenecks in the Nordic grid. Because of transmission constraints, hydro power in Norway and Sweden was not able to substitute condensing generation in Denmark. The internal transmission constraints are

demonstrated by Danish area prices twice as large as those in Southern Norway in the first week of the forecast period (NVE, 2008).

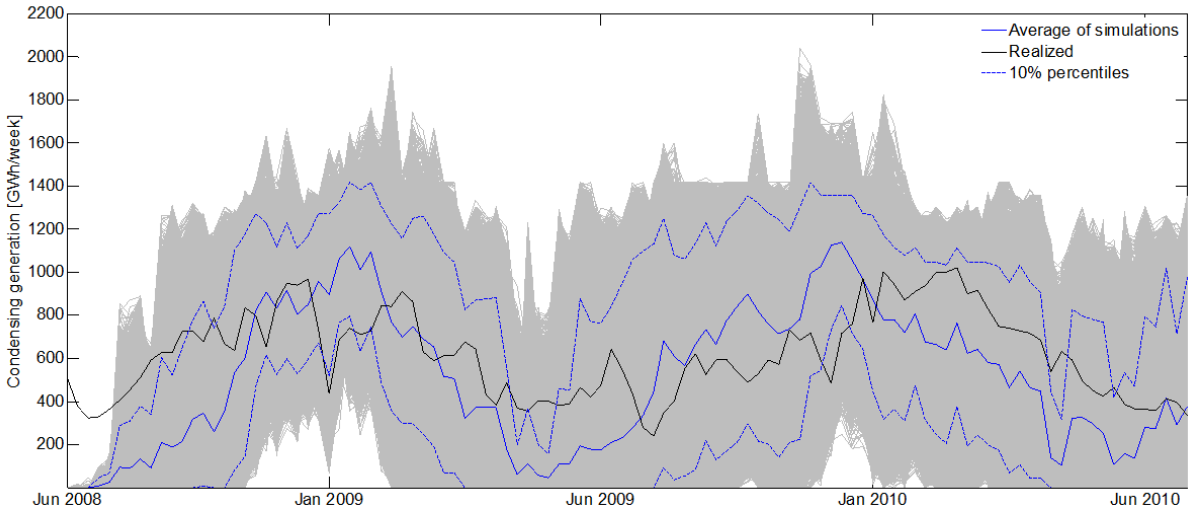

Figure 50. *Realized and simulated condensing generation*

Realized and simulated levels for exchange with the Netherlands, Germany and Poland are illustrated in Figure 51, where positive exchange indicates net import to Nord Pool. The mean of the simulations tends to be higher than realized levels, i.e. weekly net import to Nord Pool is often estimated to be too high. Although price differences is the major driver of exchange, comparing simulated EEX and Nord Pool prices with their realizations does not explain a higher simulated mean. On the other hand, it may be explained by simplifications in the modeling approach. In reality, exchange is determined by node prices in the connected areas rather than system prices. Furthermore, transmission costs complicate the picture.

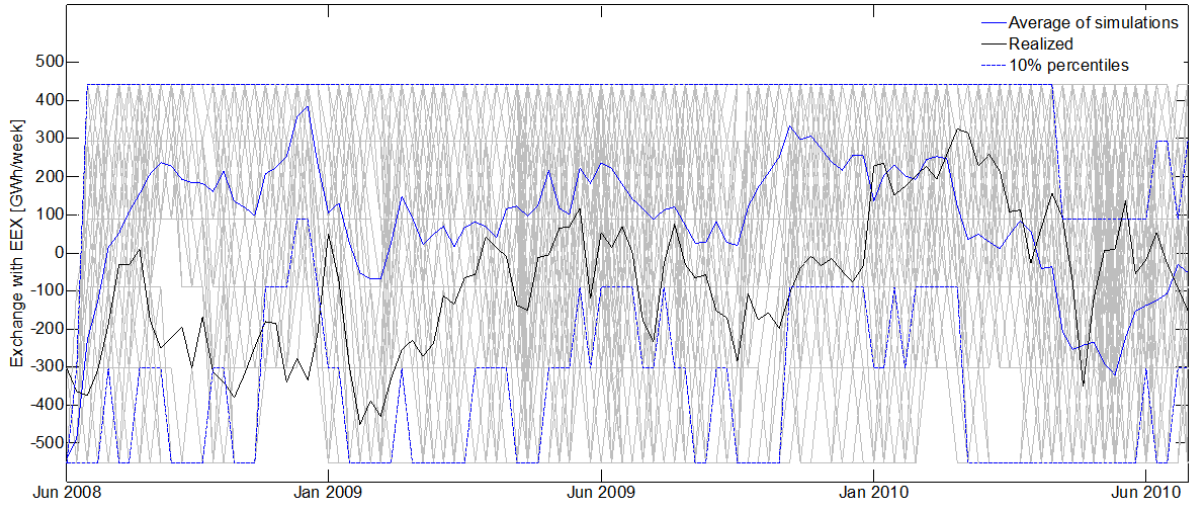

Figure 51. *Realized and simulated exchange with the Netherlands, Germany and Poland*

Figure 52 presents the resulting price scenarios. The mean of the scenarios is relatively close to the realized system price until January 2010, expect for the peak period in 2008. This price peak

seems to be a consequence of a peaking EEX price, still high fuel prices and normalization of the hydrological balance. As only one of the applied EEX scenarios spikes in this period and the water value equation underestimates the peak (Figure 41), the mean of scenarios diverges from the realized price. A rapid increase in the system price started in January 2010, due to the above discussed increase in water value. With a strongly negative hydrological balance, the system price stayed well above the mean of the simulations during the remaining forecast period.

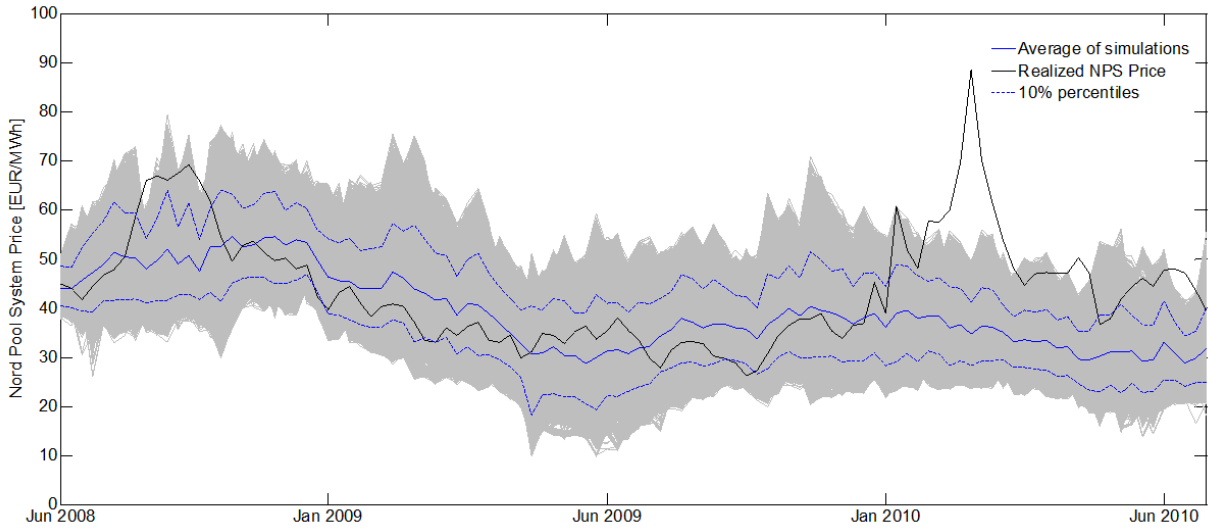

Figure 52. *Nord Pool system price scenarios*

Comparing the realized price to its simulated distribution indicates that the price risk is underestimated. For instance, no scenarios capture the price spike in February 2010. The main reason is the low number of scenarios for each stochastic factor. Thus, more unlikely values of the stochastic factors leading to extreme price scenarios are not included. In addition, the shortcomings of the inflow model discussed in 4.1.3 results in a lower inflow risk during the winter than what is realistic. In Chapter 4.8.1, we will show how an extended sample space of inflow scenarios affects the price distribution, and how the variance structure can be modeled more realistic.

4.8 Case studies

The model can be applied to learn more about the impact of different variables. First, we consider the price risk caused by inflow volatility. Then the relative influence of the stochastic factors is investigated. Finally, we study the impact of changes in the exchange capacity on the price and its distribution.

4.8.1 Inflow risk

The inflow model used in the base case simulations did not incorporate the seasonality in the variance, as previously explained. Therefore, we present two case studies which provide a more realistic picture of the price risk caused by inflow volatility.

First, the inflow scenarios for 2009 are substituted by the realized series for the years with maximum and minimum total inflow in the data sample (2000 and 1996, respectively). For the remainder of the forecast period, the original inflow scenarios are used. Snow reservoir scenarios are replaced by realized values from the autumn of 2008 and throughout 2009, to ensure consistency with inflow. Figure 53 displays the average hydro reservoir level together with the upper and lower tenth percentiles for the base case (with original inflow scenarios) and the two extreme scenarios. The shape is as expected, with large deviations between the three mean series in 2009, and convergence towards the base case in 2010.

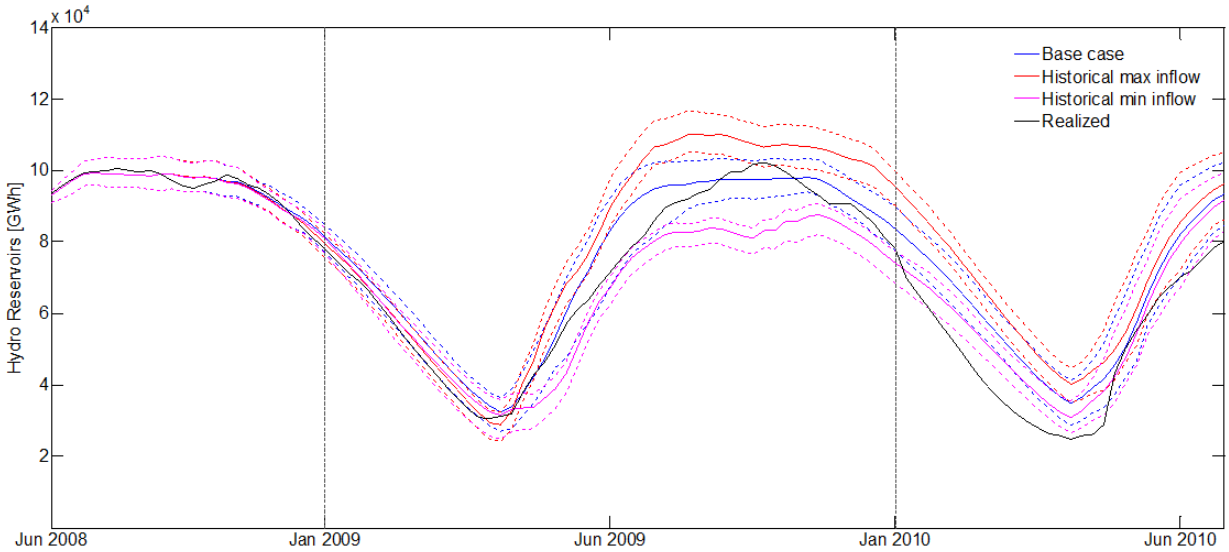

Figure 53. *Hydro reservoir scenarios for extreme inflow scenarios*

The deviations in hydro filling lead to large differences between the expected price paths, as evident from Figure 54. Deviations between the three cases appear already in the end of 2008, due to differences in snow reservoirs, and augment rapidly from January 2009. The higher price uncertainty (indicated by the percentiles) for the minimum inflow case, compared to the maximum case, is a consequence of the increasing steepness of the water value function with decreasing relative storage levels. When the original inflow scenarios are substituted back in 2010, convergence towards the base case price distribution appears as expected.

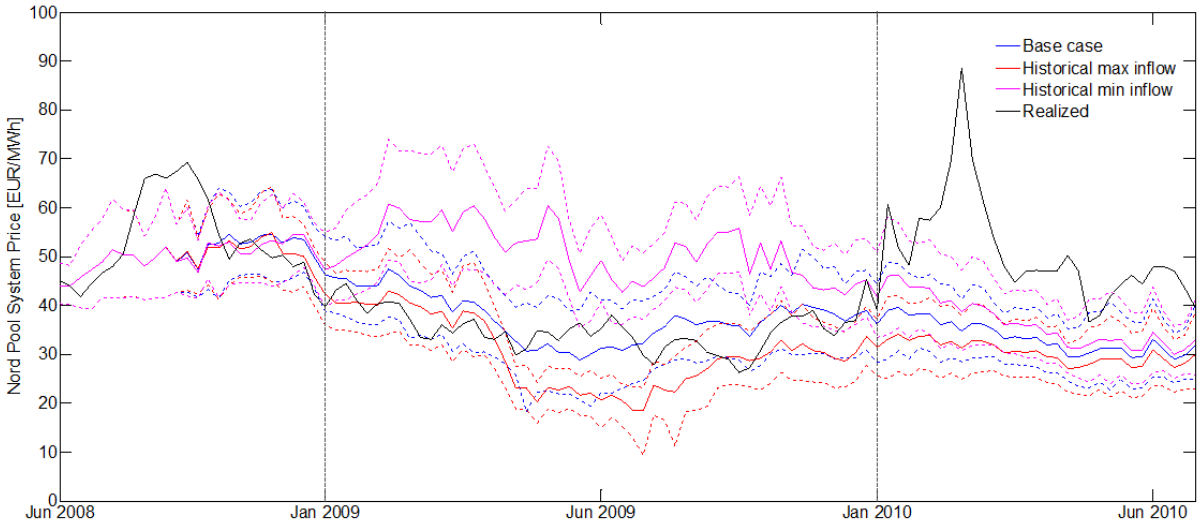

Figure 54. *System price scenarios for extreme inflow scenarios*

The above analysis provides a picture of the inflow risk and demonstrates that the model works as it should. To exploit the inflow risk in a more systematic manner, a case with 10 000 inflow scenarios is also simulated. Scenario paths for the other stochastic factors are chosen randomly from the set used in the base case simulations.

When assessing inflow risk in particular, the inflow variance should be modeled as realistic as possible. Thus, we prioritize a correct representation of the variance instead of modeling the true physical relationship with snow reservoirs. To better represent the inflow variance in this case study, we replace our original inflow model with an alternative model. In addition to the SARIMA-based dynamic regression models with logarithmic transformation proposed in 4.1.3, dynamic regression models with deseasonalized variables are potential alternatives. With the latter models, both the input and output series are deseasonalized according to (1), in line with the approach suggested by Hipel and McLeod (1994). Deseasonalizing take explicit account to the differences in variance throughout the year, thus transformations are not necessary to achieve a correct representation of the variance structure.

A model with deseasonalizing and without logarithmic transformation is chosen. Models with transformation led to forecasts slightly exceeding the historical average after convergence should have occurred. However, the explanatory power of the change in snow reservoirs disappears after deseasonalizing. Exclusion of snow reservoirs leads to an ordinary deseasonalized ARIMA model. According to the AIC criterion, the Ljung-Box test and the ADF test, an ARIMA(4,0,5) model is selected. Table 19 lists the coefficient estimates, while 10 000 simulated scenarios are shown in Figure 55. Due to the high number of simulations, convergence to the theoretical forecast is achieved without applying a Sobol sequence.

Table 19. *Coefficients in the deseasonalized inflow model*

AR1	AR2	AR3	AR4	
0.2344	-0.3721	0.1313	0.5857	
MA1	**MA2**	**MA3**	**MA4**	**MA5**
0.4337	0.6020	0.2977	-0.3605	-0.2098

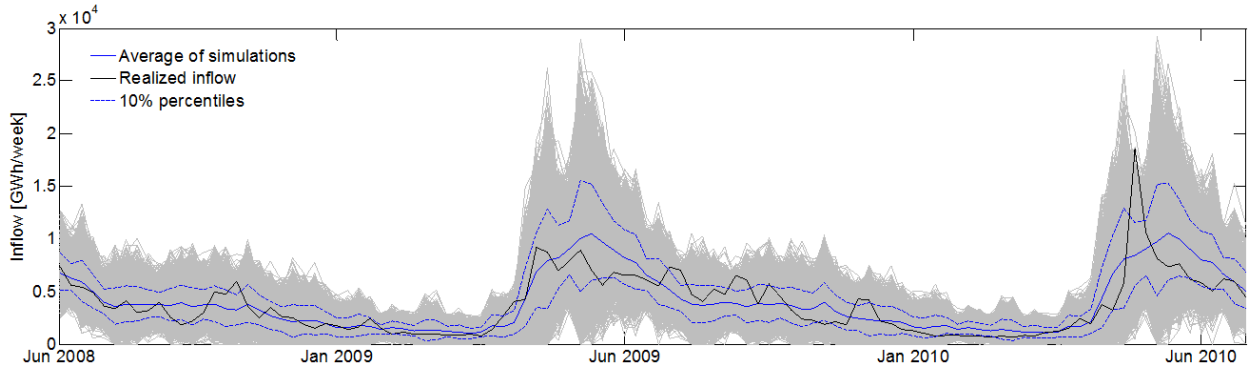

Figure 55. *Inflow scenarios from a deseasonalized ARIMA model*

Figure 55 exposes the disadvantage of deseasonalized ARIMA models discussed in Chapter 2.1.1. The lower variance in week 20 and 21 compared to 19 and 22 has no natural explanation, and may be a consequence of a smaller calibration set than necessary to achieve robust variance estimates. For the remaining part of the year, the distribution seems reasonable.

Compared to the base case simulations (Figure 48), the hydro reservoir sample space is much wider (Figure 56). This leads to occurrence of more extreme price scenarios (Figure 57). Extreme prices start to appear when inflow peaks, and the frequency is then gradually decreasing until the next hydrological cycle begins. Such behavior is not representative for the actual price distribution, but reflects the price risk caused by inflow stochasticity.

The high inflow variance in late spring will in some scenarios lead to reservoir levels deviating dramatically from the average. When the deviation is negative, the water value becomes high and the price peaks. The size of those peaks should be considered as a conceptual indication only: With an extremely negative hydro balance, it is likely that non-flexible technologies as nuclear will deviate from the scheduled maintenance periods and provide additional generation capacity. In addition, such relative storage levels are outside the sample used to calibrate the water value equation. The gradually decreasing peak frequency is tied to the gradually decrease in inflow volatility throughout the fall and winter. When the variance is lower, chances are higher that hydro producers can schedule generation such that the median trajectory policy is reached. This is shown in Figure 56, where the reservoir tenth percentiles are gradually narrowing from the summer of 2009 until the next hydrological cycle.

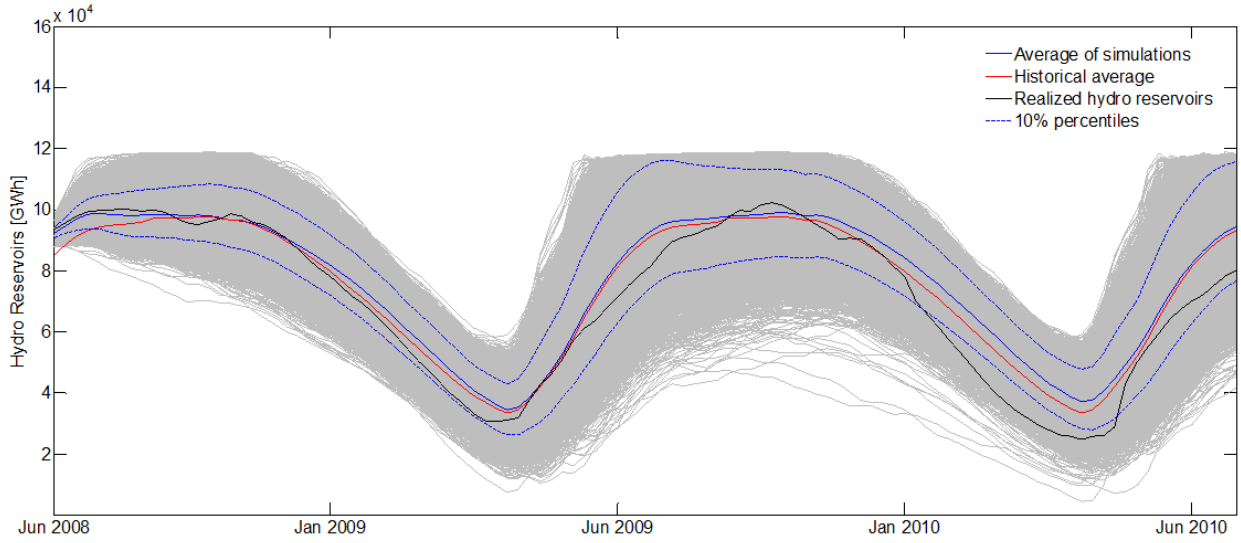

Figure 56. *Hydro reservoir scenarios for 10 000 inflow scenarios*

As pointed out, the applied inflow model was not able to capture the relationship between snow reservoirs and inflow. Thus, the snow reservoir scenario path is selected randomly for each inflow path. If the correlation structure between inflow and snow had been included, price peaks would have been more evenly distributed throughout the year.

A price equal zero appears when reservoir levels are extremely high, such that unregulated hydro cover all demand together with the other non-flexible technologies.

The expected price path is in the same range as for the base case. Most of the time, the price range within the tenth percentiles are slightly wider. Consequently, variations in inflow result in price fluctuations larger than the average price volatility caused by the other stochastic factors.

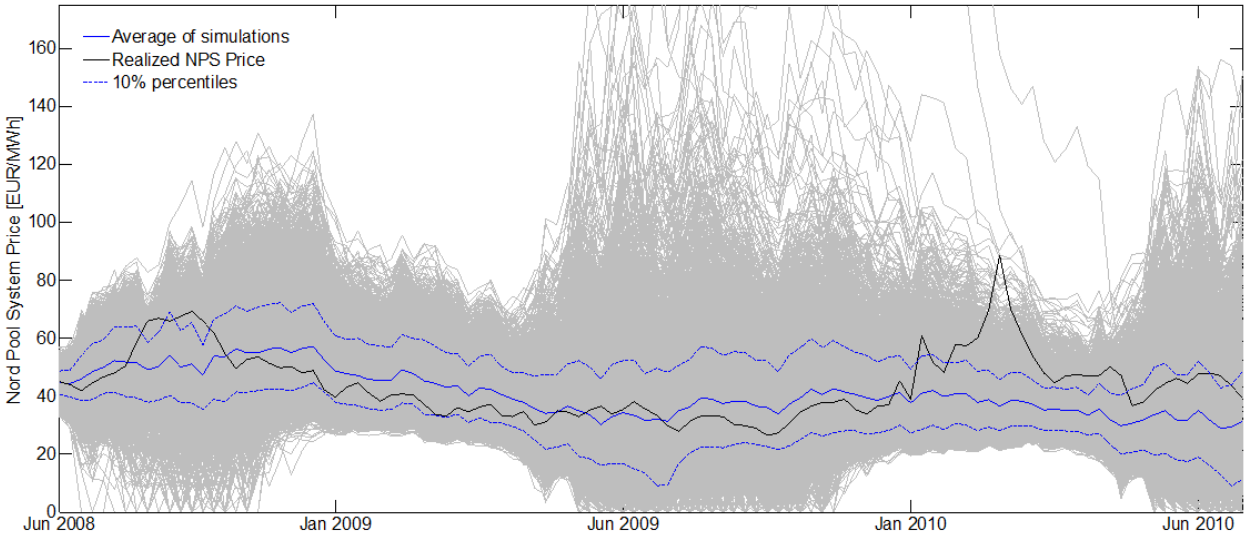

Figure 57. *System price scenarios for 10 000 inflow scenarios*

4.8.2 The relative influence of the stochastic factors

The stochastic factors have different influence on price variations. To quantify the impact of each factor, we simulate the market equilibrium using a set of scenarios for the stochastic factor under study and forecasts for the other factors. To make the results comparable, each factor is simulated by 40 scenarios. The deseasonalized inflow model is applied in order to model the variance properly.

The first column of Table 20 shows the average price volatility caused by each stochastic factor throughout the forecast period. In the second column, the risk of each factor is given by the average coefficient of variation[34] of the scenarios during the forecast period. We also present the average relative price volatilities, defined by the average price volatility divided by the average coefficient of variation.

Table 20. *Variance analysis*

	Average price volatility (EUR/MWh)	Average coefficient of variation	Average relative price volatility (EUR/MWh)
Inflow	2.5927	0.2444	10.600
HDD	0.4483	0.1694	2.6463
EEX price	2.7666	0.4885	5.6638
Nuclear generation	0.3925	0.0381	10.295
Wind power generation	0.4649	0.4841	0.9603
Coal price	3.4538	0.2469	13.986
Natural gas price	0.4149	0.2439	1.7194
CO_2 quota price	3.4958	0.3126	11.184

Inflow, EEX prices, coal prices and CO_2 quota prices are the most important factors with regard to price variations. However, due to the extreme movements in fuel and quota prices caused by the financial crisis, the modeled impact of these factors might be larger than what is the case under normal market conditions. The relative importance of these three factors is still interesting: The average price volatility caused by CO_2 prices are higher than for coal, but this result is tied to the larger variation in the CO_2 price scenarios. Coal prices cause higher relative price volatility than CO_2 prices, which is expected since coal prices represent a larger share of the short run marginal cost of condensing units. Natural gas prices have much less importance, due to three main reasons: The installed capacity of gas fueled plants is less than the capacity of coal plants, gas turbines are often staying idle as they act as peak load plants, and the marginal cost of gas fueled units is not assumed to have direct impact on the water value.

The relatively low importance of HDD is to some extent explained by the partial hedging provided by CHP district plants: Both consumption and CHP district generation are modeled as

[34] The coefficient of variation is defined as the sample standard deviation divided by the sample mean.

linear functions of HDD. In addition, the low volatility in HDD throughout the summer season results in small price variations only.

As a consequence of low variation in generation volumes, the price variations caused by nuclear generation are rather small. On the other hand, the impact is high relative to the modeled variation. If the scenarios had managed to capture the massive realized outages, the volatility of the scenarios and the influence on the system price would have been much higher. As described in 4.7, outages of nuclear generation were one of the main reasons behind the realized price peak in the 2009-10 winter season. Despite nuclear generation cause small variations in our case, the frequency of failures throughout the forecast period may support the use of nuclear generation as a stochastic factor in future use of the model.

In contrast to nuclear generation, the modeled impact of wind generation is tightly tied to the high variation in the scenarios. Relative to the variation coefficient, wind generation has by far the least impact on the system price.

4.8.3 Changes in exchange capacity

Several new interconnections between the Nord Pool area and Continental Europe are under planning (ENTSO-E, 2009). For instance, the Nord.Link and NorGer projects, both with a planned capacity of 1400 MW between Norway and Germany, are currently undergoing concession processes. New connections are partly motivated by the increasing share of renewable generation at the Continent: A tighter connection to the hydro reservoirs in the Nord Pool area will enable higher utilization of the non-flexible renewables. In addition, a power surplus in the Nordics towards 2025 will make additional export capacity profitable (Statnett, 2011; Statnett, 2010). Increased integration with Estonia (included in the Nord Pool area in 2010) and Russia is also expected in the coming decade (Statnett, 2010). Opposition against the integration trend is represented by the Minister of Petroleum and Energy in Norway, Ola Borten Moe, who wants to restrict exchange with the Continent and instead expand the domestic generation capacity (Sprenger, 2011).

In this context, evaluation of the sensitivity to changes in exchange capacity is of interest. As conceptual examples, we show how the price scenarios in the forecast period are affected by a doubling and a removal of the capacity to the Continent and Russia. Bear in mind that these examples not necessarily provide a correct picture of consequences of future capacity changes, as the price characteristics are likely to change.

Figure 58 shows the effect of changes in capacity shared with Germany, Poland and the Netherlands. Neither the expected system price nor the price distribution (indicated by the tenth percentiles) in the forecast period is much affected by changes in exchange capacity. This result is tied to the small differences between forecasted price levels for Nord Pool and EEX. Consistent with the higher historical variance of the EEX price, we find periods when increased

capacity leads to both the most extreme upper tenth percentile and the most extreme lower tenth percentile.

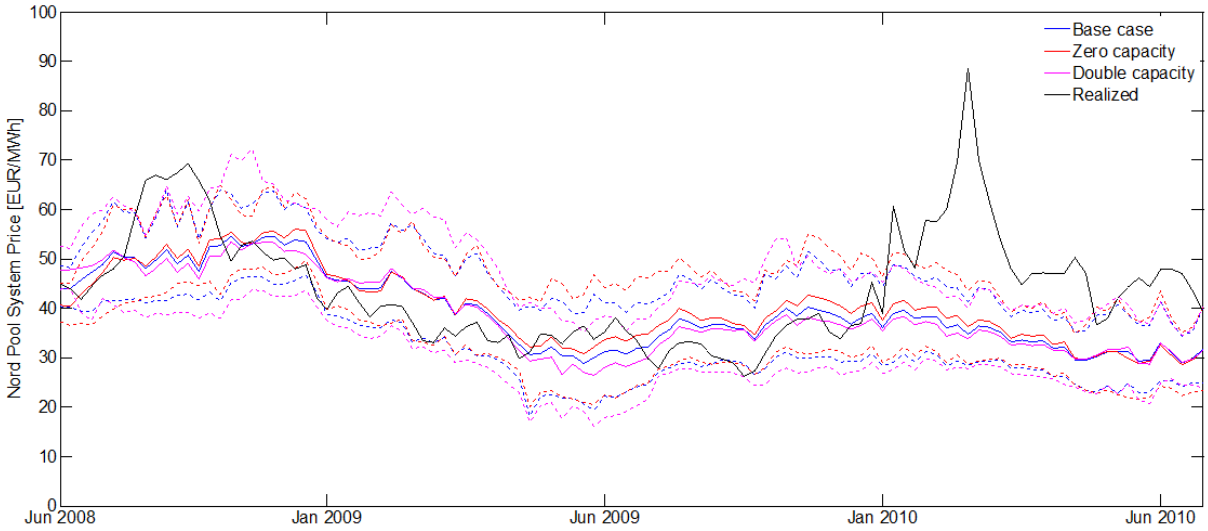

Figure 58. *System prices for different exchange capacities to Central Europe*

In Figure 59, the changes in the price distribution due to changed import capacity from Russia are displayed. Since the price of electricity imported from Russia is assumed to always be lower than the Nord Pool system price, increased capacity yields a lower system price throughout the period. On average, a doubling of the capacity results in a system price decrease of 7%.

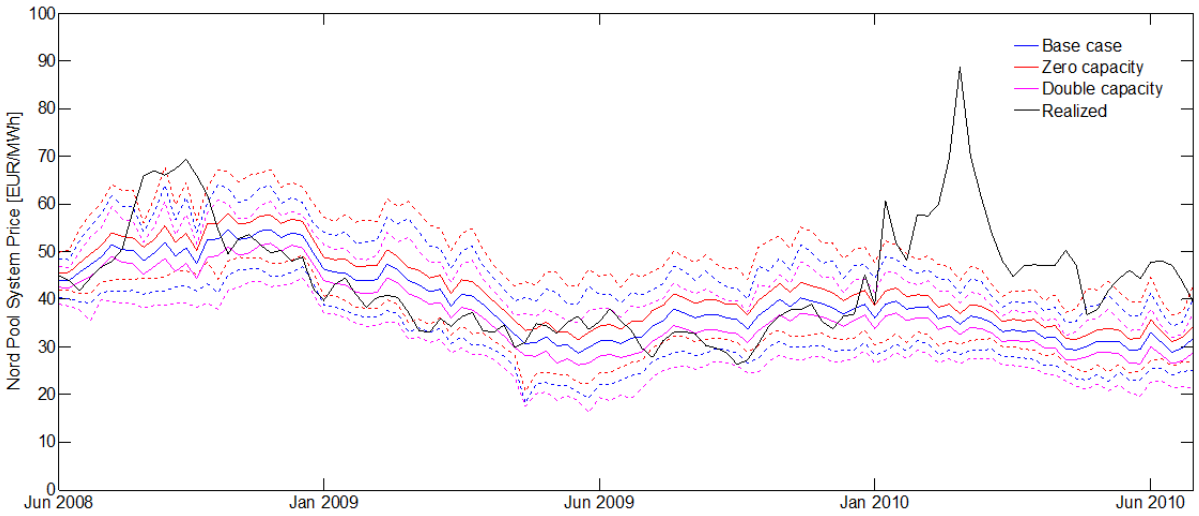

Figure 59. *System prices for different exchange capacities to Russia*

5. Discussion

As the model of this thesis considers the uncertainty in future spot prices, it is well suited for assessing risks related to price variation. It can be useful in planning with a horizon up to two years, typically generation scheduling and risk management in energy-intensive industry. The major strength of the model is inclusion of fundamental factors and relations between them.

Compared to EMPS, the use of an empirical approximation of the water value makes our model to be a less computationally intensive approach for system price forecasting. On the other hand, the high number of stochastic factors boosts up computation time. The number of scenarios for each factor should therefore be carefully evaluated when using the model. Our focus has been to show how stochastic factors influencing the price can be estimated and implemented in the model. To reduce computation time, applying forecasts for the less important factors and simulations for the most risky factors may be a good alternative in practical use.

Bottom-up modeling of electricity prices is a comprehensive task, involving a large set of models and extensive amounts of data. Consequently, we had to introduce several assumptions and simplifications. The model can therefore be improved by component wise extensions.

When modeling reservoir inflow, we did not manage to incorporate both the variance structure and the explanatory power of snow reservoirs in a single model. Thus, more advanced models outside the ARMA family should be considered. Relationships between other stochastic factors may also be implemented in the model structure. HDD can be used as an explanatory variable for snow reservoirs and inflow. The correlation between carbon quota prices, fuel prices and the EEX price can also be modeled.

We will encourage future work on the empirical water value approximation, especially concerning more accurate modeling of price peaks. Improved consumption forecasts can be obtained by including electricity price elasticity for energy-intensive industry. Another possible extension is to include internal transmission constraints and model area prices. The simulation results revealed that exclusion of transmission constraints within the Nord Pool area explained deviations between realized and forecasted levels of condensing generation and exchange.

Despite the data set is extensive; it can be improved in different ways. Longer time series for inflow and snow reservoirs should be considered, in order to obtain more robust parameter estimates. Time series for hydro reservoir spillage would also be of value. The model is sensitive to the parameter values in the water value function, and using longer time series to calibrate the function may increase its accuracy. Due to the financial crisis, we had to use hindsight in parameter estimation of the fuel price and carbon quota price processes. Testing and calibrating the model over other time periods than we did may thus be advantageous.

References

Anderson, C. L. and Davison, M. (2005) An Aggregate Weibull Approach for Modeling Short-Term System Generating Capacity. *IEEE Transactions on Power Systems*, 20(4), pp.1783-1789.

Andruszkiewicz, J. (2010) Development of cross-border transmission lines in Poland and their significance for the Central East European energy market. [online] Available at: <http://www.worldenergy.org/documents/congresspapers/314.pdf> (Accessed May 24, 2011).

Angeriz, A., and Arestis, P. (2007) Monetary Policy in the UK. [online] Available at: <http://wiztech.pk/regional/wp-content/uploads/2011/03/CJE-Philip-Arestis.ppt.pdf > (Accessed March 3, 2011).

Barz, G. and Johnson, B. (1999) Selecting Stochastic Processes for Modelling Electricity Prices. Risk publications, *Energy Modelling and the Management of Uncertainty*, Risk Books, pp. 3-21.

Batstone, S.R.J. (2003) *Aspects of risk management in deregulated electricity markets: Storage, market power and long-term contracts*. Ph.D. thesis. University of Canterbury, New Zealand.

Bishop, C.M. (1995) *Neural Networks for Pattern Recognition*. Oxford: Oxford University Press.

Bjerke E. (2006) Strømprisene stuper. *Dagens Næringsliv*, [online] April 27. Available at: <http://www.dn.no/forsiden/energi/article771215.ece> (Accessed March 11, 2011).

Brigo, D., Dalessandro, A., Neugebauer, M. and Triki, F. (2009) A Stochastic Processes Toolkit for Risk Management. Mean Reverting Processes and Jumps. *Journal of Risk Management in Financial Institutions*, 3(1), pp. 65-83.

Brown, R.L., Durbin, J. and Evans, J.M. (1975) Techniques for testing the constancy of regression relationships over time. *Journal of the Royal Statistical Society,* Series B, 37(2), pp. 149-192.

Brooks, C. (2008) *Introductory Econometrics for Finance.* (2. edition). New York: Cambridge University Press.

Burns, P. (2002) Robustness of the Ljung-Box Test and its Rank Equivalent. Working paper. [online] Available at: <http://www.burns-stat.com/pages/Working/ljungbox.pdf> (Accessed September 29, 2010).

Cartea, A. and Figueroa, M.G. (2005) Pricing in Electricity Markets: A Mean Reverting Jump Diffusion Model with Seasonality. *Applied Mathematical Finance*, 12(4), pp. 313-335.

Catalão, J.P.S., Mariano, S.J.P.S., Mendes, V.M.F. and Ferreira, L. A. (2007) Short-term electricity prices forecasting in a competitive market: A neural network approach. *Electric Power Systems Research*, 77, pp. 1297-1304.

Clewlow, L. and Strickland, C. (2000) *Energy derivatives: Pricing and risk management*. London: Lacima Publications.

Daskalakis, G. Psychoyios, D., and Markellos R.N. (2009) Modeling CO_2 emission allowance prices and derivatives: Evidence from the European trading scheme. *Journal of Banking & Finance*, 33, pp. 1230–1241.

Deng, S. (2000) Stochastic Models of Energy Commodity Prices and Their Applications: Mean-Reversion with Jumps and Spikes. Power working paper 073, University of California Energy Institute.

Dixit, A.K. and Pindyck, R.S. (1994) *Investment under Uncertainty*. New Jersey: Princeton University Press.

Doorman, G.L. (2009) Hydro Power Scheduling. Compendium in the course ELK15, Norwegian University of Science and Technology. [leaflet]

Doorman, G.L., Kjølle, G., Uhlen, K., Huse, E.S. and Flatabø, N. (2004) Vulnerability of the Nordic Power System: Report to the Nordic Council of Ministers. [online] Available at: <http://193.88.185.141/Graphics/Energiforsyning/Forsyningssikkerhed/Elforsyningssikkerhed/VulnarabilityoftheNordicPowerSystem.pdf > (Accessed May 8, 2011).

ECMWF (2009) Find out about us: our forecasts. [online] Available at: <http://www.ecmwf.int/about/forecasts.html> (Accessed May 16, 2011).

ECON (2004) Overvåkning av markedsmakt i kraftmarkedet. [online] Available at: <http://www.konkurransetilsynet.no/ImageVault/Images/id_1907/ImageVaultHandler.aspx> (Accessed February 5, 2011).

EIA (The U.S. Energy Information Administration) (2011) Statistics on Estonia. [online] Available at: <http://www.eia.gov/countries/country-data.cfm?fips=EN#data> (Accessed February 28, 2011).

Eliassen, K. (CEO, Varanger Kraft) (2011) Questions regarding exchange with Russia. [telephone] (Personal communication, February 7, 2011).

Energinet.dk (2010) Udtræk af markedsdata. [online] Available at: <http://www.energinet.dk/DA/El/Engrosmarked/Udtraek-af-markedsdata/Sider/default.aspx> (Accessed September 27, 2010).

ENTSO-E (2009) Power and Energy balances 2012. [online] Available at: <https://www.entsoe.eu/fileadmin/user_upload/_library/publications/nordic/planning/090600_entsoe_nordic_PowerEnergyBalances2012.pdf> (Accessed May 7, 2011)

ENTSO-E (2010) Principles for determining the transfer capacities in the Nordic power market. [online] Available at: <http://www.nordpoolspot.com/upload/Principles%20for%20determining%20the%20transfer%20capacities%2020100622.pdf> (Accessed February 28, 2011).

European commission (2007) ESTONIA – Internal Market Fact Sheet. [online] Available at: <http://ec.europa.eu/energy/energy_policy/doc/factsheets/market/market_ee_en.pdf> (Accessed February 12, 2011).

Ewald, C-O. and Yang, Z. (2007) Geometric mean reversion: Formulas for the equilibrium density and analytic moment matching. University of St. Andrews Economics Preprints.

Franco, J.C.G. (2003) Maximum likelihood estimation of mean reverting processes. Onward Inc. Real Options Practice.

Fridolfsson, S-O. and Tangerås, T.P. (2009) Market power in the Nordic electricity wholesale market: A survey of the empirical evidence. *Energy Policy*, 37(9), pp. 3681-3692.

Geman, H. (2007) Mean Reversion Versus Random Walk in Oil and Natural Gas Prices. *Advances in Mathematical Finance*, Applied and Numerical Harmonic Analysis, Part 2, pp. 219-228.

Gerger, C. (Head of Communication Nuclear Power, Vattenfall) (2011) Questions regarding nuclear power. [telephone] (Personal communication, February 9, 2011).

Glasserman, P. (2004) *Monte Carlo Methods in Financial Engineering*. New York: Springer.

Guimarães Dias, M.A. (2008) Stochastic Processes with Focus in Petroleum Applications. [online] Available at: <http://www.puc-rio.br/marco.ind/stochast.html> (Accessed February 1, 2011).

Hassoun, M.H. (1995) *Fundamentals of Artificial Neural Networks*. Cambridge, Massachusetts: MIT Press.

Hipel, K.W., McLeod, A.I. and Lennox, W.C. (1977) Advances in Box-Jenkins Modeling. *Water Resources Research*, 13(3), pp. 567-575.

Hipel, K.W. and McLeod, I.A. (1994) *Time series modeling of water resources and environmental systems.* Amsterdam: Elsevier Science & Technology.

Holmqvist, E. (NVE) (2010) Questions concerning snow data for Norway. [email] (Personal communication, September 21, 2010).

Hydro (2010) Annual report 2009. [online] Available at: <http://www.hydro.com/upload/Annual_reporting/annual_2009/downloadcenter/Reports/01_annual_report.pdf> (Accessed March 17, 2011).

Johansson, B. (SMHI) (2010) Question regarding median culmination in Sweden. [email] (Personal communication, September 29, 2010).

Johnsen, T.A. (2001) Demand, generation and price in the Norwegian market for electric power. *Energy Economics*, 23(3), pp. 227-251.

Johnsen, T.A. (NVE) (2011) Questions regarding the relationship between snow reservoirs and the water value. [telephone] (Personal communication, May 11, 2011).

Johnsen, T.A. and Willumsen, M.Ø. (2010) Electricity demand and temperature - an empirical methodology for temperature adjustment in Norway. [online] Available at: <http://www.nve.no/Global/Publikasjoner/Publikasjoner%202010/Rapport%202010/rapport2010_01.pdf > (Accessed September 9, 2010).

Lyngfelt, B. (SCA Sundsvall) (2011) Questions regarding CHP Industry generation at SCA Sundsvall and in general. [telephone] (Personal communication, March 10, 2011).

Manczyk, H. and Leach, M.D. (2002) Combined Heat and Power Generation and District Heating in Denmark: History, Goals, and Technology. [online] Available at: <http://www.energy.rochester.edu/dk/manczyk/denmark.pdf > (Accessed April 1, 2011).

Mansanet Bataller, M., Pardo Tornero, Á., and Valor, E. (2007) CO_2 Prices, Energy and Weather. *The Energy Journal*, 28(3), pp. 73-92.

Matilainen, J. and 17 contributors (2009) Market based analysis of interconnections between Nordic, Baltic and Poland areas in 2025. [online] Available at: <https://www.entsoe.eu/fileadmin/user_upload/_library/publications/nordic/planning/090210_entsoe_nordic_MultiregionalPlanningProjectReport.pdf> (Accessed March 5, 2011).

McDonald, R. L. (2006) *Derivatives Markets* (2. edition). Boston: Pearson Education.

Morsy, S., Rademaekers, K. and Slingenberg, A. (2008) Review and analysis of EU wholesale energy markets - Historical and current data analysis of EU wholesale electricity, gas and CO_2 Markets. [online] Available at: <http://ec.europa.eu/energy/electricity/publications/doc/wholesale_market_review.pdf> (Accessed February 28, 2011).

Murray, F.T. and Ringwood J.V. (1994) Improvement of electricity demand forecasts using temperature inputs. *Simulation Practice and Theory*, 2(3), pp. 121-139.

Nau, R.F. (2010) Seasonal ARIMA models. [online] Available at: <http://www.duke.edu/~rnau/seasarim.htm> (Accessed October 13, 2010).

NordREG (2008) Congestion Management Guidelines - Implementation within the Nordic market. [online] Available at: <https://www.nordicenergyregulators.org/upload/Reports/CMGuidelinesImplementation.pdf> (Accessed February 28, 2011).

Nordel (2009) Nordel Annual Statistics 2008. [online] Available at: <https://www.entsoe.eu/fileadmin/user_upload/_library/publications/nordic/annualstatistics/Annual%20Statistics%202008.pdf> (Accessed March 11, 2011).

Nord Pool Spot (2010) System price. [online] Available at: <http://www.nordpoolspot.com/trading/The_Elspot_market/Price-calculation/System_price/> (Accessed December 7, 2010).

Nord Pool Spot (2011a) UMM Database. [online] Available at: <http://umm.nordpoolspot.com/web/index.cgi> (Accessed January 20, 2011).

Nord Pool Spot (2011b) Info power plants >100 MW. [online] Available at: <http://www.nordpoolspot.com/umm/Generation-power-plant-Info/> (Accessed January 20, 2011).

Nord Pool Spot (2011c) History. [online] Available at: <http://www.nordpoolspot.com/about/History/> (Accessed February 7, 2011).

NVE (2008) Kraftsituasjonen pr. 9. juli. [online] Available at: <http://www.nve.no/PageFiles/1326/Monitor-uke-27%202008.pdf> (Accessed May 25, 2011).

NVE (2010a) Kraftsituasjonen veke 20, 2010. [online] Available at: <http://nve.no/Global/Energi/Analyser/Kraftsituasjonsrapporter/2010/Kraftsituasjonen%20uke%2020%202010.pdf> (Accessed April 1, 2011).

NVE (2010b) Kvartalsrapport for kraftmarkedet 4. kvartal 2009. [online] Available at: <http://nve.no/Global/Publikasjoner/Publikasjoner%202010/Rapport%202010/rapport2010_01.pdf?epslanguage=no> (Accessed May 23, 2011).

NVE (2010c) Kvartalsrapport for kraftmarkedet 1. kvartal 2010. [online] Available at: <http://nve.no/Global/Publikasjoner/Publikasjoner%202010/Rapport%202010/rapport10-2010.pdf?epslanguage=no> (Accessed May 23, 2011).

NVE (2010d) Kvartalsrapport for kraftmarkedet 2. kvartal 2010. [online] Available at: <http://nve.no/Global/Energi/Analyser/Kvartalsrapporter/Rapport%2014-10.pdf?epslanguage=no> (Accessed May 23, 2011).

Nyland, S. (Head of Analysis, SKM Market Predictor) (2011) Questions regarding calculation of marginal costs for condensing units. [email] (Personal communication, February 10, 2011)

Pankratz, A. (1991) *Forecasting with Dynamic Regression Models* (1. edition). New York: John Wiley & Sons.

Pao, H.-T. (2007) Forecasting electricity market pricing using artificial neural networks. *Energy Conversion and Management*, 48, pp. 907-912.

Patterson, W. C. (1983) *Nuclear power* (2.edition). Penguin Books [online] Available at: <www.waltpatterson.org/nppenguin.pdf> (Accessed March 8, 2011).

Pindyck, R. (2001) The dynamics of commodity spot and futures markets: A primer. *Energy Journal*, 22(3), pp. 1-29.

Pedersen, J. (Energinet.dk) (2011) Questions regarding scheduling of CHP District generation. [email] (Personal communication, February 2, 2011).

Pianosi, F. and Raso, L. (2008) Flood forecasting for heteroscedastic streamflow processes. *Proceedings of the 17th IFAC World Congress, July 6-11, Seoul, South Korea.*

Pierre, I. (2002) European Combined Heat & Power: A Technical Analysis of Possible Definition of the Concept of "Quality CHP". [online] Available at: <http://www.eurelectric.org/Download/Download.aspx?DocumentID=10278> (Accessed March 3, 2011).

Pilipovic, D. (1998) *Energy Risk: Valuing and Managing Energy Derivatives*. New York: McGraw-Hill.

RAO (2002) Company news. [online] Available at: <http://www.rao-ees.ru/en/news/pr_depart/archiv_pr/2002/show.cgi?july_december_2002.htm> (Accessed February 8, 2011).

Rasch, C.N. (Energinet.dk) (2010) Questions regarding electricity generation in Denmark. [email] (Personal communication, October 8, 2010).

Rolfsman, B. (2004) Combined heat-and-power plants and district heating in a deregulated electricity market. *Applied Energy*, 78(1), pp. 37-52.

Ross, S.M. (2007) *Probability Models* (9. edition). Burlington: Academic Press.

Sandsmark, M. and Tennbakk, B. (2010) Ex post monitoring of market power in hydro dominated electricity markets. *Energy Policy*, 38, pp. 1500-1509.

Schemde, A. (Thema Consulting Group) (2011) Data request and follow up questions related to marginal costs in the model by Thema Consulting Group. [email] (Personal communication, February 3, 2011).

Shumway, R.H. and Stoffer, D.S. (2010) Time Series Analysis and Its Applications. [online] Available at: <http://www.stat.pitt.edu/stoffer/tsa2/index.html> (Accessed September 13, 2010).

SINTEF Energiforskning (n. d.) *Redusert tilgjengelighet i Samkjøringsmodellen*. [leaflet]

SINTEF Energiforskning (2008) EMPS. [online] Available at: <http://www.sintef.no/Home/SINTEF-Energy-Research/Expertise/Hydro-thermal-operation-and-expansion-planning/EMPS/> (Accessed May 8, 2011).

SKM Market Predictor (2011) Data on condensing power plants in the Nord Pool area. [email] (Received February 14, 2011).

Sprenger, M. (2011) Ola Borten Moe vil ha billigere strøm. *Teknisk Ukeblad*, [online] March 31. Available at: <http://www.tu.no/energi/article284619.ece> (Accessed May 7, 2011).

Statnett (2010) Nettutviklingsplan 2010. [online] Available at: <http://www.statnett.no/Documents/Kraftsystemet/Nettutviklingsplaner/Statnetts%20nettutviklingsplan%202010.pdf> (Accessed May 7, 2011)

Statnett (2011) NORD.LINK starter direkte på steg to i den tyske konsesjonsprosessen. [online] Available at: <http://www.statnett.no/no/Nyheter-og-media/Nyhetsarkiv/Nyhetsarkiv-2011/NordLink-starter-direkte-pa-steg-to-i-den-tyske-konsesjonsprosessen/> (Accessed May 7, 2011)

Thema Consulting Group (2011) Data on condensing power plants in the Nord Pool area. [email] (Received February 3, 2011).

Tipping, J.P. (2007) *The Analysis of Spot Price Stochasticity in Deregulated Wholesale Electricity Markets*. Ph.D. thesis. University of Canterbury, New Zealand.

Vattenfall (2011) Annual report 2010. [online] Available at: <http://www.vattenfall.com/en/annual-report-2010.htm> (Accessed April 10, 2011).

Vehviläinen, I. and Pyykkönen, T. (2005) Stochastic factor model for electricity spot price - the case of the Nordic market. *Energy Economics,* 27(2), pp. 351-367.

VGB Powertech (2010) Availability of Thermal Power Plants 2000-2009. VBG technical-scientific report: TW 103 V e. [online] Available at: <http://www.vgb.org/vgbmultimedia/KW_Statistik/TW_103+Ve_+2010_+Outline.pdf> (Accessed March 9, 2011).

Vose, D. (2008) *Risk analysis: a quantitative guide* (3. edition). John Wiley & sons: England.

Wangensteen, I. (2007) *Power System Economics – the Nordic Electricity Market.* Trondheim: Tapir academic press.

Weigt, H. and von Hirschhausen, C. (2008) Price formation and market power in the German wholesale electricity market in 2006. *Energy Policy*, 36(11), pp. 4227- 4234.

Yang, J. and Yang, Z. (2008) Bayesian estimation of geometric mean-reversion. *International Symposium on Financial Engineering and Risk Management*, pp. 113-117.

Appendix A

A.1 Optimization of relative factors for consumption

Lagrange formulation of (32) - (33):

$$min\ z = \sum_{k\,\epsilon\,K}\sum_{j\,\epsilon\,W}\sum_{i\,\epsilon\,H}\left(f_{ijk} - \hat{f}_k\right)^2 + \lambda\left(\sum_{k\,\epsilon\,K}\hat{f}_k M_k - M\right) \tag{A.1}$$

where λ is the Lagrange multiplicator. The optimality conditions are:

$$\frac{\partial z}{\partial \hat{f}_k} = -2\sum_{j\,\epsilon\,W}\sum_{i\,\epsilon\,H}\left(f_{ijk} - \hat{f}_k\right) + \lambda M_k = 0 \tag{A.2}$$

$$\frac{\partial z}{\partial \lambda} = \sum_{k\,\epsilon\,K}\hat{f}_k M_k - M = 0 \tag{A.3}$$

A.2 Residual characteristics

Figures A.1 – A.8 display the residual characteristics for the (S)ARIMA models. The degrees of freedom in the Ljung-Box test is set equal to the particular lag length less the number of estimated coefficients, $n - (p + q + P + Q)$, according to Shumway and Stoffer (2010). Normal quantile plots (with points deviating from a straight line), density plots and Shapiro-Wilk p-values close to zero reveal that all models have non-normally distributed residuals.

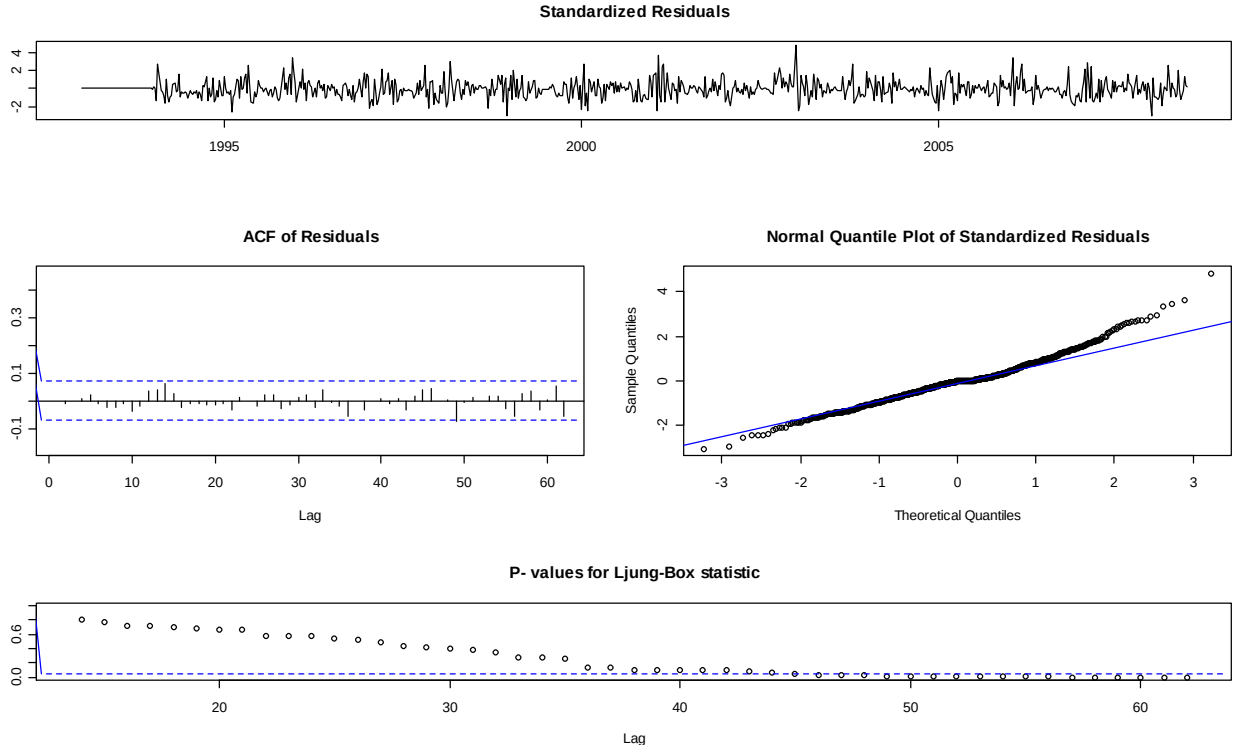

Figure A.1 *Characteristics of HDD residuals*

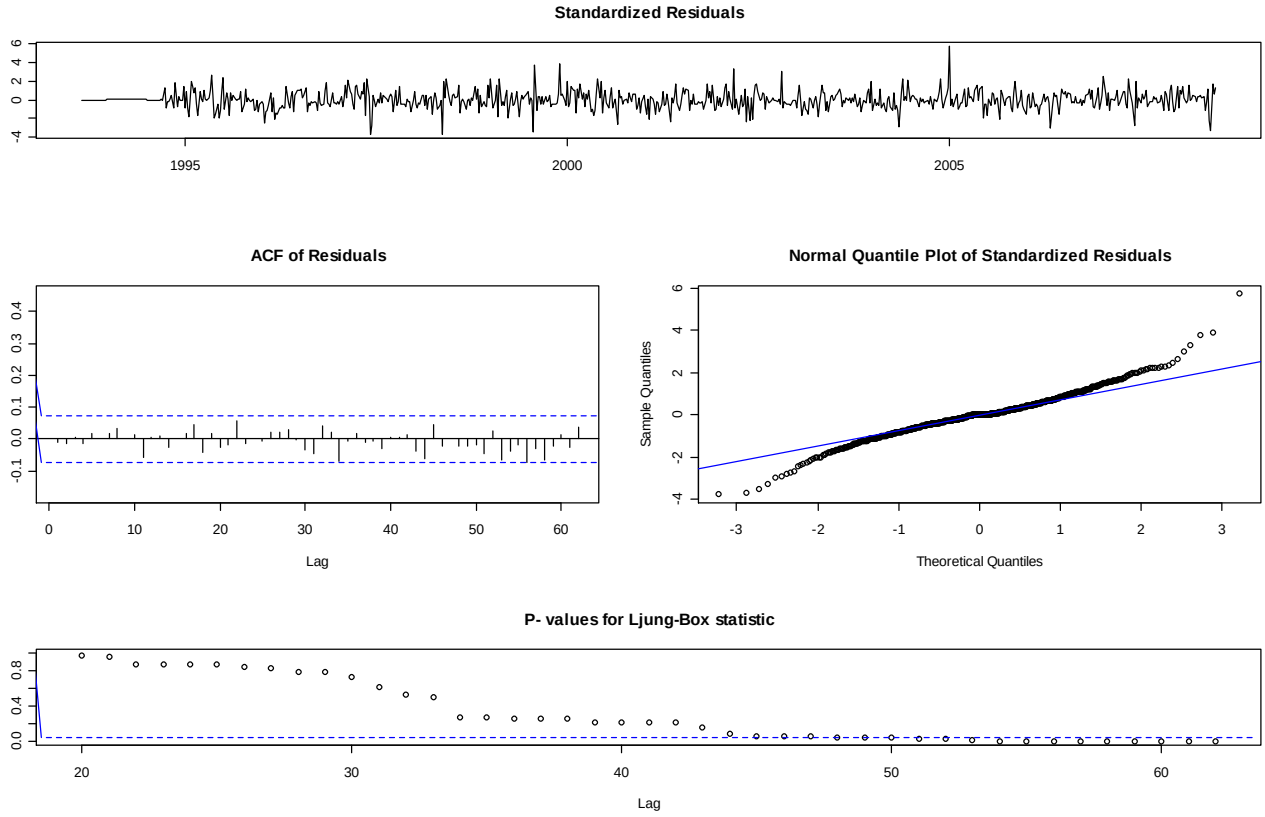

Figure A.2 *Characteristics of snow reservoir residuals*

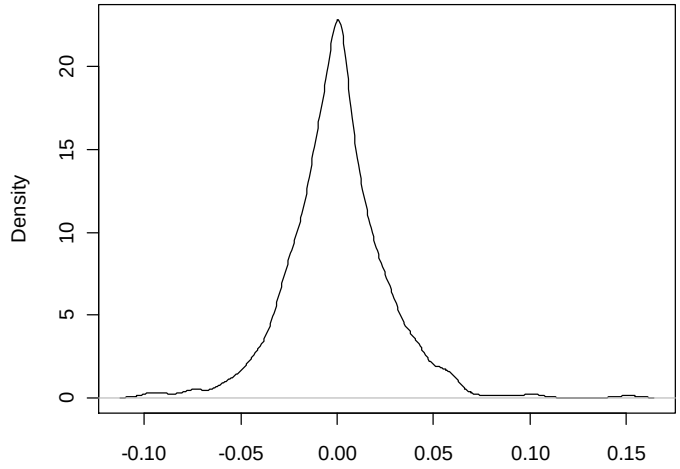

Figure A.3 *Density of snow reservoir residuals*

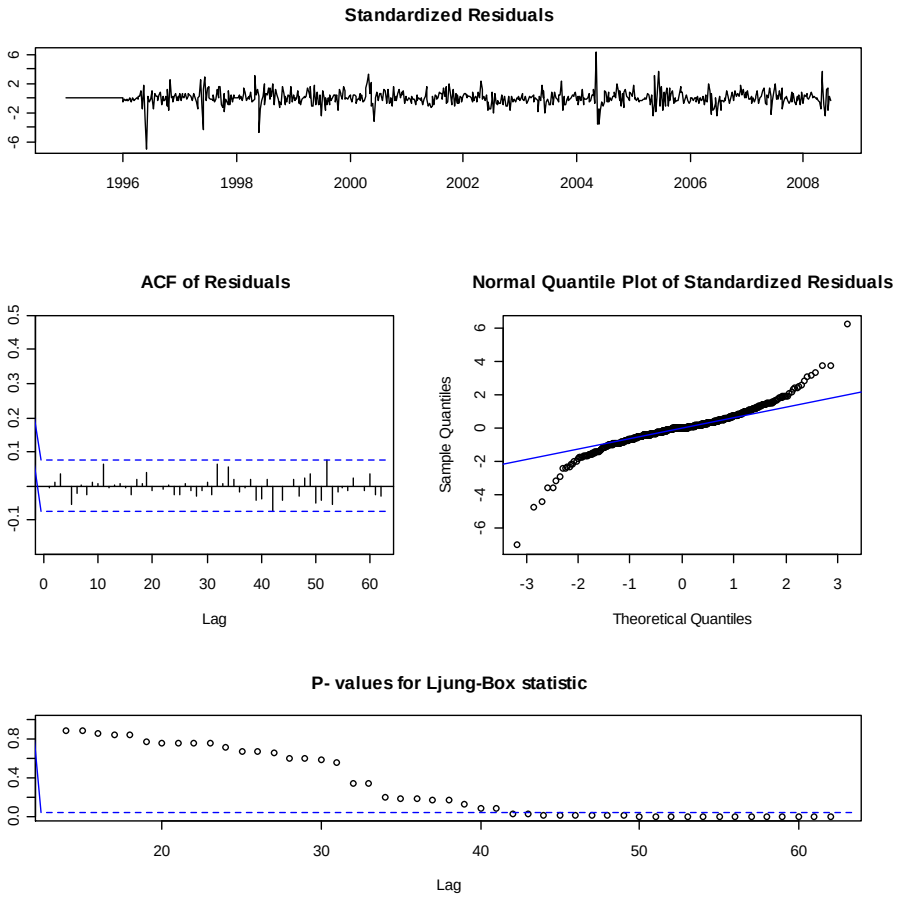

Figure A.4 *Characteristics of inflow residuals*

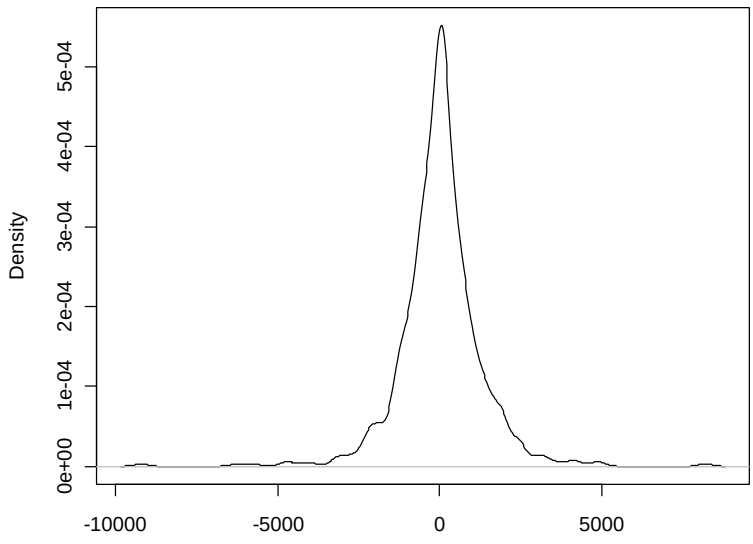

Figure A.5 *Density of inflow residuals*

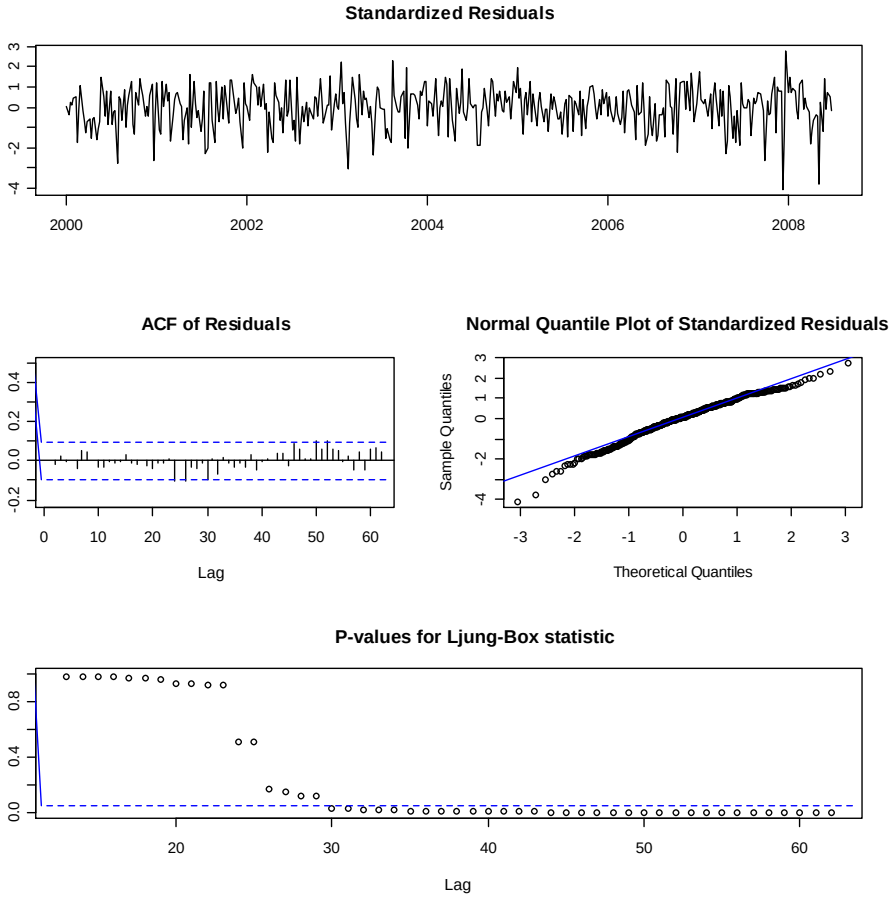

Figure A.6 *Characteristics of wind power residuals*

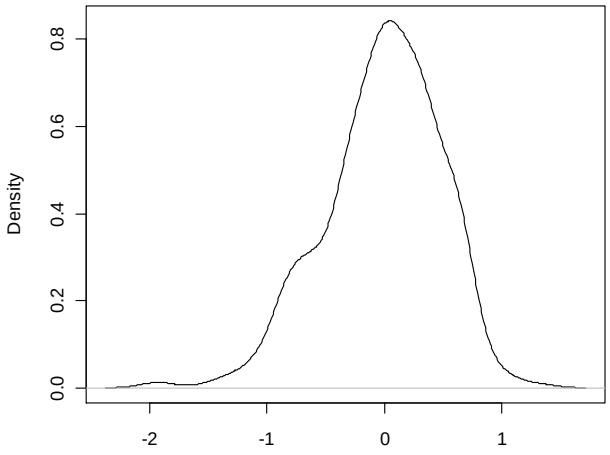

Figure A.7 *Density of wind power residuals*

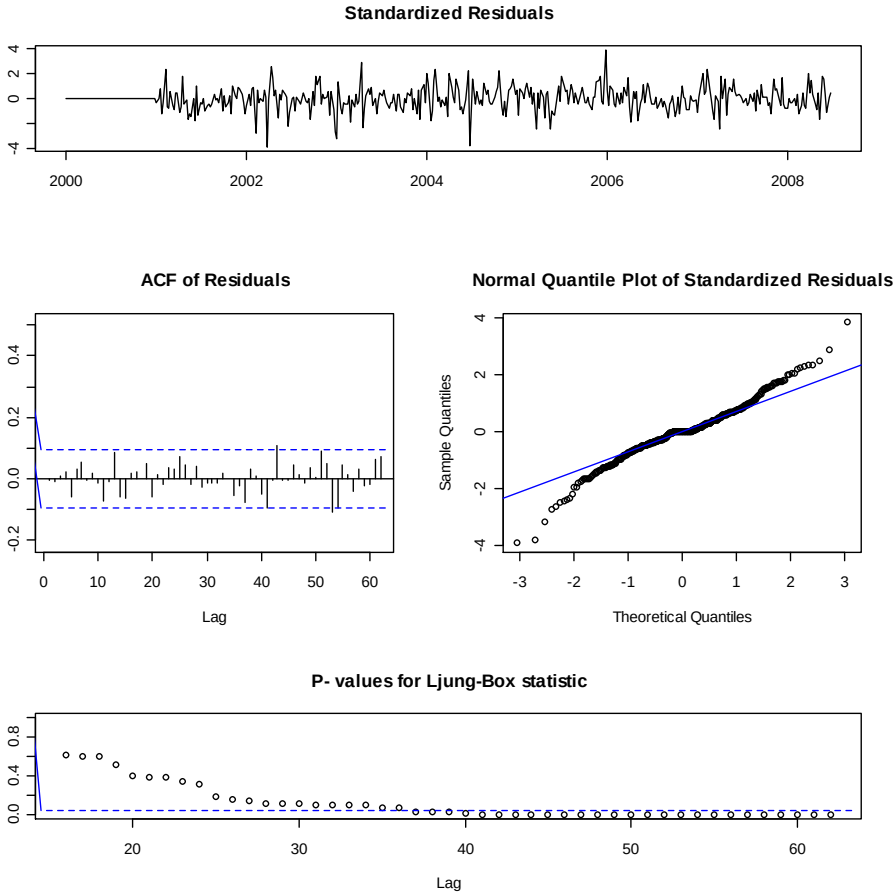

Figure A.8 *Characteristics of consumption residuals*

A.3 CUSUM charts

We create CUSUM charts to assess the stability of the SARIMA parameters, a methodology introduced by Brown et al. (1975). The cumulative sum of recursive residuals (CUSUM) is defined as (Angeriz and Arestis, 2007):

$$CUSUM_t = \sum_{i=k+1}^{t} W_{Y,i} \tag{A.4}$$

$$W_{Y,i} = \frac{\mathcal{F}_{Y,i} - Y_i}{\sigma_{Y,i}} \tag{A.5}$$

where

- Y_i is the realized value of the time series at time step i.
- $\mathcal{F}_{Y,i}$ is the one-step ahead forecast of the time series at time step i.
- $\sigma_{Y,i}$ is the standard deviation of one-step ahead forecast errors up to and including time step i.
- $W_{Y,i}$ is the one-step ahead standardized forecast error (i.e. standardized recursive residual) at time step i.
- k is the first time step for which forecasts are possible to calculate.

If the cumulative sum of standardized recursive residuals stays within a pair of critical lines, the model parameters are considered stable. The critical lines are given by the points $\left(k, \pm a\sqrt{T-k}\right)$ and $\left(T, \pm 3a\sqrt{T-k}\right)$, where T is the length of the series (Brown et al., 1975). The parameter a equals 1.143 for a significance level (α) of 1%, 0.948 when α = 5% and 0.850 when α = 10%.

CUSUM charts for the inflow, HDD and snow reservoir model are illustrated in Figure A.9, A.10 and A.11, respectively. We conclude that the parameters of the inflow and HDD models are stable, as standardized cumulative recursive residuals stay in the area between the critical lines. On the other hand, there are indications of instability for the snow reservoir model parameters. The model fails the test at the 5% significance level, but pass at the 1% level.

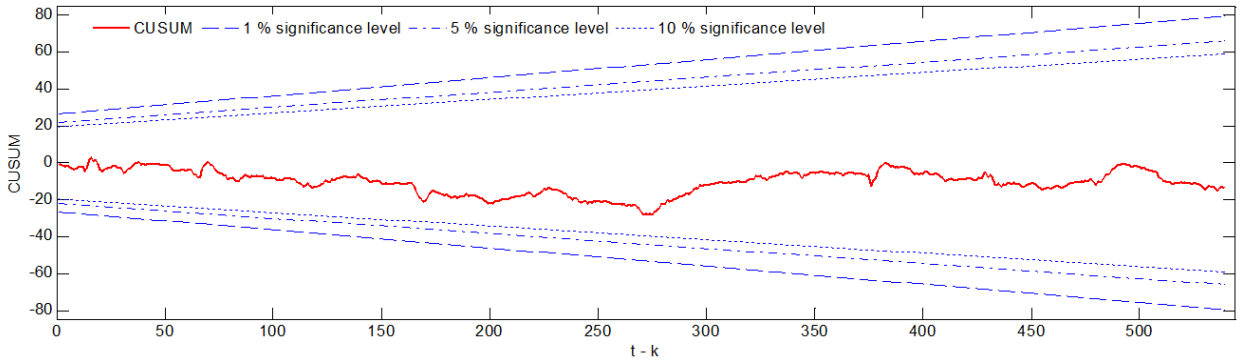

Figure A.9 *The CUSUM chart indicates parameter stability for the inflow model*

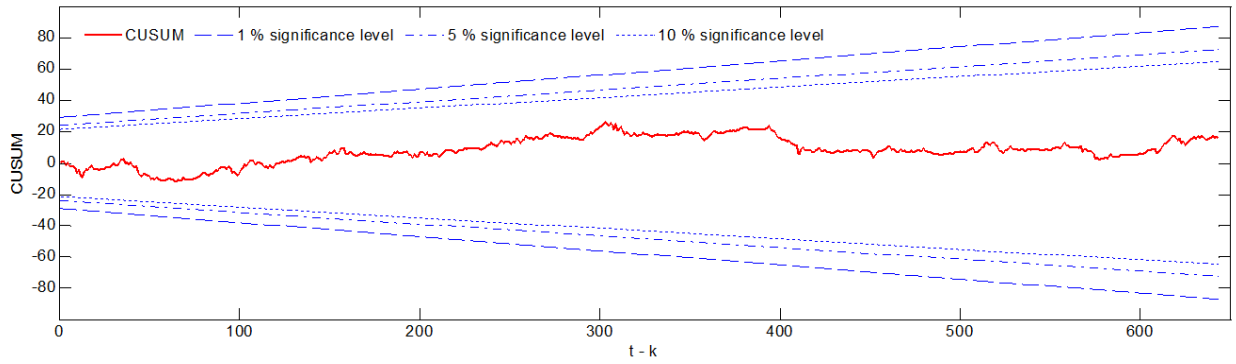

Figure A.10 *The CUSUM chart indicates parameter stability for the HDD model*

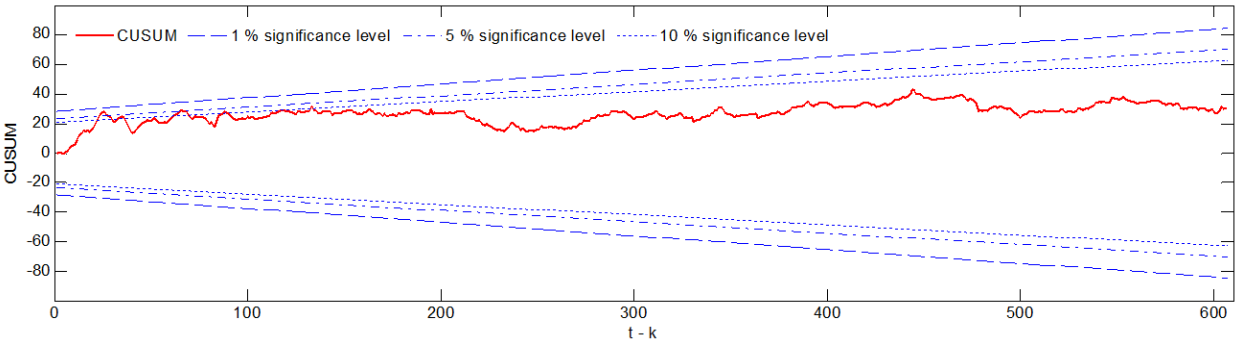

Figure A.11 *The CUSUM chart yields indications of unstable snow reservoir model parameters*

A.4 Impulse response function for inflow

Figure A.12 displays the modeled impulse response function for inflow. As apparent, snow reservoir ($\Delta R_{S\%}$) impulses in the present and previous week have a significant impact on the inflow level in the present week.

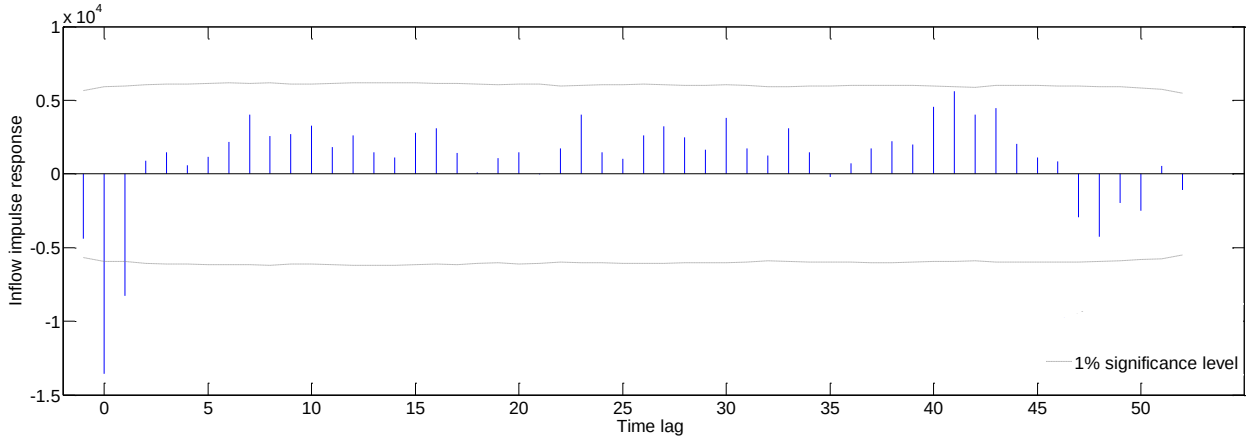

Figure A.12 *Impulse response function for inflow*

A.5 EEX logarithmic return properties

Table A.1. *Shapiro-Wilk normality tests for EEX logarithmic returns*

	Test statistic	P-value
Unfiltered returns	0.8607	0.00000
Filtered returns	0.9906	0.01269
Spikes	0.9197	0.07498

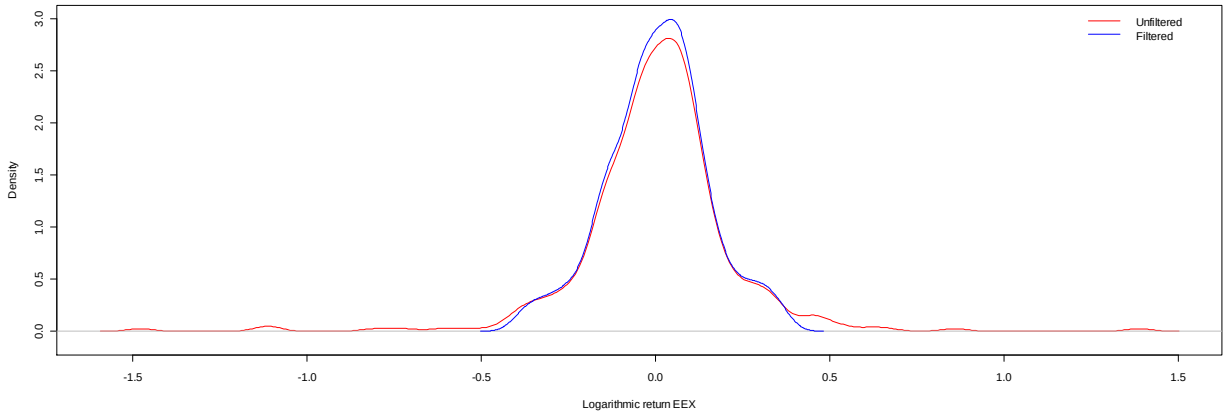

Figure A.13 *Density of unfiltered logarithmic returns compared to filtered returns*

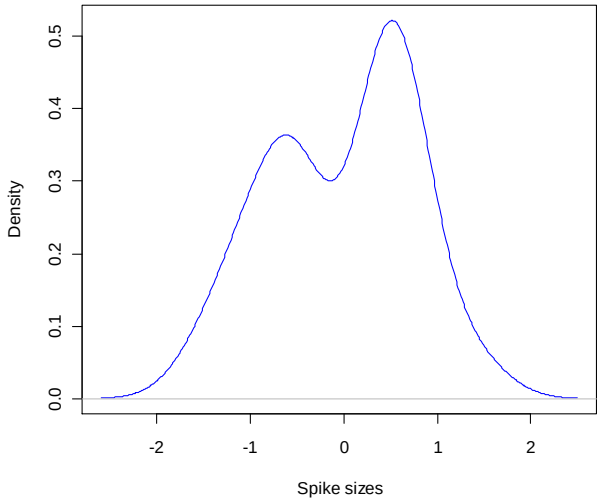

Figure A.14 *Density of (logarithmic) spikes*

A.6 Derivation of maximum likelihood parameter estimates for the discrete-time geometric mean reversion model

Starting with (44), taking the logarithm and removing constant terms, we end up with the following problem:

$$\max_{\alpha,\kappa,\sigma_{GMR}} f(\boldsymbol{Y}|Y_0,\alpha,\kappa,\sigma_{GMR},\Delta t) = \min_{\alpha,\kappa,\sigma_{GMR}} g(\boldsymbol{Y}|Y_0,\alpha,\kappa,\sigma_{GMR},\Delta t) \tag{A.6}$$

where

$$g(\boldsymbol{Y}|Y_0,\alpha,\kappa,\sigma_{GMR},\Delta t) = n\ln(\sqrt{2\pi\Delta t}\,\sigma_{GMR}) + \frac{\Delta t}{2\sigma_{GMR}^2}\sum_{i=0}^{n-1}\left(\frac{Y_{i+1}-Y_i}{Y_i} - \alpha + \kappa Y_i\right)^2 \tag{A.7}$$

First order conditions for optimal solution:

$$\frac{\partial g}{\partial \alpha} = 0, \qquad \frac{\partial g}{\partial \kappa} = 0, \qquad \frac{\partial g}{\partial \sigma_{GMR}} = 0, \qquad \sigma_{GMR} \geq 0 \tag{A.8}$$

where

$$\frac{\partial g}{\partial \alpha} = -\frac{\Delta t}{\sigma_{GMR}^2}\sum_{i=0}^{n-1}\left(\frac{Y_{i+1}-Y_i}{Y_i} - \alpha + \kappa Y_i\right) \tag{A.9}$$

$$\frac{\partial g}{\partial \kappa} = \frac{\Delta t}{\sigma_{GMR}^2}\sum_{i=0}^{n-1}\left(\left(\frac{Y_{i+1}-Y_i}{Y_i} - \alpha + \kappa Y_i\right)Y_i\right) \tag{A.10}$$

$$\frac{\partial g}{\partial \sigma_{GMR}} = \frac{n}{\sigma_{GMR}} - \frac{\Delta t}{\sigma_{GMR}^3}\sum_{i=0}^{n-1}\left(\frac{Y_{i+1}-Y_i}{Y_i} - \alpha + \kappa Y_i\right)^2 \tag{A.11}$$

Solving (A.8) is straightforward, and results in the parameter estimates (45) – (47). The solution is a global minimum since the function increases strictly for parameter values approaching $\pm\infty$.